RCA REVIEW

a technical journal

RADIO AND ELECTRONICS
RESEARCH · ENGINEERING

RCA REVIEW

a technical journal

RADIO AND ELECTRONICS
RESEARCH • ENGINEERING

VOLUME XI	SEPTEMBER 1950	NUMBER 3

CONTENTS

RCA REVIEW

BOARD OF EDITORS

REPUBLICATION AND TRANSLATION

FOREWORD

TWO new volumes in the RCA Technical Book Series — Television, Volume V (1947-1948), and Television, Volume VI (1949-June 1950) — are ready for distribution. This brings the television series up to date, and all six volumes are now available.

Information on these and other volumes published by RCA Review may be obtained by writing to:

> RCA Review
> Radio Corporation of America
> RCA Laboratories Division
> Princeton, N. J.

The Manager, RCA Review

September 25, 1950

FERROMAGNETIC SPINELS FOR RADIO FREQUENCIES*

By

R. L. Harvey, I. J. Hegyi and H. W. Leverenz

Research Department, RCA Laboratories Division,
Princeton, N. J.

Summary—Ferrospinels† are unique crystalline materials of spinel structure which are formed at high temperatures by solid-phase reaction of iron oxide and one or more of certain other metal oxides. They are ceramic-like ferromagnetic materials characterized by high permeability (up to greater than 1200), high electric resistivity (up to 10^8 ohm centimeter), and low losses at radio frequencies. Wide ranges in these and other properties are obtainable by varying the component ingredients and methods of synthesis.

While ferrospinels have been known for over forty years it is only recently that they have achieved commercial importance. In this paper there is an outline of the elementary THEORY *of ferromagnetism, and descriptions of the* STRUCTURES, SYNTHESIS, PROPERTIES, *and* USES *of some practical ferrospinels.*

HISTORICAL REVIEW

OVER 2500 years have elapsed since the ancient Greeks made the first recorded observations on attractions and repulsions of (1) certain bodies, such as amber and paper, which may be electrostatically charged by rubbing, and (2) small pieces of iron (Fe) brought near specimens of natural lodestone (magnetite = cubic-$FeO \cdot Fe_2O_3$). These basic phenomena of electricity and magnetism were impractical curiosities until 1500 years later when magnetism was used in primitive compasses. It was 600 years after the invention of the compass that Gilbert discovered that this earth itself is a magnet. Thereafter, there were few desultory qualitative experiments for 200 years more until Cavendish and Coulomb commenced quantitative research on electricity. Then, another 100 years went by before the epoch-making work of such men as Volta, Oersted, Biot, Ampere, Faraday, and Henry provided the foundation for Maxwell's unifying

---

† The coined word **ferrospinel** is used to denote a *ferromagnetic spinel*, which is a species of non-metallic cubic crystalline material containing iron in combined form. The term ferrospinel seems doubly appropriate because the materials utilize chiefly the *spin* property of unpaired electrons. Ferrospinels are sometimes called "ferrites", a term which is inappropriate because the word ferrite has long been used to denote a form of metallic (α) iron containing a fraction of a per cent of carbon (see A. F. Wells, *Structural Inorganic Chemistry*, Oxford, Clarendon Press, 1945).

Table I—Electronic Configurations and Approximate Sizes of Some Atoms and Ions

ISOLATED ATOMS

At No. Z	Element, nl: Symbol m_μ:	Quantum states and occupancy by electrons							No. of unpaired electrons N_u
		1s	2s	2p	3s	3p	3d	4s	
		0	0	0,±1	0	0,±1	0,±1,±2	0	
1	Hydrogen, H	1							1
2	Helium, He	2							0
3	Lithium, Li	2	1						1
4	Beryllium, Be	2	2						0
5	Boron, B	2	2	1					1
6	Carbon, C	2	2	1,1					2
7	Nitrogen, N	2	2	1,1,1					3
8	Oxygen, O	2	2	2,1,1					2
9	Fluorine, F	2	2	2,2,1					1
10	Neon, Ne	2	2	2,2,2					0
18	Argon, A	2	2	6	2	6			0
19	Potassium, K	2	2	6	2	6		1	1
20	Calcium, Ca	2	2	6	2	6		2	0
21	Scandium, Sc	2	2	6	2	6	1	2	1
22	Titanium, Ti	2	2	6	2	6	1,1	2	2
23	Vanadium, V	2	2	6	2	6	1,1,1	2	3
24	Chromium, Cr	2	2	6	2	6	1,1,1,1,1	1	6
25	Manganese, Mn	2	2	6	2	6	1,1,1,1,1	2	5
26	Iron, Fe	2	2	6	2	6	2,1,1,1,1	2	4
27	Cobalt, Co	2	2	6	2	6	2,2,1,1,1	2	3
28	Nickel, Ni	2	2	6	2	6	2,2,2,1,1	2	2
29	Copper, Cu	2	2	6	2	6	2,2,2,2,2	1	1
30	Zinc, Zn	2	2	6	2	6	2,2,2,2,2	2	0

Table I—Electronic Configurations and Approximate Sizes of Some Atoms and Ions

ISOLATED COMMON IONS

Ion (Atom)	Config-uration of outer electrons	No. of unpaired electrons N_u	$\mu_{eff.} = [N_u(N_u+2)]^{\frac{1}{2}}$ (theor.)	expt.	Approx. Radius in Solids Octahedral ionic (6-coord.) Å	Tetrahedral covalent (4-coord.) Å
H+	—	0	0	0		
(He⁰)	$1s^2$	0	0	0		
Li+	$1s^2$	0	0	0	0.60	
Be²+	$1s^2$	0	0	0	0.31	1.06
B³+	$1s^2$	0	0	0	0.20	0.88
C⁴±	$1s^2$ or $2p^6$	0	0	0	(4+)0.15	0.77
N³−	$2p^6$	0	0	0	1.71	0.70
O²−	$2p^6$	0	0	0	1.40	0.66
F−	$2p^6$	0	0	0	1.36	0.64
(Ne⁰)	$2p^6$	0	0	0		
(A⁰)	$3p^6$	0	0	0		
K+	$3p^6$	0	0	0	1.33	
Ca²+	$3p^6$	0	0	0	0.99	
Sc³+	$3p^6$	0	0	0	0.81	
Ti⁴+	$3p^6$	0	0	0	0.68	
V⁵+	$3p^6$	0	0	0	0.59	
Cr³+	$3d^3$	3	(3.9)	3.86	0.64	
Mn⁴+	$3d^3$	3	(3.9)	4.0	< 0.6	
Fe³+	$3d^5$	5	(5.9)	5.9	0.60	
Co³+	$3d^6$	4	(4.9)	2.5?	< 0.7	
Ni²+	$3d^8$	2	(2.8)	3	0.70	
Cu²+	$3d^9$	1	(1.4)	2	< 0.9	1.35
Zn²+	$3d^{10}$	0	0	0	0.74	1.31

"Treatise on Electricity and Magnetism" (1873).[1,2] From this era on, there was such a rapid increase in study and use of electricity and magnetism that electromagnetism is now a vital ingredient of our civilization.[1,3]

Since the ancient beginnings of our knowledge of magnetism, iron and certain iron-containing (ferrous) materials have provided out-standingly intense magnetic effects which were called **ferromagnetism.** Elemental iron, then, was one logical starting point for the preparation of new magnetic materials, and so there has been much empirical re-search on making alloys of iron with other metals which influence magnetic properties. This work has afforded dozens of superior mag-netic alloys, some of which have initial magnetic permeabilities (mag-netizabilities) over 100 times that of iron. Many of the best ferro-magnetic alloys, such as Supermalloy [Ni(79%), Mo(5%), Fe(15%)], have iron as a minor constituent, and one permanent-magnet alloy [Pt(77%), Co(23%)] contains no iron at all.[1]

These large increases in intrinsic permeability have not benefited the radio industry which has, until recently, used chiefly iron in powdered form for high-frequency devices, such as transformer cores.[4,5] Finely divided iron is used because peripheral eddy currents at high frequencies produce large losses and act to reduce the penetration of alternating fields into a conducting solid. Iron has a resistivity of only 10^{-5} ohm centimeter, and so it is necessary to decrease losses and magnetic self-shielding (magnetic skin effect) by subdividing the con-ducting solid into thin laminations or fine particles. The particles are insulated from each other, usually by coatings of phenolic resins. These nonmagnetic coatings reduce greatly the apparent intrinsic permea-bility to provide a low effective permeability. The effective permeability μ_e of a toroidal core made of sufficiently fine iron particles having an intrinsic permeability μ_i is given by

$$\mu_e = (\frac{V_i}{\mu_i} + V_b)^{-1} \tag{1}$$

where V_i is the fraction of the total volume occupied by the iron, and

[1] R. M. Bozorth, "Magnetism", *Revs. Mod. Phys.*, Vol. 19, No. 1, pp. 29-86, January, 1947.

[2] F. K. Richtmyer and E. H. Kennard, INTRODUCTION TO MODERN PHYSICS, McGraw-Hill Book Company, Inc., New York, N. Y., 1947.

[3] F. Bitter, "Magnetism", *Physics Today*, Vol. 2, No. 11, pp. 21-28, November, 1949.

[4] H. G. Shea, "Magnetic Powders", *Electronic Industries*, Vol. 4, No. 8, pp. 86-89, 186, 190, 194, 198, 202, August, 1945.

[5] G. O. Altmann and H. Beller, "Radio-Frequency Cores of High Perme-ability", *Electronic Industries*, Vol. 4, No. 11, pp. 86-89, 152, 154, November, 1945.

$V_b = 1 - V_i$ is the fraction of the volume occupied by the nonmagnetic resin coating between the particle. For a practical core with $\mu_i = 80$ and $V_i = 0.95$ (3-micron particles), μ_e is only 16. There is little advantage in going to higher intrinsic permeabilities here, because V_b limits μ_e to a maximum value of 20 even if μ_i were infinitely large. Further reduction in V_b has been impractical because thinner insulating coating (binder) results in (1) insufficient mechanical strength, and (2) increased electrical contact of the particles. The increased electrical contact increases the effective particle size and eddy-current pathlength.

Another logical starting point for research on new magnetic materials was the previously mentioned magnetite. Here, iron and oxygen are combined in a crystal wherein the iron ions (1) exist in two different states of ionization or oxidation, and (2) are located in two crystallographically dissimilar sites in spinel-type crystals.[6] It was found that magnetite is useful for radio transformer cores, but it too must be pulverized and insulated to minimize eddy-current losses, even though its resistivity of 0.01 ohm centimeter is 10^3 times that of iron.[6,7] Although the μ_e of practical magnetite cores is usually less than 8, there has been considerable use of such cores because natural magnetite is only about one-tenth as expensive as iron powder produced by the carbonyl process.[4]

Just as elemental iron can be combined with other metals to make superior magnetic alloys, so magnetite can be modified by incorporating other elements in it to produce improved magnetic spinels. This was reported by many experimenters, notably Hilpert before 1910, and later Serres, Forestier, Kato, Kawai, Cobb, Snoek, and others. [8-21] Thus far, the most useful magnetic spinels have been:

[6] E. J. W. Verwey and P. W. Haayman, "Electronic Conductivity and Transition Point of Magnetite ("Fe₃O₄")", *Physica*, Vol. 8, No. 9, pp. 979-987, November, 1941.

[7] J. C. Lee and E. H. Colpitts, "Magnetic Core for Inductance Coils", U.S. Pat. 705,935, 7/29/02 (*cf.*, U.S. Pat. 2,418,467, 4/8/47).

[8] S. Hilpert, "Verfahren zur Herstellung magnetisierbarer Materialen von gleichzeitiger geringer Leitfähigkeit für elektrische und magnetische Apparate", Ger. Pats. 226,347, 1/7/09 and 227,787, 2/25/09; *cf.*, *Z. physik. Chem.*, Vol. 18, pp. 291-315, 1932.

[9] A. Serres, "Recherches sur les moments atomiques", *Ann. Phys.*, Ser. 10, Vol. 17, pp. 5-95, January, 1932.

[10] H. Forestier, TRANSFORMATIONS MAGNETIQUES DU SESQUIOXIDE DE FER ET SES COMBINAISONS FERROMAGNETIQUES, Paris, 1928; *cf.*, *Compt. rend.*, Vol. 192, pp. 842-845, 1931.

[11] H. Forrestier and M. Vetter, "Etude des systemes Fe₂O₃ NiO-Fe₂O₃ MgO, Fe₂O₃ NiO-Fe₂O₃ CuO, Fe₂O₃ NiO-Fe₂O₃ ZnO", *Compt. rend.*, Vol. 209, pp. 164-167, 1939.

[12] Y. Kato, "Characteristics of Metallic Oxide Magnets", *Jour. Inst. Elec. Eng. (Japan)*, Vol. 53, pp. 408-412, 1933.

(1)   Permanently magnetic (hard) ferrospinels formed by heating pressed mixtures of, for example, equimolecular proportions of finely divided $FeO \cdot Fe_2O_3$ and $CoO \cdot Fe_2O_3$ (or half $CoO \cdot Fe_2O_3$ and half $NiO \cdot Fe_2O_3$) to temperatures above $600°C$.[13] The solid products are permanently magnetized by applying a strong magnetic field while the crystallized materials are cooling through the temperature range near $300°C$.

(2)   Impermanently magnetic (soft) ferrospinels formed by heating pressed mixtures of, for example, equimolecular proportions of finely divided $NiO \cdot Fe_2O_3$ and $ZnO \cdot Fe_2O_3$ (or 1NiO plus 1ZnO plus $2Fe_2O_3$) to temperatures above $800°C$ in air or oxygen.[11,12,15,17–19]

It is the latter (soft) magnetic spinels whose preparations and properties are described in this article. The completed materials are rigid sintered ceramic bodies which have resistivities ranging from about 10^2 to 10^7 ohm centimeter. They can be used without subdivision because eddy currents are reduced to very low values. Furthermore, the effective permeabilities μ_e of these ferrospinel bodies generally are ten to a hundred times greater than those of powdered-iron cores.

THEORY OF MAGNETISM

Magnetism is a property of matter which is manifested as attractions or repulsions arising from *motions* of charged particles. For purposes of this paper, it is electrons in motion which produce magnetism. On an atomic scale, magnetism is produced by two kinds of electron motion (Figure 1). These are (1) the variable motion of an electron moving in a so-called "orbital" around the atomic nucleus to which it is bound, and (2) the invariant (presumed) rotation or spin of an electron about an axis passing through it. In iron and other

---

[13] Y. Kato and T. Takei, "Permanent Magnet", U.S. Pats. 1,976,230, 10/9/34 and 1,997,193, 4/9/35.

[14] H. L. Cobb, "Magnetic Material", U.S. Pat. 1,946,964, 2/13/34.

[15] N. Kawai, "Studies of Ferrites: Formation of Solid Solutions Between Some Ferrites", *Jour. Soc. Chem. Ind. (Japan)*, Vol. 37, No. 4, pp. 392-394, and 174B (supplementary issue), 1934.

[16] D. P. Raychaudhuri, "Ferrites—Formation and Magnetic Properties", *Indian Jour. Phys.*, Vol. 9, pp. 383-414, 425-432, 1935.

[17] J. L. Snoek, "Magnetic and Electrical Properties of the Binary Systems $MO \cdot Fe_2O_3$", *Physica*, Vol. 3, No. 6, pp. 463-483, June, 1936.

[18] J. L. Snoek, "Non-metallic Magnetic Material for High Frequencies", *Philips Tech. Rev.*, Vol. 8, No. 12, pp. 353-360, December, 1946.

[19] J. L. Snoek, NEW DEVELOPMENTS IN FERROMAGNETIC MATERIALS, Elsevier, New York, 1947.

[20] A. Kussman and H. Nitka, "Ferromagnetismus und Struktur von Manganferriten", *Physik. Zeits.*, Vol. 39, No. 6, pp. 208-212, March, 1938.

[21] J. W. Mellor, A COMPREHENSIVE TREATISE ON INORGANIC AND THEORETICAL CHEMISTRY, Vol. 13, pp. 905-929, Longmans, Green and Co., London, 1934.

ferromagnetic solids it is chiefly the additive effect of many spinning electrons which produces the observed intense magnetic effects. The "orbital" contribution is generally of minor importance. This is so because the "orbital" magnetic moment approaches zero in the intense distorted electric fields which are produced by atomic interaction in crystals.[22] On the other hand, the electron spin contribution is not affected by the electric fields in crystals (except as these fields are involved in the electron pairing to be discussed subsequently). An electron spin moment in an atom is neutralized, however, when the spin
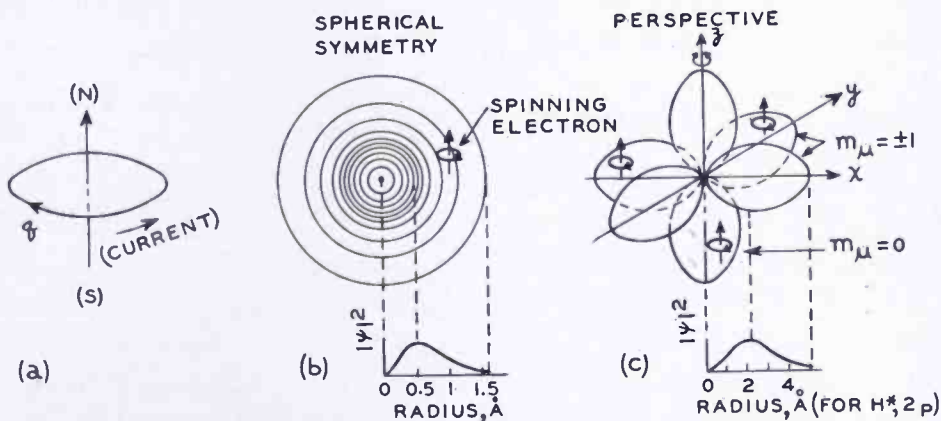
Fig. 1—Magnetism produced by electron motion. Note that the electron "clouds" ("shells") of atoms are *not* sharply bounded, and the pictorial representation of electron spin is hypothetical.[23]

(a) Angular motion of a negative charge q about an axis produces a magnetic field corresponding to that of a magnetic dipole with the indicated polarity. (N) is the north-seeking pole. Arrow shows direction of resultant field (H) impelling an extraneous north pole.

(b) The single electron in a (paramagnetic) free hydrogen atom (1) moves around the central nucleus, and (2) spins around an axis passing through the electron. $|\Psi|^2$ is the relative probability of the electron being at a given point along the radius of the atom.

(c) The three valence electrons of a (paramagnetic) free nitrogen atom move in three configurations with different values of m_μ. The three electrons keep their spins parallel as they move about in dumbbell-shaped regions (the $m_\mu = \pm 1$ "clouds" merge to a doughnut shape).

remains antiparallel (opposite) to that of another spinning electron sharing the same spatial configuration (same "orbital" quantum numbers). Such antiparallel spins are commonly called **paired spins.** Pairing of electron spins is an important factor in the formation of atoms and in the combining of atoms to form molecules and crystals.[22,23]

The process of building atoms will be discussed, noting that a

[22] F. O. Rice and E. Teller, THE STRUCTURE OF MATTER, J. Wiley and Sons, New York, N. Y., 1949, pp. 182-192 (See also p. 550 of the article by C. Kittel, reference 24).

[23] H. W. Leverenz, AN INTRODUCTION TO LUMINESCENCE OF SOLIDS, J. Wiley and Sons, New York, N. Y., 1950, pp. 6-39.

maximum number of unpaired electrons is required in order to have a proportionately large maximum magnetization. Table I shows numerically the electron configurations of some free atoms and ions arranged in order of increasing atomic number, Z. The Z electrons around the nucleus of a normal free atom have discrete energy levels; that is, they have sharply defined strengths of bonding to the nucleus. Although the electrons are moving, some with velocities near 10^7 meters per second, they occupy states of constant energy which are called **stationary states**. These stationary states can be specified completely (neglecting nuclear motion) by four **quantum numbers, n, l, m_μ, and s_μ,** which may be only integers or half integers according to

$$s_\mu = \pm \tfrac{1}{2} \text{ and } |m_\mu| \leqslant l < n = 1, 2, 3, \cdots . \tag{2}$$

The principal quantum number n is correlated with the bulk of the energy of a bound electron in a stationary state. The other three quantum numbers characterize more specifically the electronic configurations; that is, the angular momentum quantum number, l, denotes the possible angular momenta of an electron with a given n, m_μ denotes the projection of these angular momenta on an axis corresponding to an external magnetic field, and s_μ denotes the projection of the independent spin angular momenta along the same axis.

Another qualification for the building of atoms is given by the Pauli **exclusion principle** which postulates that no two electrons in a system, such as an atom, can have identical n, l, m_μ, and s_μ. From Equation (2) and the exclusion principle, it follows that the maximum number of bound electrons with a given l is $2(2l+1)$. In practice, $l = 0, 1, 2, 3, \ldots$ is denoted by the spectroscopic symbols s, p, d, f, ..., and the maximum number of electrons with a given n and l may be arranged in groups ("shells") according to Table II.

Table II—Some Electron Configurations and Their Notation

	n:	1	2		3			4
	nl:	$1s$	$2s$	$2p$	$3s$	$3p$	$3d$	$4s$
$2(2l+1)$		2	2	6	2	6	10	2
Designation when "shell" is full.		$1s^2$	$2s^2$	$2p^6$	$3s^2$	$3p^6$	$3d^{10}$	$4s^2$

The electron configurations corresponding to the lowest (ground) energy states of atoms may be derived by using Equation (2) and the

exclusion principle. This is done by starting with $Z = 1$ and $n = 1$ (lowest energy), and increasing Z while keeping the energy of the system as low as possible. Table 1 shows this atom-building process which has been outlined in more detail elsewhere.[23] In what follows, the spin aspects of the process will be emphasized.

Electrons occur with unpaired spins in most species of free atoms because (1) when Z is odd there must be at least one unpaired spin, and (2) whether Z is even or odd, the interaction of electrons with each other often requires that their spins be unpaired, when possible, to minimize the energy of the atom. Electrons with identical n, and $l \geq 1$, can adopt parallel spins by using different spatial distributions corresponding to the different allowed values of m_μ. These electrons minimize their mutual electrostatic repulsion by staying, on the average, as far apart as possible. In a free nitrogen atom (Figure 1c), for example, each of the three $2p$ electrons has a different value of m_μ. When each of the three m_μ configurations is occupied by an electron, then additional electrons pair with those already present. On proceeding from nitrogen to neon, it is found that the latter atom finally has all its electrons paired in the highly stable configuration $1s^2$, $2s^2 2p^6$.

The lower part of Table I shows the building of a series of **transition-group elements** containing electrons, with $l = 2$, in *inner incompleted "shells"*. As shown, the inner $3d$ shell acquires electrons *after* the $4s$ shell has been completed, and there are some irregularities in the electron distributions of the $3d$ and $4s$ shells. The irregularities are attributed to the interactions of electrons with each other. These interactions comprise (1) classical electrostatic (repulsion) energies, and (2) difficultly comprehensible quantum-mechanical **exchange energies**. Exchange energies, which have no classical analogue, arise in a system, (atom, molecule, or crystal) which has two or more possible electronic configurations of nearly equal energy. Such a system can form a *hybrid* configuration wherein it has lower energy than it would have if it were "frozen" in only one of the possible configurations. The resultant change in energy is a measure of the exchange or resonance energy.

At the right of Table I are shown the electron configurations of some common **cations** (positive ions) and **anions** (negative ions). All the ions listed in the upper series have no net spins because the unpaired electrons of the corresponding atoms are in the outermost (bonding, or valence) shell where the electrons are readily removed or paired. In the lower transition-group series, however, one of the cations (Fe^{3+}) has five unpaired electrons in its incompleted $3d$ shell. Atoms *and* ions of certain transition-group elements are, therefore,

especially suitable for making magnetic materials. Although there are other suitable transition-group elements, notably gadolinium with seven unpaired $4f$ electrons and one unpaired $5d$ electron per isolated atom, this discussion will chiefly concern the elements listed in Table I.

To make materials with maximum **saturation magnetization,** it is desirable to have (1) atoms with highest numbers of unpaired electrons N_u (Table I), (2) a maximum number N_m of these atoms per unit volume, preferably without decreasing N_u, and (3) parallel alignment of all the N_uN_m unpaired spins per unit volume. *If* these conditions were met in magnetic (α) iron,* with $N_u = 4$ and $N_m = 7.86 \times 6.02 \times 10^{23}/55.85 = 8.5 \times 10^{22}$ atoms per cubic centimeter, then the saturation magnetization, that is, the total magnetic spin moment per cubic centimeter, would be

$$I_s = N_uN_m\mu_e = 4 \times 8.5 \times 10^{22}\,\mathrm{cm}^{-3} \times 9.3 \times 10^{-21}\,\mathrm{erg\ oersted}^{-1}$$

$$= 3160\ \mathrm{erg\ oersted}^{-1}\,\mathrm{cm}^{-3},$$

where μ_e is the elementary Bohr magneton.[2] From experiments, it is found that I_s for α-iron is 1707 at room temperature (300° Kelvin) and extrapolates to 1752 at 0° Kelvin.[24] In iron, the value of $N_u = 4$ for free atoms is decreased to an effective nonintegral value $n_{eff} = (1752/3160)\,4 = 2.22$ by the combining and packing together of atoms with a center-to-center spacing of 2.47Å. This decrease is caused by electronic interaction of the iron atoms which results in increased pairing of an average of about $4 - 2.22 = 1.78$ electron spins per atom. It is seen, then, that the distance between atoms, which distance influences the degree of their interaction and electron pairing (sharing), should be made a compromise optimum rather than a minimum. Optimum interatomic spacing is essential for ferromagnetism, not only with one species of atom, as in elemental iron, but also with different species of atoms, such as iron and oxygen in magnetite. Interatomic spacings in solids are determined by the natural sizes of atomic electron "clouds", as modified by interaction with neighboring atoms. This spacing, at a given temperature, is a characteristic of the composition and crystal structure of the solid. In solid chromium and manganese, the internuclear separations are so small that the high value of N_u (Table I) for the free atoms are largely nullified by pairing.

---

* α-iron is the body-centered-cubic form which is stable below 910°C.

[24] C. Kittel, "Physical Theory of Ferromagnetic Domains", *Revs. Mod. Phys.*, Vol. 21, No. 4, pp. 541-583, October, 1949; see also the papers by J. H. Van Vleck, *et al.*, in *Physica*, Vol. 15, Nos. 1, 2, pp. 1-12, 197-271, April, 1949, and H. J. Williams, "Ferromagnetic Domains", *Elec. Eng.*, Vol. 69, No. 9, pp. 817-822, September, 1950.

Figure 2 shows, as a general function of kinetic energy and atomic spacing, the magnetic properties of matter composed of atoms which in the free state have unpaired electrons. Using iron as an example, each iron atom in the gas (Figure 2a) has four unpaired (parallel) spins and the gas is predominantly paramagnetic; that is, it moves in

(a) Paramagnetic gas. Randomly oriented spins.

(b) Paramagnetic liquid or solid. Randomly oriented spins at $T > T_0$.

(c) Ferromagnetic solid. Parallel spins in single domain at $T = 0°$ Kelvin.

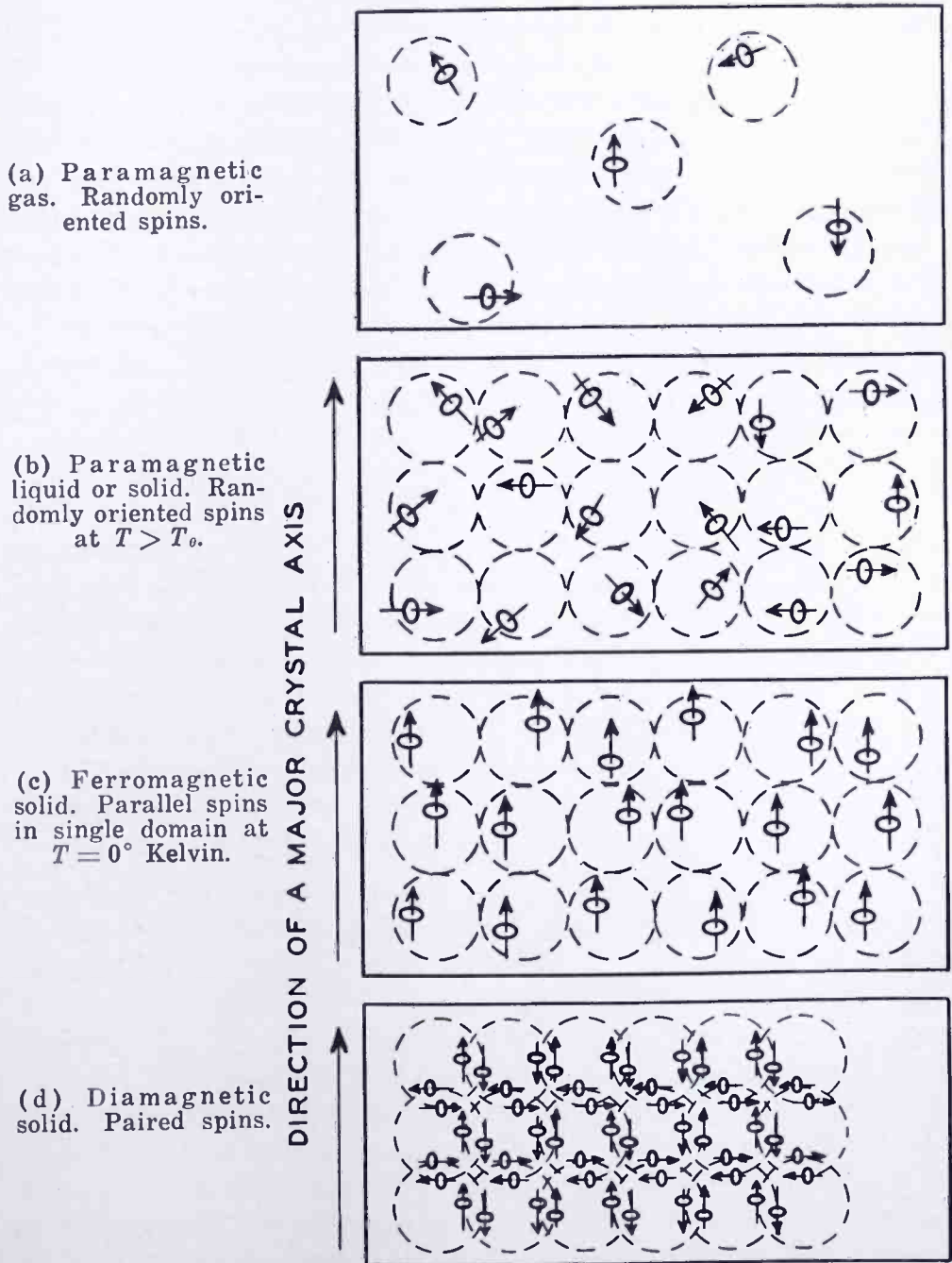(d) Diamagnetic solid. Paired spins.

DIRECTION OF A MAJOR CRYSTAL AXIS

Fig. 2—Schematic of some electron spin orientations in atoms of several different kinds of magnetic materials. The shapes of real atoms in solids, that is, their external electron "clouds", are generally nonspherical.[23]

the direction of increasing density of a non-uniform applied magnetic field. In the absence of an applied field, the spins of the separate atoms are randomly and transitorily oriented, and therefore the gas has no net magnetic moment. On decreasing the temperature (kinetic energy) of the gas it condenses to form first a liquid and then a solid. In the condensed state there is transfer and exchange of electrons among the atoms to an extent which depends on their natures, groupings, and proximities. All the 4s electrons and an average of 1.78 of the 3d electrons in a crystal of α-iron are exchanging places (pairing spins) with electrons on neighboring atoms. This bodily exchanging of electrons gives rise to a bonding energy which holds the atoms together. The remaining average of 2.22 unpaired inner 3d electrons, which are not exchanging, seek to move in configurations which minimize their electrostatic interaction from atom to atom. This ideally requires the electrons to maintain parallel spins aligned throughout the crystal, and the energy associated with such overall spin alignment is called an *exchange energy*. The exchange energy per atom for α-iron is approximately

$$E_e \approx kT_\theta = 1.44 \times 10^{-13} \text{ erg} \qquad (4)$$

where $k = 1.38 \times 10^{-16}$ erg degree^{-1}, and T_θ is the Curie temperature, which for iron is 1043° Kelvin. At temperatures above 1043° Kelvin, solid α-iron is paramagnetic (Figure 2b) because the exchange energy is too small to produce a net spin orientation when the energy of random thermal agitation of the atoms exceeds kT_θ. Below T_θ, however, the spins align to an increasing extent until at 0° Kelvin they are almost perfectly aligned (Figure 2c) within extended regions called **domains**.

It was previously mentioned that in ferromagnetic α-iron, which has an internuclear spacing of 2.47 Å, an average of 1.78 of the original four 3d spins per atom are cancelled (paired) by electron exchange. If the internuclear spacing were greatly increased, the system would become paramagnetic because the interatomic spin-aligning exchange energy decreases with increasing spacing. On the other hand, decreasing internuclear spacing increases spin pairing, and can eventually produce complete pairing which makes the solid diamagnetic (Figure 2d). A diamagnetic material moves in the direction of decreasing intensity of an applied magnetic field. (All atoms are diamagnetic to some degree, although the slight diamagnetism component may be overwhelmed by strong paramagnetism arising from unpaired spins. The diamagnetic effect is caused by precession of "orbital" electronic

motion in a direction such that the resultant magnetic field opposes the applied field).

Ferromagnetism requires not only an optimum spacing between atoms with unpaired electrons, but also a crystalline arrangement of the atoms, preferably with highest (cubic) symmetry. A crystalline array is essentially anisotropic and has major axes which provide preferred directions for orientation of unpaired spins. The spin orientation apparently occurs through intermediate spin-"orbital" coupling with the nearly nullified "orbital" component which orients according to the symmetry of the crystal.[24]

Given only the foregoing information regarding spin alignment and orientation, one might expect single crystals of ferromagnetic materials to be single magnetic domains with all the unpaired spins oriented parallel to one major crystal axis. Such single-domain crystals do occur when their size is sufficiently small; for example, α-iron crystals smaller than 10^{-6} centimeter. Larger crystals, however, do not spontaneously form single domains. Instead, they generally have complex multidomain structures which depend strongly on the composition, structure, size, and shape of the crystal. Multidomain structure forms spontaneously whenever the crystal thereby achieves a state of lower energy than it would have as a single domain. Figure 3 shows some possible domain structures for a hypothetical simple crystal. In a given ferromagnetic crystal, the domain structure attempts to equilibrate the size and shape factors of the overall crystal and the following internal energies:

(1) *exchange energy* (produces parallel spins),
(2) *anisotropy energy* (attempts to orient spins along one crystal axis),
(3) *magnetostatic energy* (energy of net oriented spins producing magnetic poles),
(4) *magnetoelastic energy* (energy of magnetostatically produced mechanical strain in the crystal; for example, strain caused by attraction of opposite magnetic poles at the ends of the crystal),
(5) *wall energy* (energy in distorted spin-reorientation regions between domains).[24]

Suitable arrays of small domains can reduce the magnetoelastic energy by providing high-permeability flux-closure paths to reduce the magnetostatic energy, but small domains increase the wall energy per unit volume. Detailed analyses of the listed component factors and a review of domain theory in general are presented in a recent article by Kittel.[24] Here it should be emphasized that real ferromagnetic crystals, with

irregular shapes and sizes, generally have complicated domain structures. These internal structures are sometimes deducible from the visible "powder patterns" produced by their external fields acting on a coating of colloidal magnetite in liquid suspension.[25] The colloidal magnetite particles concentrate near domain boundaries and indicate the terminal outlines of domains.
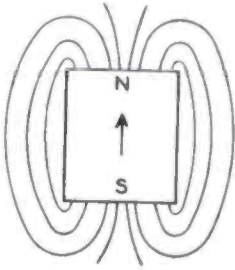
(a) Single domain (see Figure 2c).
   No walls.
   Two poles.
   Strong magnetization.

(b) Four domains, parallel.
   Three walls.
   Eight poles.
   Weak magnetization.
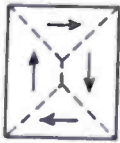
(c) Four domains, abutted.
   Five walls.
   No poles.
   No magnetization.
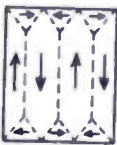
(d) Ten domains, abutted.
   Fifteen walls.
   No poles.
   No magnetization.

Fig. 3—Possible domain structures for a single crystal in the absence of an external field. Dotted lines indicate Bloch walls which are narrow regions wherein spin orientations change gradually between domains.[24] Note that in the lower drawings the domains act as flux closures ("keepers") for each other.

The process of magnetizing a crystal with multidomain structure is sketched in Figure 4. As the intensity of the applied magnetic field is increased, domains which have a component of magnetization in the direction of the applied field grow at the expense of domains which oppose the applied field. Here, thermal agitation facilitates wall

---

[25] C. Kittel, "Theory of the Formation of Powder Patterns on Ferromagnetic Crystals", *Phys. Rev.*, Vol. 76, No. 10, p. 1527, November 15, 1949.

displacements, as contrasted with the disorienting effect of thermal agitation within domains.[3] In weak applied fields there are small inter-domain wall displacements which are spontaneously reversible; that is, the initial equilibrium domain structure is resumed when the weak field is removed. As the field strength is increased, there are larger wall displacements which are difficultly reversible. Wall movements, particularly those which are difficultly reversible, proceed *stepwise* and so the process of magnetization is discontinuous (Barkhausen effect). The stepwise motion is attributed to scattered impurity atoms and other localized structural imperfections which increase the activation energy required to move the wall through a (perturbed) site in the
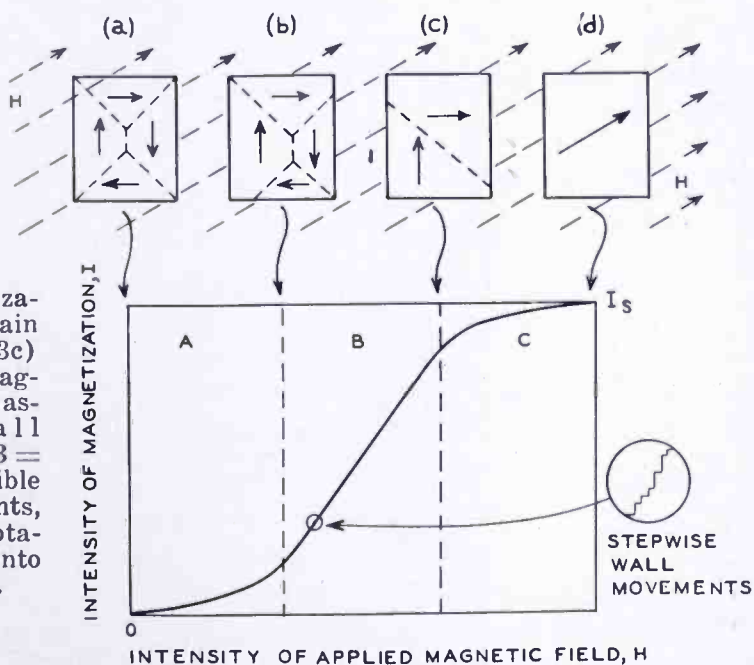
Fig. 4 — Magnetization of a four-domain crystal (Figure 3c) by an applied magnetic field. A = Easily reversible wall displacements, B = difficultly reversible wall displacements, C = reversible rotation of spin axes into direction of H.

solid. When all the domains opposed to the applied field have been transformed into domains having a major component in the field direction (Figure 4c), then further increase in the applied field rotates the spin orientations away from the preferred crystallographic directions into the direction of the external field.

The I versus H curve of Figure 4 resembles the upper part of common B versus H curves (Figure 5) because the resultant **magnetic induction** B is related to the magnetization I by

$$B = H + 4\pi I \text{ gausses,} \qquad (5)$$

where H (applied) is expressed in oersteds, and B (produced in the solid by H) is expressed in gausses. The maximum value of I was

shown in connection with Equation (3) to be set by the number of effective unpaired spins per unit volume ($n_{eff.}$ cm^{-3}).

Of practical importance is the **susceptibility** (ease of magnetization) per unit volume. The susceptibility χ is the ratio of I to H; that is,

$$\chi = I/H \text{ electromagnetic units,} \qquad (6)$$

and the correlated magnetic **permeability** is

$$\mu = 1 + 4\pi\chi \qquad (7)$$

$$= B/H. \qquad (8)$$

Materials with negative χ are diamagnetic, and those with positive
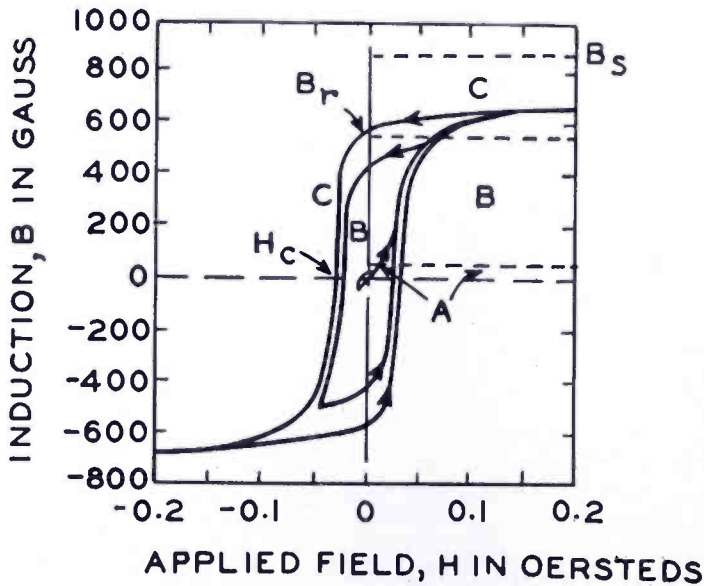
Fig. 5 — Typical B versus H curves for a high permeability alloy (Bozorth[1]) showing increasing hysteresis loops (losses) obtained with increasing intensities of the applied field. A = region of reversible wall displacements, B = irreversible wall displacements, C = reversible rotation of spin axes (see Figure 4). B_r = remanence or residual induction, H_o = coercive force required to reduce B_r to zero. B_s = saturation value of B.

χ are paramagnetic or ferromagnetic according to the magnitude of χ. The susceptibility of α-iron can exceed 500 electromagnetic units.[1] A large value of χ (and μ) with moderate H indicates that (1) the solid has domains, (2) the domain walls are easily moved, and (usually to a lesser extent), (3) the spin orientations are easily rotated. Permanent magnets should have wall movements which are as difficultly reversible as possible, whereas magnetic materials for use in high-frequency alternating fields should have wall movements which are as easily reversible as possible. Permanent magnets have high **remanence** (residual induction) and high hysteresis, whereas the ferrospinels described in this article have low remanence and low hysteresis.

Structural imperfections in solids can impede wall movements and thereby decrease χ (and μ) and decrease the reversibility of wall displacements. For example, Yensen has determined the influence of varying the carbon content of α-iron and reported that (1) a hypothetical single crystal of α-iron containing only 0.001 per cent of carbon should have a permeability of about 500,000, whereas an actual crystal containing 0.011 per cent carbon has a permeability of 20,000, and (2) 0.01 per cent of carbon in a single crystal of α-iron operated with a B_{max}. of 10,000 gauss at 50 cycles per second produces a hysteresis loss of 0.37 watt per kilogram as against zero hysteresis loss for a hypothetical perfectly pure ideal single crystal.[26] Similarly, local and long-range anisotropy produced by other crystal imperfections, strain from mechanical working, and departures from cubic symmetry decrease μ and increase hysteresis losses. In contrast with these impurity- and structure-sensitive properties, the saturation magnetization, I_s, and Curie temperature, T_θ, are relatively insensitive to small crystal imperfections and anisotropy.

When the magnetization of a ferromagnetic solid is changed by an applied field, there is often an appreciable change in length of the solid in the direction of the field. This phenomenon is called **magnetostriction** even though the change Δx in length x may be positive or negative with increasing H. The saturation value of $\Delta x/x$ is -4×10^{-5} for solid nickel, and $+1.6 \times 10^{-5}$ for the alloy [Ni(68%), Fe(32%)].[1] Positive magnetostriction (expansion) is generally obtained when the normal internuclear spacing between atoms with unpaired spins is less than the optimum spacing for maximum magnetization, whereas negative magnetostriction (contraction) is obtained when the normal internuclear spacing exceeds the optimum. In both cases, the applied field facilitates closer approach to the optimum internuclear spacing. Reciprocally, it is possible to alter the magnetization of a solid by compression or tension. Compression, for example, increases magnetization when the normal internuclear spacing exceeds the optimum, and decreases magnetization when the normal spacing is less than optimum. All these effects diminish in magnitude as the temperature of the solid is raised; that is, as an increasing proportion of the unpaired spins are randomly oriented. For high permeability and low hysteresis loss, it is essential to have low magnetostriction, because magnetostriction is an indicator of nonoptimum conditions.

The optimum spacing and arrangement of iron atoms are changed on going from solid elemental iron to the ferrospinels wherein iron is

---

[26] G. C. Richer, et alia, "Magnetism", *Physics in Industry*, Institute of Physics, London, 1938.

combined with oxygen and other elements. *Ferromagnetic* α-iron has each iron atom 2.47 Å (center-to-center) away from 8 nearest iron atoms located at the corners of a hexahedron, and 2.86 Å away from 6 next-nearest iron atoms located at the corners of an octahedron. *Non-ferromagnetic* normal-cubic $ZnO \cdot Fe_2O_3$ has its iron atoms (ions to some degree) all in octahedral sites relative to the face-centered-cubic array of oxygen atoms (see Figure 8). Each iron atom has, as near neighbors, 6 oxygen atoms 2.1 Å away and 6 other iron atoms 3 Å away. In *ferromagnetic* inverse-cubic $NiO \cdot ZnO \cdot 2Fe_2O_3$ the iron atoms occupy both octahedral and tetrahedral sites relative to the oxygens (see Figure 9). Iron atoms in octahedral sites have, as near neighbors, 6 oxygen atoms 2.1 Å away and an average of only 2 other iron atoms 3 Å away, whereas iron atoms in tetrahedral sites have, as near neighbors, 4 oxygen atoms 1.8 Å away, an average of 4 other iron atoms (in octahedral sites) 3.5 Å away, and an average of 4 other iron atoms (in tetrahedral sites) about 3.7 Å away.* The distributions, spacings, and degrees of ionization of iron and other atoms (ions) in a ferrospinel are adjustable by varying the ingredients and the atmosphere during crystallization and cooling of the solid.

The changeable amount of sharing and transfer of electrons between atoms in ferrospinels leads one to denote the oxidation numbers (effective ionic charges or formal valencies) of, for example, iron and oxygen as $Fe^{<3+}$ and $O^{<2-}$, because these atoms (ions) may have non-integral charges in solids.[23] As the degrees of ionization and covalent bonding (by electron sharing) of atoms in solids are changed, the sizes of the atoms alter, as shown at the right of Table I. At the same time there is a change in electric conductivity of the solid. Ferrospinels are semiconductors whose low direct-current bulk conductivity is occasioned by (1) stronger bonding of valence electrons to atomic nuclei than is found in metals, (2) possible high resistances of distorted intercrystal boundaries in these granular sintered bodies, and (3) impurities and other imperfections which can trap electrons and thus build up space charge in the solid.

COMPOSITIONS AND STRUCTURES OF FERROSPINELS

The chief requirements for strong magnetism in solid iron com-

---

* L. Néel has hypothesized that iron atoms in adjacent tetrahedral and octahedral sites balance each other magnetically by assuming opposite electron spin orientations. The unbalanced electron spins of the nickel atoms in octahedral sites, then, are presumed to produce the observed ferromagnetism (see L. Néel, et al., "Propriétes magnétiques des ferrites," *Ann. de phys.*, Vol. 3, pp. 137-195, 1948; *Compt. rend.*, Vol. 230, No. 2, pp. 190-194, Jan. 9, 1950; *Compt. rend.*, Vol. 230, No. 3, pp. 280-282, Jan. 16, 1950; *Compt. rend.*, Vol. 230, No. 4, pp. 375-377, Jan. 23, 1950).

pounds are: (1) The iron atoms should be combined with other atoms which have sufficient electron affinity to ionize the iron, while leaving a maximum number of the electrons of iron unpaired, as it has been shown (Table I) that free iron ions, particularly Fe^{3+}, have a relatively large number of unpaired spins. (2) The iron atoms* should be spaced near enough to each other to obtain sufficient interaction for spin alignment. (3) The iron atoms should be arranged in a cubic array.

For low loss operation at radio frequencies, it is essential to have the crystals as isotropic as possible; hence, only stable iron compounds which crystallize in the cubic system are considered. Of these, the most useful thus far have been certain oxygen-dominated[23] iron-containing solids which crystallize with spinel structures. The original spinel was a mineral specimen of magnesium aluminate, $MgAl_2O_4$. Compounds which have the same structure as $MgAl_2O_4$ are classified as spinel structures. One class of such compounds can be generalized by the formula XFe_2O_4, where X is a metallic cation nominally assigned the valence of 2+, Fe has a nominal valence of 3+, and the oxygen anion is 2—, i.e., $X^{2+}Fe^{3+}{}_2O^{2-}{}_4$. For simplicity of discussion the term valence will be used without implying that the cation or anion have integral ionic charges, but rather as signifying the capacity of the element to combine with one or more atoms of another element. The hydrogen atom taken as unity is the standard of comparison, e.g., in water, H_2O, the valence of oxygen by this definition would be 2—; for Fe_2O_3 the iron would be 3+, as oxygen is 2—. Compounds of the type XFe_2O_4 are ferromagnetic when X^{2+} is Co^{2+} (ionic radius of 0.72 Å), Fe^{2+} (0.75 Å), Mg^{2+} (0.65 Å), Mn^{2+} (0.80 Å), Ni^{2+} (0.69 Å), and Cu^{2+} (0.9 Å). If the cations are larger, e.g., Sr^{2+} (1.35 Å) or Pb^{2+} (1.18 Å) the structures are hexagonal and the materials are weakly ferromagnetic. There are two known exceptions where the X cations are of proper size to give a cubic ferrospinel, but the compounds are not ferromagnetic; these are Zn^{2+} (0.83 Å) and Cd^{2+} (0.97 Å). The ferromagnetic spinel-structure compounds are not necessarily restricted to the formula type XFe_2O_4, as there are materials,[27-29] e.g., $LiFe_5O_8$, cubic-Fe_2O_3, and $Mn_3O_4 \cdot 3Fe_2O_3$, which are cubic spinels and are ferromagnetic. In order to more clearly understand how such dif-

---

* The word atom is here used to include both atoms and ions.[23]

[27] Alex Hoffman, "Crystal Chemistry of Lithium Ferrites", *Naturwissenschaften*, Vol. 26, pp. 431 (1938).

[28] E. J. W. Verwey, "The Crystal Structure of γ-Fe_2O_3 and γ-Al_2O_3, *Zeitschrift für Kristallographie*, Vol. 91A, pp. 65-69, 1935.

[29] E. J. W. Verwey and M. G. van Bruggen, "Structure of Solid Solution of Fe_2O_3 in Mn_3O_4", *Zeitschrift für Kristallographie*, Vol. 92, pp. 136-138, 1935.

ferent materials are similar in structure the crystallography of ferro-spinels will be discussed.

The metallic cations and oxygen anions of oxides are held together partly by ionic and partly by covalent forces. In cases where either the cations or anions are appreciably larger than the other, the larger arrange themselves in closest packing. When equivalent spheres are packed so that the interstitial spaces are minimized, the spheres arrange either in cubic or hexagonal symmetry. For the ferrospinels the ionic radius of the oxygen anions (1.40 Å) is approximately twice as large as the radius of the cations (about 0.7 Å), and the anions are close-packed in a face-centered cubic array with the cations being distributed in the interstices between the oxygens. A crystal is made up of a periodic distribution of cations and anions, and one can imagine a unit cell, which when repeated in space will reproduce the crystal. For ferrospinels of the type XFe_2O_4 there are $8(XFe_2O_4)$ in a unit cell, i.e., 8 X^{2+} cations, 16 Fe^{3+} cations, and 32 O^{2-} anions. Figures 6a, 6b, and 6c, show the close packing of 32 oxygen anions in a cubic unit cell.

The geometrical arrangement of the close-packed oxygens produces two types of interstices between the anions: one surrounded by 4 oxygen anions called a tetrahedral interstice, and one surrounded by 6 oxygen anions called an octahedral interstice (the oxygens are at the 6 apexes of the octahedron). Figure 7a illustrates the geometric arrangement of a cation surrounded by 4 oxygen neighbors, and Figure 7b the arrangement of six oxygen neighbors around a cation. There are in a spinel unit cell a total of 96 interstices between the oxygens, 64 being tetrahedral and 32 being octahedral. The cations have been found to be distributed two ways in these sites:[30,31] one a distribution having all 8 of the X^{2+} cations in tetrahedral sites with 16 of the Fe^{3+} cations in octahedral sites, the other distribution having 8 of the Fe^{3+} cations in tetrahedral sites, and the other 8 of the Fe^{3+} cations together with 8 of the X^{2+} cations being in octahedral sites. The first distribution (or structure) is called a normal spinel, e.g., $ZnFe_2O_4$, where the Zn^{2+} cations are in tetrahedral sites, and all the Fe^{3+} cations are in octahedral sites. The other distribution is called an inverse spinel, e.g., $NiFe_2O_4$, where one-half of the Fe^{3+} cations are in tetrahedral sites, and the other half together with the remaining cations are all in octahedral sites. Figures 8a and 8b show the cation

[30] F. W. Barth and E. Posnjak, "Spinel structures: with and without variate atom equipoints", *Zeitschrift für Kristallographie*, Vol. 82, pp. 324-341, 1932.

[31] E. J. W. Verwey and E. L. Heilman, "Cation Arrangement in Spinels", *Jour. Chem. Phys.*, Vol. 15, pp. 174-180, 1947.

distribution for a normal spinel, and Figures 9a and 9b the distribution for an inverse spinel. Some of the useful normal and inverse ferrospinels are listed in Table III.

A ferrospinel of the type XFe_2O_4 can, therefore, be described as a close-packed array of 32 oxygen anions in a face-centered-cubic unit
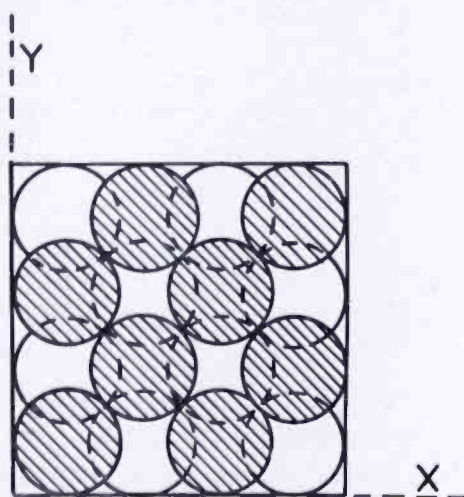
Fig. 6a—Plan view of close-packed oxygens in a spinel unit cell. First layer of 8 oxygens represented by open circles. Second layer of 8 oxygens represented by hatched circles. Third layer of 8 oxygens directly above the first layer. Fourth layer of 8 oxygens directly above the second layer. A total of 32 oxygens in a cubic unit cell.
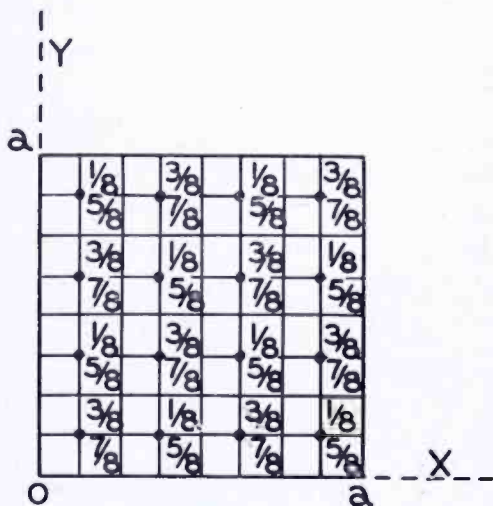
Fig. 6b—Plan view of positions of 32 close-packed oxygens in a spinel unit cell. Points represent oxygen centers. The X, Y distances are drawn to scale, and the Z distances are given as fractions of a unit cell dimension, a, set equal to one.
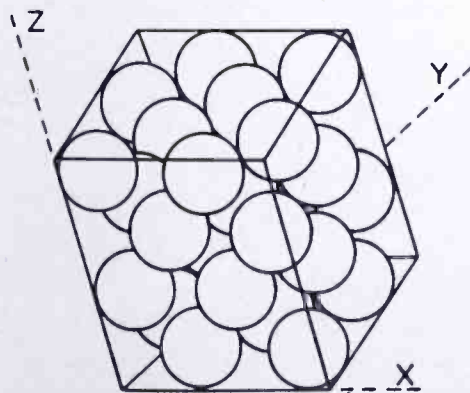
Fig. 6c—Perspective view of the arrangement of 32 close packed oxygens in a spinel unit cell.

cell with 8 cations of X^{2+} and 16 cations of Fe^{3+} distributed in the oxygen interstices. As the material is electrically neutral, there are in a unit cell $X^{2+}_8Fe^{3+}_{16}O^{2-}_{32}$, that is, ideally a balance of 64+ valencies
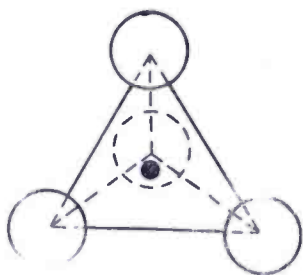
Fig. 7a — *Tetrahedral Interstice.* Cation (small dark sphere) surrounded by 4 oxygens (large open spheres).
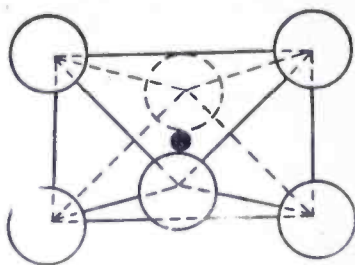
Fig. 7b — *Octahedral Interstice.* Cation (small dark sphere) surrounded by 6 oxygens (large open spheres).
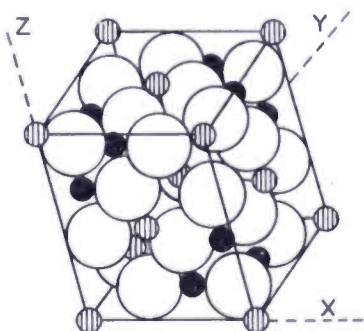
Fig. 8a—*Normal Spinel.* Perspective view of X^{2+} cations (hatched spheres), Fe^{3+} cations (black spheres), and O^{2-} anions (large open spheres), in a cubic unit cell.[31]
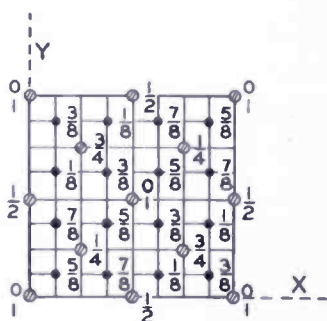
Fig. 8b—*Normal Spinel.* Plan view of position of X^{2+} cations (hatched circles), and Fe^{3+} cations (dark circles) in a cubic unit cell. The X, Y, distances are drawn to scale, and the Z distances are given as fractions of a unit cell dimension.
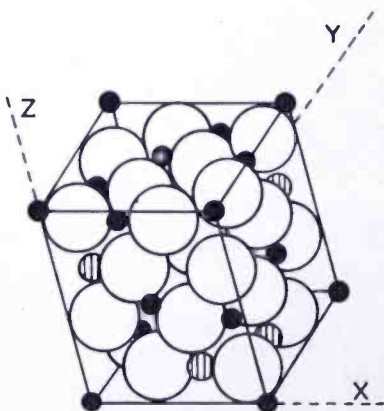
Fig. 9a—*Inverse Spinel.* Perspective view of X^{2+} cations (hatched spheres), Fe^{3+} cations (black spheres), and O^{2-} anions (large open spheres) in a cubic unit cell.
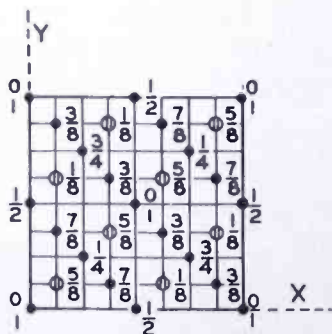
Fig. 9b—*Inverse Spinel.* Plan view of positions of X^{2+} cations (hatched circles), and Fe^{3+} cations (dark circles) in a cubic unit cell. The X, Y, distances are drawn to scale, and the Z distances are given as fractions of a unit cell dimension.

for the cations, i.e., $(8 \times 2+) + (16 \times 3+) = 64+$, against $64-$ valencies for the anions, i.e., $(32 \times 2-) = 64-$. The number of cations need not be limited to 24 or be limited to the $2+$ and $3+$ type, but the total cation valencies must equal the total anion valencies. Therefore, other cations of different valencies but of similar size may be distributed in the oxygen interstices, as long as the total cation valencies are kept constant. This occurs for the compound $LiFe_5O_8$ where there are $Li_4Fe_{20}O_{32}$ in a unit cell, giving ideally a total of $(4 \times 1+) + (20 \times 3+) = 64+$ valencies for the cations. In the compound cubic-Fe_2O_3, 32 oxygen anions are close-packed in a cubic unit cell, with an average of $21\frac{1}{3}$ of Fe cations in the oxygen interstices. In reality there are 20 cations in each of 3 cells with one cation being statistically distributed on the average among 3 cells throughout the crystal. In manganese ferrospinel, the compound is more nearly $Mn_3O_4 \cdot 3Fe_2O_3$ $(= Mn^{2+}O \cdot Mn_2^{3+}O_3 \cdot 3Fe_2^{3+}O_3)$ rather than $Mn^{2+}Fe_2^{3+}O_4$. That is, there are variable proportions of different cationic valencies of manganese present. This structure is explained in similar manner to the cubic-Fe_2O_3 compound, that is, 32 oxygen anions are close-packed in a cubic unit cell with a sufficient number of different Mn cations distributed throughout the interstices to balance the $64-$ valencies of the oxygen anions.

Experiments[8-21] have shown that improved magnetic and electric properties are obtained from materials which are solid solutions* of two or more ferrospinels of the types discussed. These solid solutions are not restricted to cationic distributions of normal or inverse structures. In fact, the most useful materials are solid solutions of normal and inverse cationic distributions. For example, solid solutions of nickel and zinc ferrospinels most likely have Zn and Fe cations in tetrahedral sites and Ni and Fe cations in octahedral sites. The exact locations and ionic charges of the cations are not determinable by present techniques, as the intensity of x-ray scattering by the different cations are of similar magnitude, and consequently no clear-cut interpretation is possible from the x-ray patterns. In Table III are listed some spinels from which useful ferrospinels are prepared by making solid solutions of two or more of the listed compounds.

Small proportions of materials such as hexagonal-Fe_2O_3 and $BeFe_2O_4$, both of hexagonal structure, can be put in solid solution with mixtures of the above cubic ferrospinels, and improved properties obtained. The hexagonal-Fe_2O_3 can be thought of as going into solid

---

* Two or more constituents are said to be in solid solution when a homogeneous one-phase solid results from their combination. If the combination produces more than one phase then the resultant solid is a mixture of phases and is called heterogeneous.

solution as cubic-Fe_2O_3, while some Be can be distributed throughout the interstices without forming a new phase.

Table III—Characteristics of some spinels from which useful ferrospinels are prepared.

	a ($\AA$)	Approximate μ_o	Curie-Temp. ($^\circ C$)
Normal Ferrospinels			
$CdFe_2O_4$	8.69	1.00	—
$ZnFe_2O_4$	8.42	1.00	—
Inverse Ferrospinels			
$CuFe_2O_4$	8.37	90	410
$CoFe_2O_4$*	8.36	1.1	520
$FeFe_2O_4$	8.39	70	590
Cubic-Fe_2O_3	8.32	—	620†
$LiFe_5O_8$	8.31	30	590
$MgFe_2O_4$	8.36	60	325
$Mn_3O_4 \cdot 3Fe_2O_3$	8.55	250	290
$NiFe_2O_4$	8.36	30	580

* Magnetically hard.   † Extrapolated value.
a = Average value of cube edge, found in the literature, for a unit cell of 32 close-packed oxygens.

In general, solid solutions of two or more of the above materials give varied and improved electric and magnetic properties, e.g., permeability, remanence, saturation, resistivity, magnetostriction, and Q.

SYNTHESIS OF FERROSPINELS

Ferrospinels are generally synthesized by mixing their constituent oxides in predetermined proportions, pressing the mixture into rigid shapes, and heating the pressed material (without melting) for several hours in a furnace. The finely divided and intimately mixed solid components react and diffuse on an atomic and molecular scale to form a new crystal structure. This is called an additive solid state reaction.[23] The procedures in the synthesis are similar for the ferrospinels listed in Table III and for their solid solutions. The nickel-zinc ferrospinels have been found to be practical for many applications and the remainder of this paper will deal almost exclusively with these materials. The synthesis is here exemplified by outlining the preparation of a typical material, such as an equimolar solid solution of nickel ferrospinel and zinc ferrospinel in a form suitable for measurement pur-

poses. This material can be prepared from chemically pure oxides as follows:

(1) *Mixing*—The pure fine-particle oxides are rough-mixed in the proportion of 25 mole per cent of zinc oxide, ZnO (20.35 grams), 25 mole per cent of nickelous oxide, NiO (18.67 grams), and 50 mole per cent of ferric oxide, Fe_2O_3 (79.84 grams). Intimate mixing is accomplished by wet ball milling, that is, tumbling a water slurry of the oxides with porcelain balls in a closed porcelain jar for about four hours. The mixed slurry is dried at about 200°C, and the dry cake is ground and sieved to a fine powder.

(2) *Sintering*—The powder is placed in a clay crucible, and heated in an electric furnace at 1050°C for one hour in air.

(3) *Comminuting*—The sintered mixed-oxide material is ground to a fine powder, by wet ball milling in a steel ball mill, or by dry hammer milling in a rotary hammer mill.

(4) *Adding Organic Binder and Lubricant**—To 120 grams of the dry sintered ground powder are added 1 per cent "Carbowax" (1.2 grams), and 4 per cent "Trigamine Stearate" (4.8 grams), emulsified in 30 milliliters of hot water. These are mixed together using additional water if necessary to obtain a uniform distribution of the added organics. The water is evaporated by heating at about 75°C, and the residue is sieved to a fine powder.

(5) *Molding*—The prepared powder is molded in a polished steel mold to a toroid shape of 0.25 centimeter cross section with 3.0 centimeters outside diameter and 2.5 centimeters inside diameter. A weight of about 2.2 grams of the powder pressed at about 20,000 pounds per square inch will give a square cross section.

(6) *Final Thermal Reaction and Crystallization*—The molded sample is placed on a sillimanite setter plate and heated in an electric furnace. The organic binder and lubricant are volatilized by heating the formed body from room temperature to 300°C in air and holding at that temperature for two hours. Completion of reaction and crystallization is accomplished by increasing the temperature in about five hours to 1400°C and holding at this temperature for one hour. This entire procedure is carried out in an air atmosphere.

(7) *Cooling*—The power is shut off and the material is allowed to cool to room temperature in the furnace. This takes about 16 hours.

The synthesis of ferrospinels with other compositions is similar to the foregoing procedure, but procedural variations are required to obtain optimum characteristics. Some possible variations, and their

---

* The cited materials were suggested by L. R. Shardlow, Ceramist, RCA Victor Division, Harrison, N. J.

effects upon the characteristics of the formed material, are discussed below.

(1)   Mixing may be done alternatively by coprecipitating from solution the required proportion of oxides, or ingredients which upon heating decompose into oxides. Mixtures obtained by this procedure are more intimately mixed, and so they react and crystallize at lower temperatures. The previously described process of mixing the solid ingredients, however, is generally more practical.

(2) and (3)   The sintering and grinding operations help control the shrinkage and porosity of the product. It is essential to control shrinkage in order to obtain products of uniform size and shape. The porosity of the material may be varied by sintering at different temperatures and grinding to different particle sizes, or by adding inorganic "fluxes" such as silicon dioxide, SiO_2. The control of porosity is required in order that the material will be in proper form for heat treatment. The importance of this control of porosity will be more fully discussed later.

(4)   Binders are added to make the powder particles cohere after they are pressed into different shapes. Lubricants may also be added to facilitate molding. The binders and lubricants added are usually organic compounds, which can be volatilized by heating the formed bodies at low temperatures.

(5)   The pressures used for molding these materials are less critical than for the molding of powdered iron cores with organic binders. Pressures of about 10,000 to 20,000 pounds per square inch have been found to be satisfactory. The material may also be extruded. For extrusions the content of the organic binder, lubricant, and water are usually higher, and the correct amount needed must be experimentally determined. In general, different shapes may be produced by processes similar to those used in the preparation of ceramics.

(6)   The final reaction and crystallization must be controlled carefully. In this procedure, the molded mixed oxides are heated to some temperature between 950°C and 1450°C in oxygen, air or nitrogen, depending upon the composition chosen and the properties desired. At these high temperatures the cations and anions of the mixed oxides diffuse, and a new material of spinel structure results. The formation of the spinel is so rapid that when unsintered molded mixed oxides are heated from one to five minutes at about 1300°C they show complete spinel x-ray diffraction patterns. Further heating influences chiefly the rate of growth of the crystals. Low temperatures and/or short periods of crystallization give small crystals, and high temperatures and/or long periods of crystallization give large crystals.

At these high crystallization temperatures dissociation of the oxides may also occur. At high temperatures there is an appreciable probability that oxygen anions will separate from the cations and escape as oxygen gas, and as a result the positive charge on some or all of the cations is reduced. This dissociation is illustrated by the conversion of ferric oxide, Fe_2O_3, to magnetite, $Fe_3O_4 (= Fe^2+O \cdot Fe_2^{3+}O_3)$, at high temperatures. Ideally,

$$3(Fe_2^{3+}O_3) \rightarrow 2(Fe^2+O \cdot Fe_2^{3+}O_3) + \tfrac{1}{2}O_2.$$
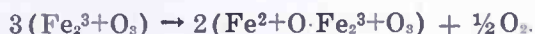
This reaction is appreciable at temperatures above $1300°C$ in air and may be readily carried out in nitrogen or vacuum at much lower temperatures. Correspondingly, manganic oxide, Mn_2O_3, changes to Mn_3O_4 at temperatures above $900°C$ in air. The degree of dissociation varies not only with temperature, duration of heating, and atmosphere, but also with the presence of other oxides. This often occurs in ferrospinels containing excess Fe_2O_3 over the stoichiometric (equimolar) amount. When such materials are heated to $1300°C$, larger amounts of ferrous cation, Fe^2+, are found on analysis than when Fe_2O_3 is heated by itself to the same temperature. This occurs in mixtures of MgO and Fe_2O_3,[32] mixtures of ZnO and Fe_2O_3,[33] and mixtures of NiO and Fe_2O_3. At temperatures approaching and above the melting point of the mixture the dissociation is rapid and difficult to control. Consequently, the crystallization temperature is kept below the melting point of the mixture, and the solid state reaction is made in the region of sintering temperatures.

The maximum permeabilities for the $NiO-Fe_2O_3$, as well as for the $ZnO-Fe_2O_3$ systems, as shown in Figure 12, are not at the stoichiometric compositions but rather at compositions containing excess Fe_2O_3. Because of dissociation, these materials contain some magnetite (Fe_3O_4) in solid solution with nickel or zinc ferrospinel. X-ray diffraction patterns of nickel ferrospinels, containing up to 80 mole per cent of Fe_2O_3, crystallized in air at $1400°C$ show only a spinel phase, while compositions containing Fe_2O_3 in excess of 80 mole per cent contain both a spinel, and a hexagonal-Fe_2O_3 phase. Chemical analysis of the composition containing 80 per cent of Fe_2O_3 shows that not all the excess Fe_2O_3 dissociates to Fe_3O_4, and such compositions can be thought of as solid solutions of $NiFe_2O_4$, Fe_3O_4, and cubic-Fe_2O_3. The dissociation can be brought to completion by heating the materials in an atmosphere of pure nitrogen or vacuum. Compositions made this way have higher permeabilities than if processed in air. The higher permeabilities in the case of the nickel ferrospinels are the result of the lowering of the negative magnetostriction of nickel ferrospinels by the positive magnetostriction of the magnetite in solid solution. Maximum permeabilities are obtained at minimum magnetostriction values. The high permeabilities for the zinc ferrospinels with excess Fe_2O_3 are probably caused by both the

[32] H. S. Roberts and H. E. Merwin, "The System $MgO \cdot FeO \cdot Fe_2O_3$ in Air at One Atmosphere", *American Journal of Science*, Vol. 21, pp. 145-157, 1931.

[33] Yagoro Kato and Takeshi Takei, "Studies on Zinc Ferrite, Its Formation, Composition, and Chemical and Magnetic Properties", *Trans. Amer. Electrochem. Soc.*, Vol. 57, pp. 297-312, 1930.

reduction of the Curie temperature of magnetite by the zinc ferrospinel in solid solution and the reduction of the positive magnetostriction of magnetite. In Table IV data is given for different compositions in the $NiO-Fe_2O_3$ system crystallized in air, in nitrogen containing about ½ per cent oxygen, and in purified nitrogen.

Table IV—$NiO-Fe_2O_3$ System—1300°C Crystallization Temperature

NiO (Mole %)	Fe_2O_3 (Mole %)	μ_o	Crystallized in air Q (500 Kc)	μ_o	Crystallized in N_2 (½ % O_2) Q (500 Kc)	μ_o	Crystallized in purified N_2 Q (500 Kc)
50	50	27	60	—	—	25	42
40	60	29	81	52	57	81	40
30	70	28	106	61	64	118	10
20	80	14	91	40	87	80	4
10	90	4	53	28	85	41	22
0	100	1	25	7	65	30	2

For the $ZnO-Fe_2O_3$ system, also formed at 1300°C, permeabilities of about 200 with Q of 50 at 500 kilocycles were obtained in the composition region of 33 mole per cent ZnO and 67 mole per cent Fe_2O_3 ($ZnO \cdot 2Fe_2O_3$) when the heating is made in purified nitrogen. The $ZnO-Fe_2O_3$ system has been studied by Kato and Takei[33] who heated in air and vacuum.

(7)   Because of the partial dissociation of the oxides at the crystallization temperatures, certain compositions require an increase in the positive charge of some or all of the cations for optimum ferromagnetic properties. A post-crystallization heat treatment will sometimes accomplish this. This process is a reversal of dissociation; that is, oxygen is absorbed by the material, and the oxidation states of the cations are increased. The rate of this absorption is controlled by the porosity and temperature of the material, and by the ambient atmosphere. These heat treatments are made at temperatures of about 350°C to 950°C, i.e., below the normal temperature of crystallization. For the NiZn ferrospinel composition previously given, satisfactory results may be obtained by turning the furnace off after the required heating at 1400°C, and allowing the material to cool to room temperature in air. Slightly better ferromagnetic properties may be obtained if an atmosphere of oxygen is used and the cooling rate experimentally determined for the optimum property desired. In some cases, it is desirable to have a definite ratio of cations of different oxidation states, which have been formed during high-temperature crystallization, remain in the finished material. This condition may be attained by quenching, (rapid cooling), or by making the final material non-porous.

In the latter case, absorption of oxygen is minimized during cooling of the material.

It is thus evident that different materials may be produced by variation of ingredients, and procedures of synthesis. These different materials have varied properties, and because the properties are directly affected by such factors as the mode of preparation, particle size, crystallinity, and shape of specimen, these materials and their properties are called structure-sensitive.

ELECTRIC PROPERTIES

The electric and magnetic characteristics of the nickel-zinc-ferro-spinels, crystallized at 1400° C in air, will be given as illustrative of the general behavior of ferrospinels. Because the methods and equipment used in obtaining the data are useful in the interpretation of the results they will also be given in this section.

For consistency and ease of comparing the data, the compositions are expressed in mole per cent of the ingredients used. For mixtures containing three component oxides the data is plotted on *triaxial diagrams*. On such plots each apex of the triangle represents 100 mole per cent of one of the oxides, and the side opposite that apex represents zero per cent of the same oxide. A point on one of the sides of the triangle represents the composition of a mixture of two oxides, while a point within the triangle represents the composition of a mixture of all three oxides. Every point within the triangle has the property that the sum of the perpendiculars from the point to the sides is equal to the height of the triangle, and so the lengths of the perpendiculars from the points to the sides are equal respectively to the fractional amounts of the three components. In Figure 10 several mixtures are plotted for the nickel-zinc-ferro-spinel system.
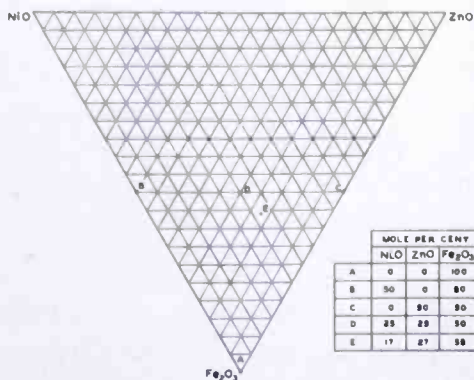
Fig. 10—A plot of the ternary system NiO-ZnO-Fe_2O_3.

The most important properties to be measured on a soft magnetic material of this kind are, permeability, saturation, losses, resistance, magnetostriction, and Curie temperature.

In making measurements on such materials, one of the first considerations is the shape and size of the magnetic specimen. In this work most of the measurements have been made on two standardized

configurations: (1) a *rod-shaped specimen* of square cross section, having approximate dimensions of 0.25 by 0.25 by 4.1 centimeters, has been used for a rapid measurement of permeability, relative losses, resistance, magnetostriction, and Curie temperature; (2) for a more precise measurement of permeability, loss components, and saturation, a *torus specimen* is used having the following approximate dimensions: 3.0 centimeters outside diameter, 2.5 centimeters inside diameter, and 0.25 centimeter height. The square cross section as well as the nearly equal inside and outside diameters of the torus are important factors in producing a uniform flux density within the magnetic body, a condition which is desirable for obtaining accurate measurements.

The rod specimens are used because they are suited to rapid measurements, and while they are not useful for basic measurements of permeability and loss components a great deal of comparative data can be easily and rapidly obtained. They are, however, well suited for the basic measurement of resistance, magnetostriction, and Curie temperature.

Table V—Design Data of Coils Used for Measurement of Permeability and *Q*.

	Kilocycles Per Second	
Coil Form	500	5000
Shape of Cross Section	□	□
Inside Dimension—centimeters	0.445 × 0.445	0.445 × 0.445
Wall Thickness—centimeters	0.013	0.013
Winding		
Type	Solenoid	Solenoid
Wire Size—Centimeters	0.02 (#32)	0.25 × 0.01 strap
Wire Insulation	Formex	None
Spacing Between Turns—centimeters	None	0.01
Length of Coil—centimeters	4.05	4.05

For the measurement of **permeability** and **Q value**, two helical test coils are used with Boonton Q Meter, type 160A. The design data of these coils are given in Table V. One of the coils is used at a frequency of 500 kilocycles and the second at a frequency of 5000 kilocycles. The first coil, without a magnetic core, is found to be resonant at 500 kilocycles with a shunt capacitance of 5000 micromicrofarads. When the ferrospinel rod specimen, or core, is symmetrically inserted in the field of the coil the circuit is found to be resonant, at the same

frequency, with a smaller value of shunt capacitance. The ratio of this capacitance to 5000 micromicrofarads is the effective permeability. When the core is $0.25 \times 0.25 \times 4.1$ centimeters in size the curve of Figure 11 may be used to convert the effective permeability to actual, or toroidal, permeability. The curve of Figure 11 was obtained experimentally by measuring comparable rod and torus specimens. The Q value is read when the circuit is tuned to resonance with the ferrospinel core in place. The Q value found by this method will have no simple relation to the Q value measured using a torus specimen but is valuable comparative information between two or more specimens.

Using the second or high-frequency coil with the same Q meter, but now operating at 5000 kilocycles per second, the same ferrospinel rod is measured by placing the specimen symmetrically in the field of this coil and reading the Q value at resonance. This frequency is chosen because, with the present materials and techniques, it gives a wide spread in the high frequency losses. For some ferrospinel bodies having low losses at this frequency, a third coil, resonating at a still higher frequency, should be used.
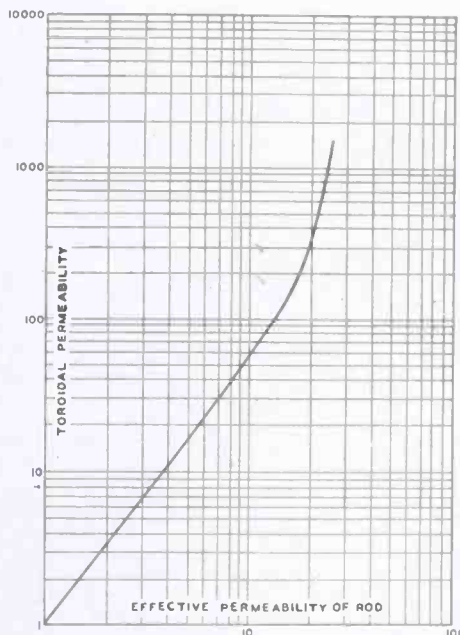
Fig. 11—Permeability conversion curve.

The *initial permeability* versus *composition* is shown in Figure 12. The measurements were made on the rod specimens and checked by measurements on toroidal specimens.

It should be emphasized that the compositions represented by this figure represent only the proportions of the ingredients used in preparing the materials, and not the compositions of the finished products. For 100 mole per cent of Fe_2O_3 a permeability value of 1.02 is shown, which in reality is the permeability of a small proportion of Fe_3O_4 (magnetite) contained in the hexagonal Fe_2O_3. The magnetite was formed during the heating of the hexagonal Fe_2O_3 at 1400°C by the dissociation process as previously discussed in the synthesis section.

Along the NiO-Fe_2O_3 side of the composition triangle (ZnO = 0) the peak value of permeability is about 60 for the composition 40NiO — 60Fe_2O_3. On maintaining a constant proportion of Fe_2O_3 and replacing

some of the NiO with ZnO, it is found that the permeability is increased
to about 220 where the composition is $12.5NiO - 27.5ZnO - 60Fe_2O_3$.
Thus, the addition of ZnO to the system has increased the permeability
by the process of reducing the Curie temperature. This will be ex-
plained in more detail later under the discussion of the Curie tempera-
ture. The highest value of permeability ($\mu_o = 1200$) is found for the
composition $15NiO - 35ZnO - 50Fe_2O_3$. The peak value of permeabil-
ity can be maintained only by a strict control of composition and
processing.
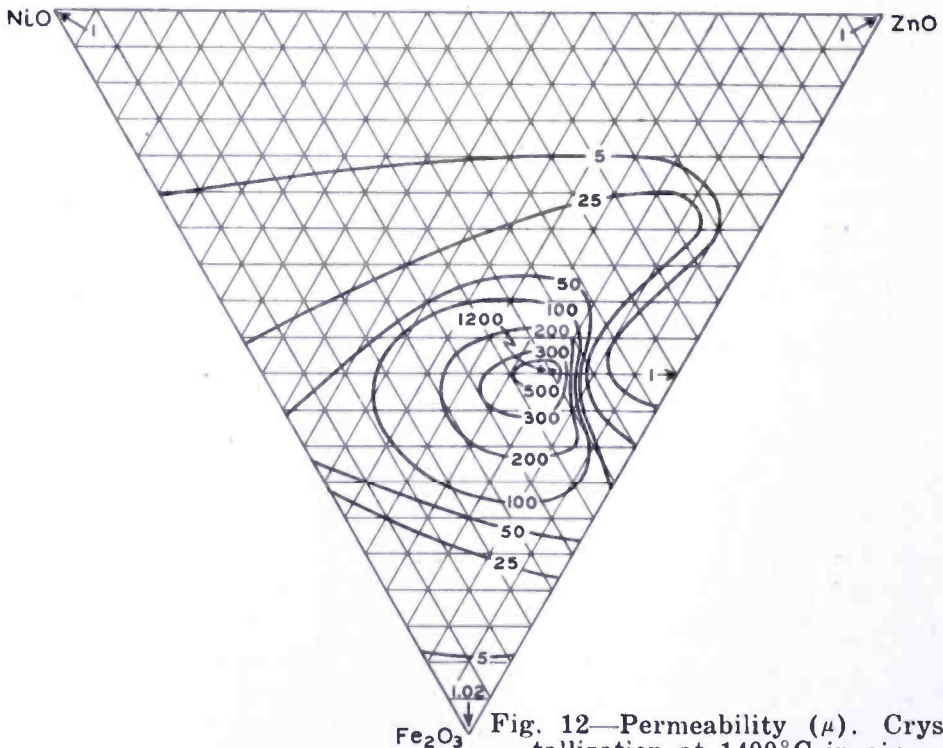
Fig. 12—Permeability (μ). Crys-
tallization at $1400°C$ in air.

As more ZnO is added to the composition of maximum permeability,
the contour lines of permeability converge where there is a rapid
decrease in permeability. In this region, the Curie temperature de-
creases from above to below room temperature.

It has been found expedient to measure the *total losses* of the rod
specimens inserted in the test coils previously described. Figure 13
shows the Q value of the circuit with the specimen in the coil, for
various ferrospinel compositions measured at 500 kilocycles. The coil
alone, resonated at this frequency has a Q value of 26, as shown for
the compositions 100NiO and 100ZnO.

The total losses have a minimum value at the composition 25NiO-
$5ZnO-70Fe_2O_3$ where the Q value is 100. As the composition is altered
to contain more ZnO the losses increase as shown by the decrease in

Q value. For compositions in the region of $15NiO\text{-}40ZnO\text{-}45Fe_2O_3$ the total Q value is less than the coil Q value. This shows that the ratio of the *resistance* added to the coil by the ferrospinel to the *reactance* added to the coil by the ferrospinel is greater than the corresponding ratio of the coil alone.

Figure 14 is also a plot of the *total Q value versus composition* but at 5000 kilocycles, using the second helical coil previously described. The coil alone has a Q value of 26. The contour lines are very different at this higher frequency because the predominant type of loss is a function of frequency. It is also interesting to note that the region of maximum losses (minimum Q) at 5000 kilocycles is the region of maximum permeability (see Figure 12). The separation and discussion of the various loss coefficients is presented next.
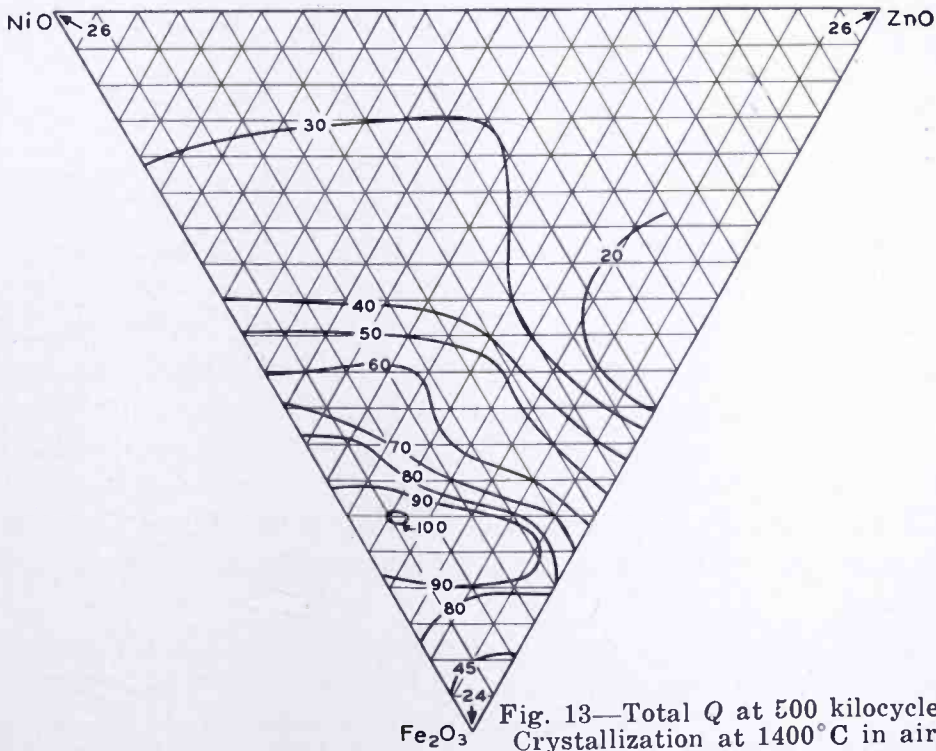
Fig. 13—Total Q at 500 kilocycles. Crystallization at 1400°C in air.

The more *basic measurements* of *permeability, flux density,* and *loss separation* will now be considered, using the toroidal specimen which is uniformly wound with a low loss winding such as a single layer of litz wire containing 30 strands of number 44 wire.

The simple circuit shown in Figure 15 was found to be satisfactory for measuring these properties. Since it is desirable to measure the voltages across the inductance, the resistor, and the generator, with a single vacuum-tube voltmeter, and at the same time maintain one side of the voltmeter at ground potential, the same circuit containing a
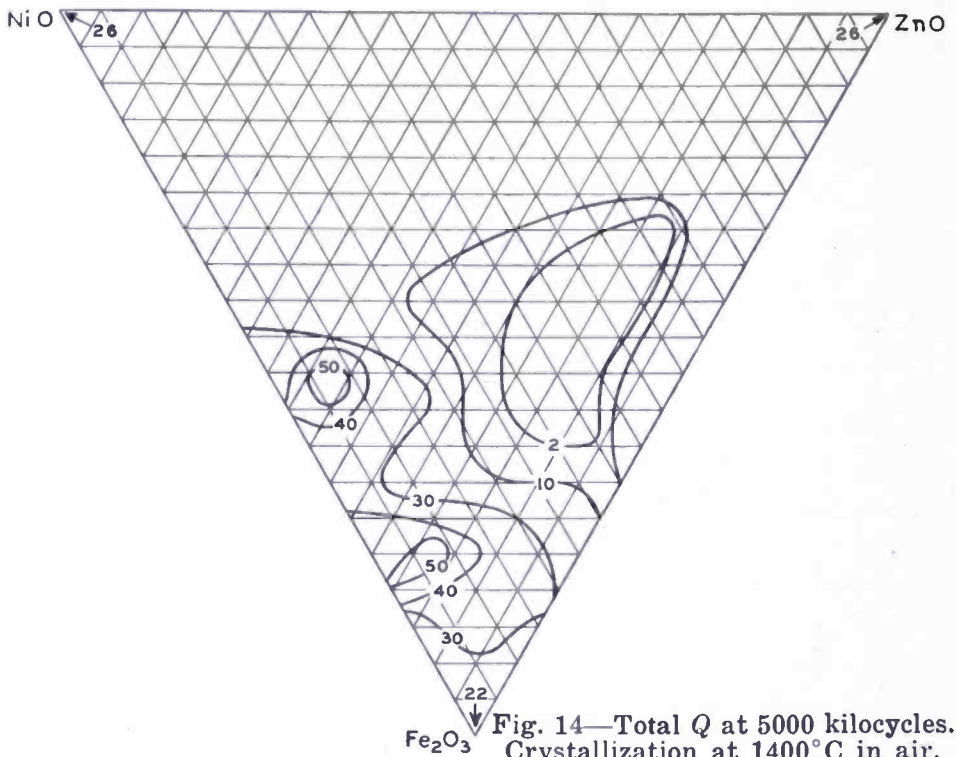
Fig. 14—Total Q at 5000 kilocycles. Crystallization at 1400°C in air.

switching arrangement was actually used. The toroidal ferrospinel specimen is the core for the inductance L.

Resonance is obtained by varying the capacitor C until a minimum voltage reading is obtained across the resistor R. This is the condition for maximum impedance of the tuned circuit with unity power factor.[34]

To obtain full information on a ferrospinel torus it is necessary to take a series of readings at each frequency for various values of flux densities, obtainable by varying the intensity of the input signal. The frequencies used in most of these tests were 100, 200, 500 and 1000 kilocycles.

If measurements are made at lower frequencies it is necessary to have a multi-layer bank winding on the torus in order to keep the value of the capacitor (C) at a reasonable value. When the value of (C) becomes large the resistive component is appreciable and must be eliminated or considered in the calculation of the total resistance of the circuit. The input voltage should not exceed that required to increase the permeability to a value of $1.2\mu_o$.
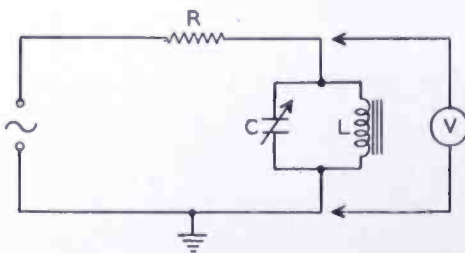
Fig. 15—Schematic diagram of test equipment used for loss separation measurements.

[34] R. S. Glasgow, PRINCIPLES OF RADIO ENGINEERING, pp. 35-45, McGraw-Hill Book Company, Inc., New York, N. Y., 1936.

For best sensitivity and accuracy it is necessary to use a non-inductive type of resistance, R, of such a value as to keep the voltage across the resistor equal to, or less than, the voltage across the tuned circuit.

The permeability, μ, is calculated from the convenient equation

$$\mu = kL, \tag{9}$$

where

$$k = \frac{d \times 10^8}{0.4\,AN^2},$$

$d =$ Average diameter of torus in centimeters,

$A =$ Cross sectional area of torus in square centimeters,

$N =$ Number of turns on the winding.

Also,
$$H = KI_L \text{ oersteds}, \tag{10}$$

where
$$K = \frac{0.4N}{d}.$$

The total line current, I_0, is

$$I_0 = I_R = \frac{E_R}{R}. \tag{11}$$

The current through the condenser, I_c, is

$$I_c = \omega C E_c, \tag{12}$$

and
$$Q = \frac{I_c}{I_R}. \tag{13}$$

The current through the inductance, I_L, is

$$I_L = \sqrt{I_R^2 + I_c^2}, \tag{14}$$

and the inductance, L, is

$$L = \frac{1}{\omega^2 C} \frac{Q^2}{1 + Q^2}. \tag{15}$$

The total effective (coil and core) resistance, R_T, is:

$$R_T = \frac{\omega L}{Q}.$$

(16)

To obtain the effective resistance, R_m, of the ferrospinel material alone it is usually satisfactory, when using a low-loss coil as described, to assume the copper loss resistance is equal to the direct-current resistance and subtract this from the total, R_T. This is not true for high values of Q (coil and core) and low values of inductive reactance, X_L. The Q of the ferrospinel material is:

$$Q_m = \frac{\omega L}{R_m}.$$

(17)
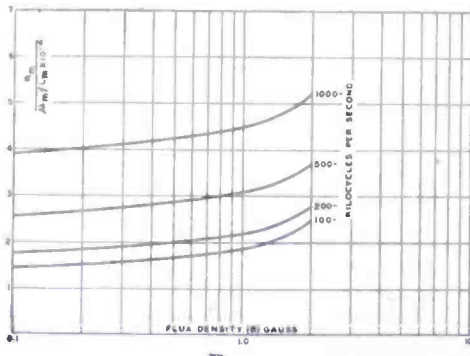
Fig. 16— $\dfrac{R_m}{\mu_m f L_m \cdot 10^{-4}}$ versus flux density, as a function of frequency.
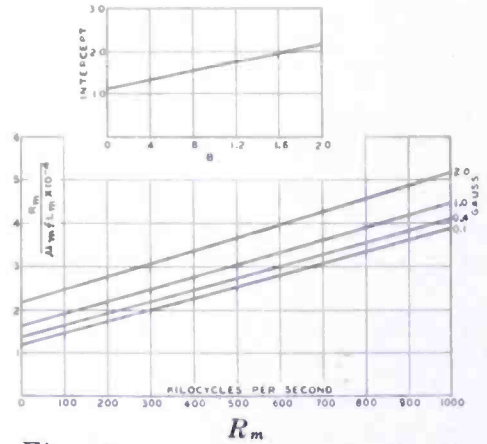
Fig. 17— $\dfrac{R_m}{\mu_m f L_m \cdot 10^{-4}}$ versus frequency, as a function of flux density.

From Equations (9), (15) and (16) it is possible to compute

$$\frac{R_m}{\mu_m f L_m},$$

where the subscript (m) denotes a single point where R, μ, and L are related.

Plotting $\dfrac{R_m}{\mu_m f L_m}$ versus B ($B = \mu H$), a family of curves is obtained as illustrated by Figure 16.

Then plot $\dfrac{R_m}{\mu_m f L_m}$ versus frequency (Figure 17) by taking points

from the curves of Figure 16 having constant value of B. For certain ranges of frequency and flux density a family of straight parallel lines results. This permits the use of a simple graphical method of separating the three types of losses and the loss constants by means of the well known relation as deduced by Legg:[35]

$$\frac{R}{\mu f L} = \frac{2\pi}{\mu Q} = aB + c + ef, \tag{18}$$

where

$a =$ hysteresis resistance constant,

$c =$ residual resistance constant,

$e =$ eddy current resistance constant.

By plotting B versus the intercept of the straight lines (top chart of Figure 17) the value of the residual constant, c, can be found at the intercept value where $B = 0$.

The slope of the straight lines gives the value of the eddy current constant, e, and the slope of the intercept line gives the value of the hysteresis constant, a.

For the equimolar Ni-Zn ferrospinel, crystallized at 1400°C, the constants were found to be

$$a = 0.5 \times 10^{-4},$$

$$c = 1.15 \times 10^{-4},$$

$$e = 0.27 \times 10^{-9},$$

$$\mu_0 = 280.$$

Most of the ferrospinel materials obey the above relation up to a frequency of about 1000 kilocycles, above which frequency the relation is no longer linear. Within this frequency limitation, the four constants, μ, a, c and e fully describe the behavior of the ferrospinel materials at low flux densities ($\mu \leq 1.2\mu_0$) and, knowing these, the applications engineer can evaluate each ferrospinel material for his specific usage.

At frequencies above which Equation (18) is no longer valid, one

[35] V. E. Legg, "Magnetic Measurements At Low Flux Densities Using the Alternating Current Bridge", *Bell Sys. Tech. Jour.*, p. 39, January, 1936.

may plot the term $\dfrac{2\pi}{\mu Q}$ versus frequency and have, for a specific ferro-spinel body, a relation between the total losses and frequency.

Equation (18) may be rewritten in terms of Q thus:

$$Q = \frac{2\pi}{\mu(aB + c + ef)}. \tag{19}$$

At low frequencies and for low values of flux density, the Q value is limited by the residual constant, c. At low frequencies and high values of flux density the Q value is limited by the hysteresis contant, a.

Many applications in communications where ferrospinels have possible use will be seriously limited by the value of the eddy current constant, e, because of the high frequency impressed on the ferrospinel. The flux density may be low and therefore the hysteresis loss as well as the residual loss will be negligibly low compared to the eddy current loss. As can easily be seen by Equation (19), it is probable that ferrospinels for high frequency use will have reduced values of permeability.

Because the measurement of **Curie temperature** requires a relatively long time, a simple, automatic equipment has been developed for this purpose. This equipment employs a signal source exciting an inductive reactance in series with a fixed resistor. The rod ferrospinel specimen is the core of the coil comprising the reactance. The radio-frequency voltage across the reactance is rectified by means of a silicon crystal rectifier and is impressed on the meter of an Engelhard recorder. As the ferrospinel core changes permeability, the reactance, and thus the voltage supplied to the recorder is altered. At the Curie temperature a rapid change of reactance is recorded. A thermocouple is placed adjacent to the ferrospinel core and the recorder is arranged in such manner that alternately the temperature and effective permeability are recorded.

The Curie temperature of the various Ni-Zn ferrospinels is shown in Figure 18. For the purposes of this paper the Curie temperature is defined as the temperature at which the initial permeability is reduced to 10 per cent of the peak initial permeability. Ferrospinels with a wide range of Curie temperatures may be obtained by varying the ZnO content. The nickel ferrospinel (ZnO = 0) has a Curie temperature of 580°C. As the ZnO content is increased the Curie temperature is decreased. The ferrospinel whose Curie temperature equals room temperature has the approximate composition $12NiO{-}38ZnO{-}50Fe_2O_3$. Ferrospinels with Curie temperatures considerably below room tem-
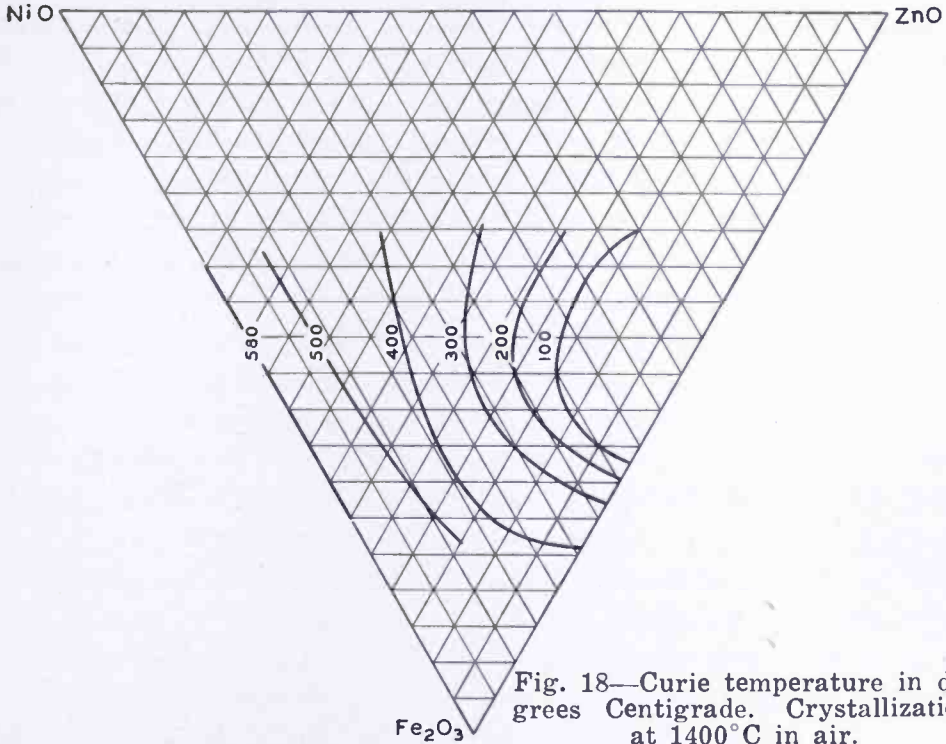
Fig. 18—Curie temperature in degrees Centigrade. Crystallization at 1400°C in air.

perature are possible with a further increase in the ZnO content. An equimolar solid solution of ZnO and Fe_2O_3 is paramagnetic at all temperatures at which it has been studied in these Laboratories.

The permeability is a function of the Curie temperature as illustrated by the curves of Figure 19. When part of the NiO is replaced by ZnO the Curie temperature is reduced as previously illustrated and also the permeability is increased. By the replacement of 35 mole per cent of NiO with ZnO the Curie temperature is reduced from 580°C to 100°C, and the permeability (at room temperature) is increased from 30 to 1200. This means of increasing the permeability must be used with some caution because, as clearly shown by Figure 19, the permeability stability with temperature is confined to a narrow range and the normal ambient
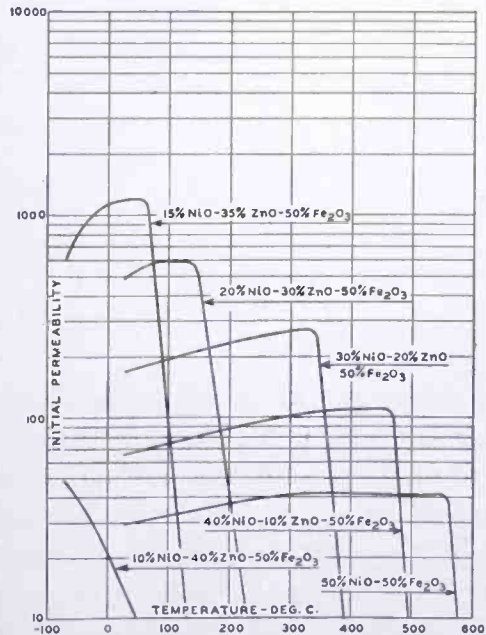
Fig. 19—The variation of initial permeability and Curie temperature as a function of composition.

temperature variation of the equipment using the ferrospinel may exceed this narrow range of stability.

The direct-current measurement of **volume resistivity** is made by affixing metallic electrodes to the opposite ends of the rod specimens. This can be accomplished by spraying molten metal or by using a low-conversion-temperature silver paste, or paint, as used by some resistor manufacturers. The measured values are converted to the usually accepted unit of ohm centimeter. The validity of the method may be checked by successively reducing the length of the ferrospinel rod and measuring the resistance as zero length is approached.

The volume resistivity of the ferrospinels is almost entirely a function of the Fe_2O_3 content as shown by Figure 20. The highest value of resistivity is found in the ferrospinels containing a small amount
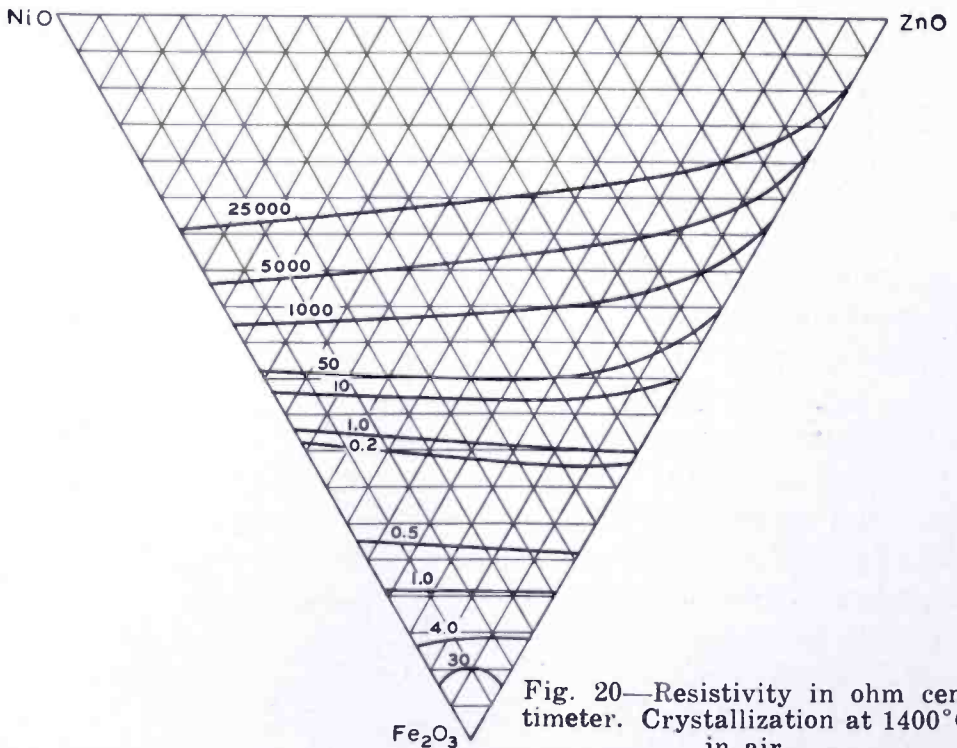
Fig. 20—Resistivity in ohm centimeter. Crystallization at 1400°C in air.

of Fe_2O_3, and as the Fe_2O_3 content is increased the resistivity decreases to a minimum value of less than one ohm centimeter when the Fe_2O_3 content is about 60 per cent. As the Fe_2O_3 content is further increased the resistivity also increases but at a rather slow rate. The resistivity is also a function of crystallization temperature. Ferrospinels can be made with resistivities of several megohm centimeter by using lower temperatures of crystallization.

One might expect that ferrospinels having high electric resistivity would be completely devoid of eddy current loss. However, this is not

borne out by experimental data. For example, two ferrospinels which were measured, were found to have values of volume direct-current resistivity which differed by a factor of 2×10^4, and yet they had the same eddy current loss constant. This leads to the belief that in a polycrystalline structure of this kind, the resistivity may not be uniform throughout the body. Indeed the experimental data strongly indicates that the crystals may have low resistivity and that the crystal boundaries are responsible for the high overall resistivity.

The sign and magnitude of the **magnetostriction** is measured by an apparatus which combines mechanical and optical means of amplification. The rod ferrospinel is held in the anvil of a mechanical system of levers having a magnification of 500. The magnified end of the mechanical system is viewed by an optical system having a magnification of 100. A coil containing a direct current is symmetrically placed around the ferrospinel rod, so that, as the direct current flux is varied through the ferrospinel rod, the change in length of the rod is magnified by a factor of 5×10^4 as viewed by the observer. A calibrated scale within the optical system is used to obtain the magnetostriction sensitivity in terms of parts per million.

The coil used in the above equipment was not sufficiently long to produce a uniform field and therefore it is not possible to give specific data as to the magnetostriction sensitivity of the ferrospinels of the system. However, this is unimportant for the present discussion. Figure 21 shows two regions of maximum magnetostriction sensitivity, one positive and one negative. In the region between these two maximums, the positive and negative magnetostriction effects are combined to produce a resultant smaller effect and thus a smaller sensitivity. Along the dotted line as indicated, the magnetostriction is found to be zero. As pointed out by Snoek[19] this seems to be one of the requirements for maximum permeability and is shown by comparing Figures 12 and 21.

USES

Ferrospinels are being used increasingly in electronic equipment operating in the frequency range of 10 to 5,000 kilocycles. At power and low audio frequencies the ferrospinels are not competitive with laminated ferromagnetic materials, and at very high frequencies the losses in the ferrospinels are excessive when high permeability is required. It is possible, however, to produce a ferrospinel, with low permeability, useful at frequencies in the order of 100 megacycles. The application of ferrospinels as core bodies in the deflection yoke, horizontal deflection transformer, and high voltage transformer for

television receivers is now finding wide acceptance. The ferrospinels are especially suited to television video frequencies as their use in these components results in improved performance, at lower cost and with smaller space.

In the standard broadcast receiver, the ferrospinels are expected to be used in the radio frequency circuits as "trimmers" and as permeability tuning cores. With a properly designed coil it is possible to tune a circuit, by the movement of a ferrospinel rod, from 500 to 3000 kilocycles, or to cover the standard broadcast band (540 to 1730 kilocycles) with only three-eighths of an inch movement of the ferrospinel rod. Interesting uses of the ferrospinels are shown in the photograph of Figure 22. The ferrospinel antenna rod, three eighths
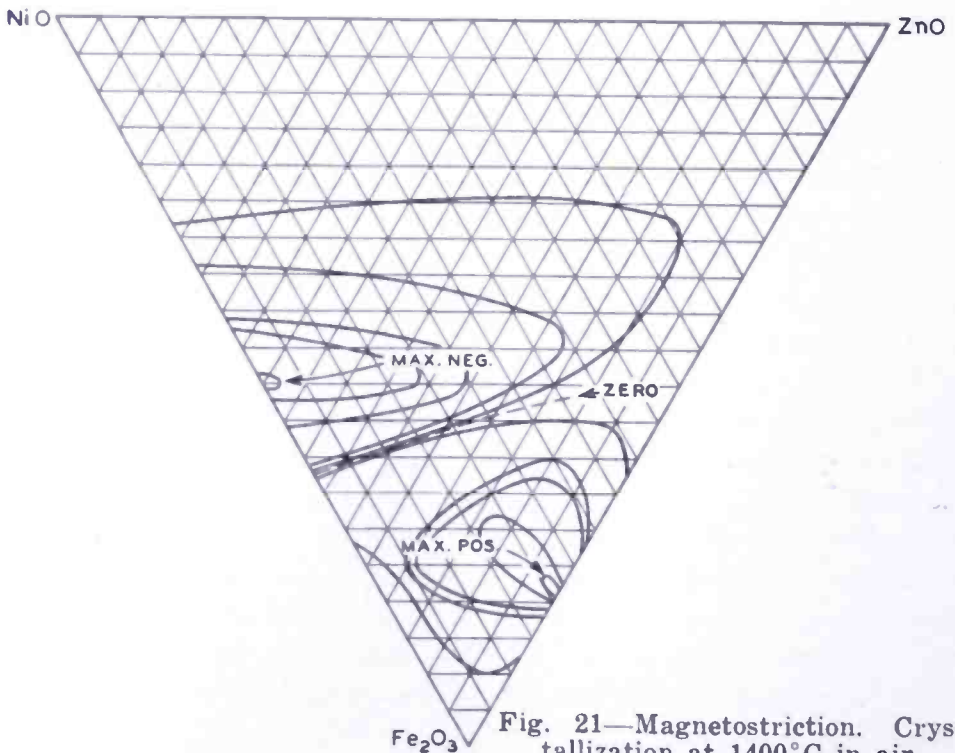
Fig. 21—Magnetostriction. Crystallization at 1400°C in air.

of an inch in cross section and seven inches long, with the small coil as shown, has equal to or better performance than the standard table model loop also shown. Figure 22 also shows the possible reduction in size of a 455-kilocycle intermediate-frequency transformer. At the right is a widely used transformer containing powdered iron parts. The transformer at the left has the same performance and can be reduced in size because of the ferrospinel liner shown in the center. This liner is placed between the coils and the metal shield and because of its high permeability, contains all the magnetic flux, thus removing the detrimental effects of the metal shield.
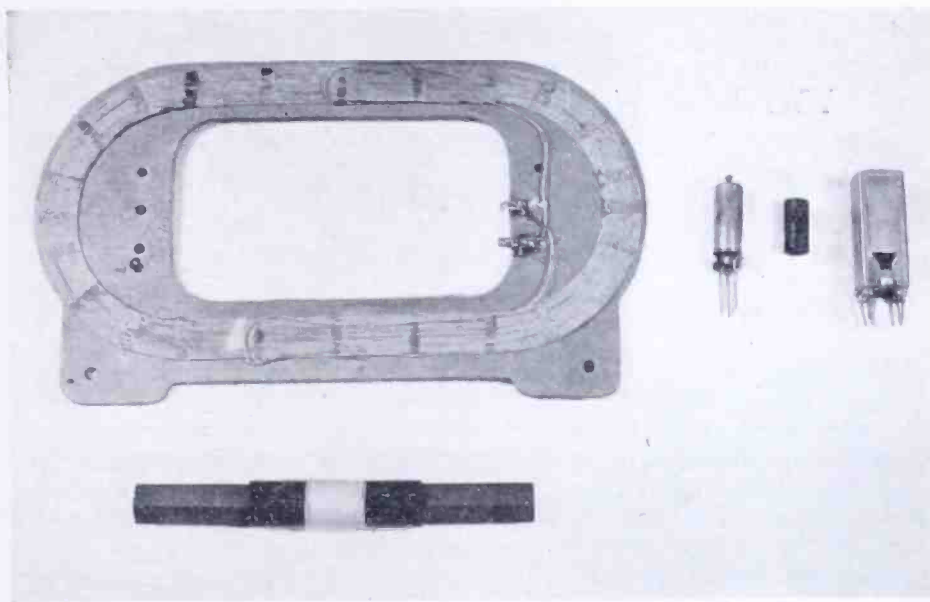
Fig. 22—Two uses of ferrospinels in receiver design.

As previously indicated, some of the ferrospinels are useful for magnetostriction applications and have been used as "driver" and "take-off" elements for resonant metal filters. The details of this application have been published by Roberts and Burns.[36]

By using a ferrospinel with a high electric resistivity as the core body for radio frequency inductances, the wire may be placed on the ferrospinel without additional insulation. In fact, the conductor may be affixed by the printed circuit technique for some applications.

The authors record their appreciation of administrative aid given by W. L. Carlson and V. K. Zworykin, and technical aid given by R. S. Weisz, P. H. Werenfels and D. G. Linz.

---

[36] W. van B. Roberts and L. L. Burns, Jr., "Mechanical Filters for Radio Frequencies", *RCA Review*, Vol. X, No. 3, pp. 348-365, September, 1949.

LIGHT-TRANSFER CHARACTERISTICS OF IMAGE ORTHICONS*†

By

R. B. JANES AND A. A. ROTOW

Tube Department, RCA Victor Division,
Lancaster, Pa.

Summary—Transfer characteristics (signal output versus light input) of image orthicon tubes have been studied at different target voltages and with tubes having different target-mesh spacings. The light input includes both the simple case of a small white square on a dark background and a photographic step tablet in a dark and white field. The results are used to indicate the optimum light levels for image orthicons, types 5820 and 5826. Measurement of the light-transfer characteristics brings up the many effects caused by redistribution of secondary electrons on the target at high lights. The particular redistribution causing ghosts is discussed in detail and possible changes in tube design for minimizing these ghosts are reviewed.

INTRODUCTION

THE function of a pickup or camera tube is to transfer an optical image into an electrical signal. How well this transfer is accomplished can be determined by measuring three properties of the electrical signal: the signal-to-noise ratio, the resolution, and the gray-scale reproduction[1]. The first two properties have been discussed in detail in a previous paper[2]. The third property was covered only to the extent that a very simplified transfer curve was included. Schade[1] had previously, however, published curves which more closely represented normal operating conditions.

The gray-scale reproduction or, as it has sometimes been called "the light-to-signal transfer characteristic," determines in part how the final image will compare with the original in tone gradation. A knowledge of the transfer characteristic is especially important when an attempt is made to match pictures from two or more cameras and in the ever-present problem of kinescope photography. In order to

---

[1] O. H. Schade, "Electro-Optical Characteristics of Television Systems", Part III, *RCA Review*, Vol. IX, No. 3, p. 490, September, 1948.

[2] R. B. Janes, R. E. Johnson and R. S. Moore, "Development and Performance of Television Camera Tubes", *RCA Review*, Vol. X, No. 2, p. 191, June, 1949.

establish more thoroughly the types of transfer curves to be expected from image orthicons, this paper gives the results of data taken on many tubes under widely varying conditions.

In the image orthicon, the transfer characteristics are determined almost entirely by the potentials and the electron redistribution at the target-mesh assembly. It will be necessary to discuss only this part of the tube in order to reach an understanding of the problem. As shown in Figure 1, the optical picture which is focused on the photocathode gives rise to photoelectrons which are imaged, by means of an axial magnetic field and an accelerating voltage, onto the target-mesh assembly. The target-mesh assembly consists of a target of very thin glass with a mesh mounted only a few thousandths of an inch from it on the photocathode side. In operation, the other side of the
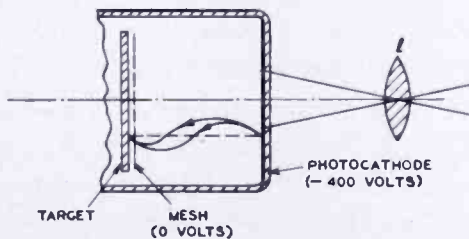
Fig. 1 — Electrons f r o m photo-cathode imaged onto target-mesh assembly.
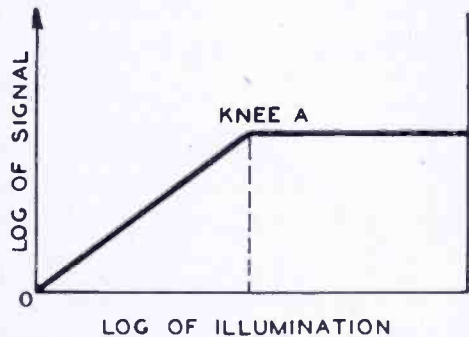
Fig. 2—Simplified transfer curve.

target is held at a potential near zero by the electron beam from the gun. The mesh in turn is held at a potential of about two volts above that of the beam side of the target. When an illuminated scene is picked up, the electron image from the photocathode will strike the target and cause secondary electrons to be emitted. With low illuminations nearly all the secondary electrons will be collected by the mesh. As the illumination is increased the potential of the glass target rises almost to that of the mesh until a point is reached at which there is no field at the mesh to collect the secondaries. At and about this point the secondaries will be distributed over the target and will land on other target areas. On the basis of these simplified considerations a transfer curve can be drawn. According to such a curve, as plotted in Figure 2 on a log-log scale, the signal output will be a straight line with a slope of one at low lights until a point, usually called the knee of the curve, is reached where the target reaches mesh potential. Above this point the signal output is constant. Such a curve is greatly simplified since it does not take into account the interelement capacitance which must be considered for all but very close target-to-mesh spacings, electron redistribution over the target, and the variation in

initial velocity of the secondary electrons. Actually, such a curve holds most closely for a tube such as the RCA-5826 having a close-spaced target and operating with a small illuminated area on a black background—a combination which is seldom found in actual operation.

INTERELEMENT CAPACITANCE EFFECTS

Since the effects of interelement capacitances do not change the transfer curve as radically as the effects of electron redistribution, and since these effects have already been covered in a previous paper[2] they will be only briefly mentioned. As shown in reference (2) the interelement capacitance puts a second knee in the simple transfer curve for tubes having wide-spaced target such as the 5820. Such a simplified transfer curve is shown in Figure 3. In ordinary use, the illuminations are such that the second knee is not reached; the major effect of interelement capacitance in the 5820 is to introduce white-edge effects.[2] The presence of these white edges is disturbing and is one reason that close-spaced and wide-spaced tubes c a n n o t be matched.

Fig. 3—Simplified transfer curve including effects of interelement capacitance.

Data have been taken on a group of tubes illuminated with a small white square on a black background in order to check the simplified curves. When the data were taken, a light box, covered except for a small square in the center, was used. Ambient light was kept at a minimum and the signal output of the tube was read on an oscilloscope having a horizontal line selector. If a horizontal line that runs through the square of light is selected, the effect of multiplier shading is held to a minimum. Figure 4 shows the transfer curves obtained under such conditions. Only when the target-to-mesh spacing is less than one thousandth of an inch does the second rise disappear. For wider spacings the amount of the second rise increases with spacing. This amount is a rough measure of the "white-edge" effect. These curves differ from the theoretical ones in that the knees are rounded. The variation in the initial velocity of emission of the secondary electron from the target is a partial explanation for this difference. Since the curves are all plotted at the same value of 100 per cent for maximum signal output, they are not useful for determining absolute values.
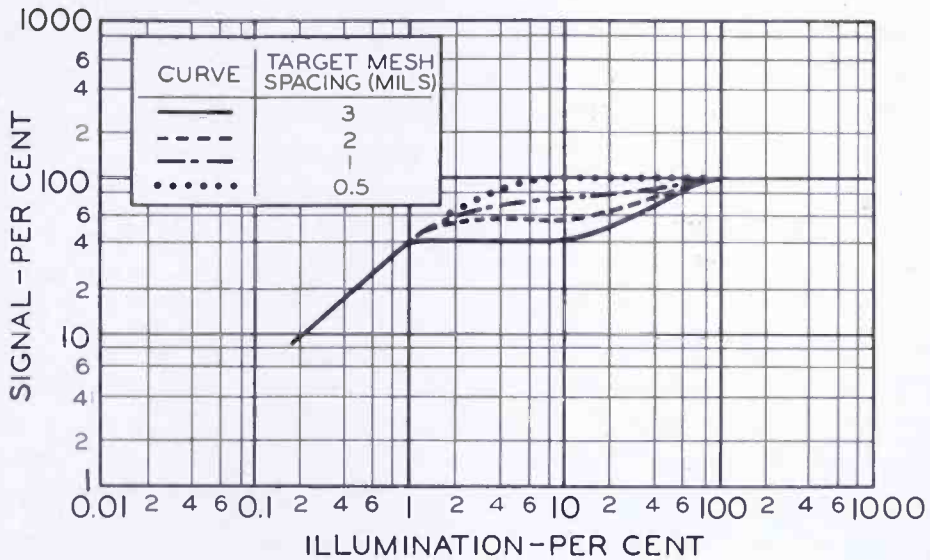
Fig. 4—Transfer characteristic for image orthicons having different target-mesh spacings.

ELECTRON REDISTRIBUTION EFFECTS

As mentioned previously, after the knee of the signal-output curve is reached, the secondary electrons emitted by the target will no longer be collected by the mesh but will be redistributed over the target. The signal from any element of the target, hence, depends not only on the illumination of its corresponding photoelement but also on the illumination of the corresponding photoelements of other parts of the target. This electron redistribution causes three different effects around any high-lighted element as shown in Figure 5. These effects are (A) the black border, (B) the white halo, and (C) the ghost. The black border is a very desirable effect in that it serves to preserve some contrast between signals when both are above the knee. The white halo is undesirable and is most evident when there are large areas of intense highlights in the picture. Under these conditions the white halo will actually destroy the contrast of much of the remainder of the picture, particularly if it is in low lights. The ghost is evident when there are highlighted spots on a dark background near the edges of the picture. It will be considered in detail in a later section of the paper.

The cause of these different effects can be found by examining the initial velocity distribution of secondary electrons as shown in Figure 6. The initial velocities can roughly be divided into three

Fig. 5—Effects of electron redistribution.

groups. Those of group one, which comprise the bulk of the electrons, have a velocity of a few (approximately 3) volts. Because of their low velocity, their secondary-emission ratio on relanding is less than one. As a result, the target is discharged and the black border is caused. Also, because of their low velocity these electrons do not travel far. Consequently, contrast is preserved in highlights only for small objects or for the edges of large objects. Group two contains electrons with velocities of more than about ten or twelve volts and which will themse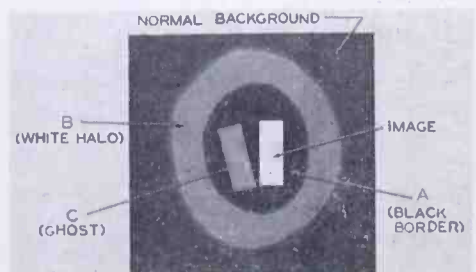lves produce more than a 1-to-1 secondary-emission ratio when they reland on the target. These electrons are partly responsible for the white halo and because of their higher velocities may travel a long distance on the target. The white halo effect, however, may also be caused by optical reflections in the tube. Group three contains reflected electrons which, because they comprise a group of very nearly the same velocity, will produce a nearly focused secondary picture or ghost. In commercial tubes the ghost is rotated counter-clockwise with respect to the highlight which causes it.
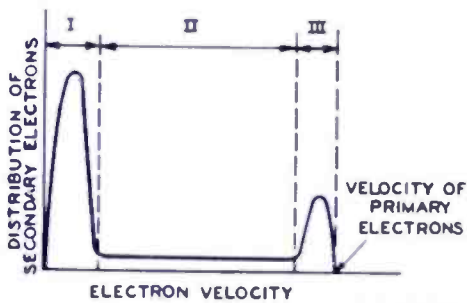
Fig. 6—Initial velocity distribution of secondary electrons.

TRANSFER CURVES

In order to measure the transfer characteristics of tubes where redistribution is present, a photographic step wedge with equal logarithmic steps of 0.2 is used. The wedge itself has ten steps making, with the clear illuminated background, a total of eleven steps. An illuminated light box is used with the step wedge horizontal and covering about one half of the picture width. The lens stop is set to put the highest white (the highest of the wedge, not the clear background) at the knee of the curve or several stops above the knee. The tubes are measured with a black background and with a border of white of the same intensity as the clear background all around the wedge. In all cases an oscilloscope having a horizontal line selector was used, and the maximum output of the tube was considered as 100 per cent.

Early in the investigation it was found that the results were confused, as shown in Figure 7, by the ghost from the highlights of the wedge and particularly from the white background. The ghost from the white background lifts the lower end of the curve of signal output and makes it appear nearly straight. For this reason, it is necessary

to take the curves with the ghost minimized by slightly defocusing the photocathode voltage or by using an "anti-ghost" tube to be described later. Because the ghost is made up of electrons which go through the image section three times instead of once, a slight change of photocathode voltage will defocus it rapidly.

The first curves were taken with a target voltage two volts above cutoff and are shown in Figure 8. The curves are plotted on log-log paper and for each tube the maximum signal is set at 100 per cent. All illuminations were also taken above or below the knee, thus eliminating the effects of varying photo-sensitivity from tube to tube. In
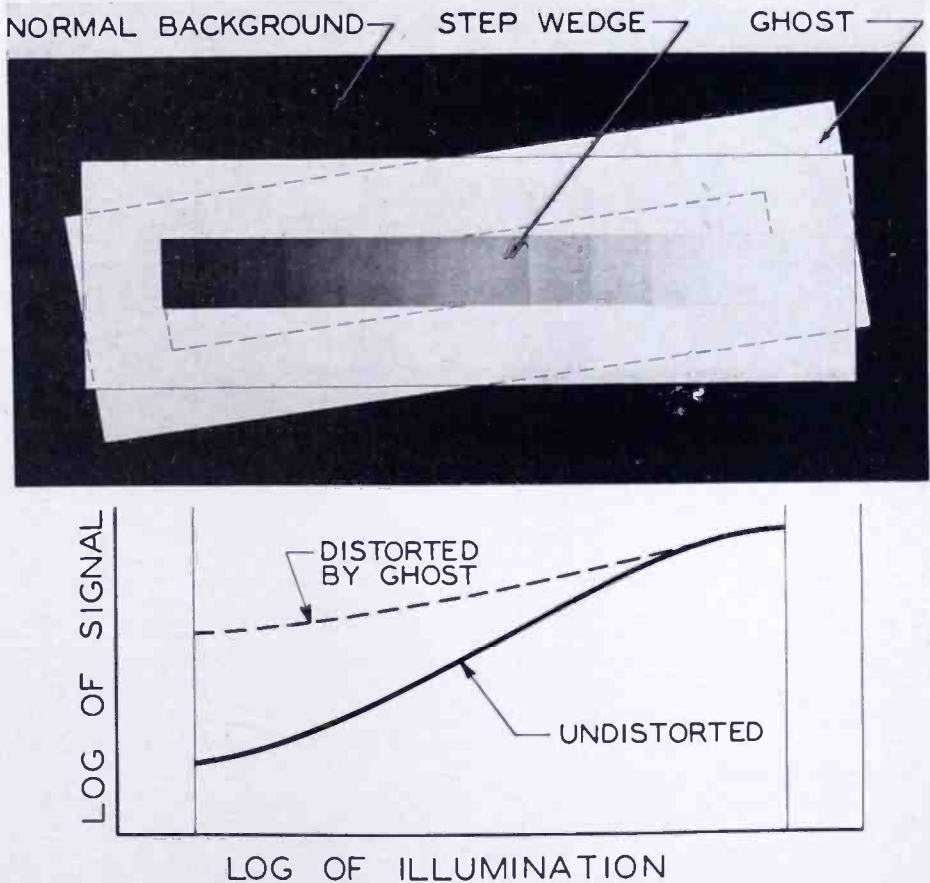
Fig. 7—Effect of ghost on signal-output curve.

taking the curves of tubes of various target spacings at a target voltage of two volts, it was found that the curves were essentially independent of target spacing. For this reason the curves of Figure 8 are drawn for the average of several tubes of various spacings. If the curves are examined more closely, it is seen that the curve with the highlight at the knee is essentially straight (the extra point above the knee corresponds to a square of the clear area). The curves for a black or a white background are the same, as would be expected, since in this

case there is little redistribution below the knee. However, conditions are different for the curves above the knee. It should be noted that the curve does not flatten out above the knee as much as the curves of Figure 4 which were taken with a small square. This difference is, of course, a measure of the preservation of contrast caused by redistribution. (If the curves were taken for very large areas in the steps, the contrast would only be preserved near the edges.) Also, when a
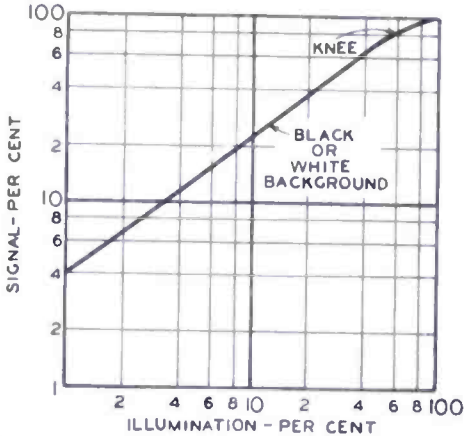
(a) Lens stop set so that highest light of the wedge is at the approximate knee of the curve.
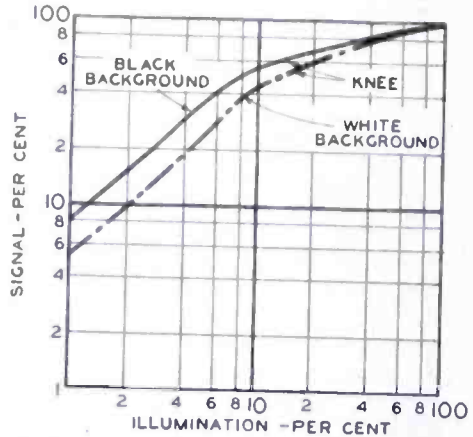
(b) Lens stop set so that highest light of the wedge is two stops above the approximate knee of the curve.
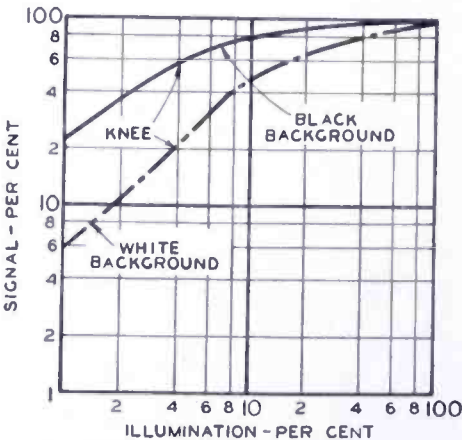
(c) Lens stop set so that highest light of the wedge is four stops above the approximate knee of the curve.

Fig. 8—Transfer characteristic for tubes having mesh-target spacing of 1 and 3 mils and target voltage of 2 volts. Ghost is defocused.

white background is present the signal curve is compressed at low lights. This compression is still more true of curve C, taken with the lens stop set so that the highest light of the wedge is four stops above the knee.

The curves were then repeated for target voltages of 1.0 and 1.5 volts above cutoff. In these cases the curves differ somewhat for wide-

spaced (RCA 5820) and close-spaced tubes (RCA 5826). Figures 9 and 10 show the results at 1.5 volts for wide- and close-spaced tubes. The principal difference appears to be the fact that for the wide-spaced tubes there is a sign of a second rise occurring at high light levels. The significant point is the tremendous amount of compression in the blacks that occurs when a white background is used. Even below the knee there is a certain amount of compression because not all of the

(a) Lens stop set so that highest light of the wedge is at the approximate knee of the curve.
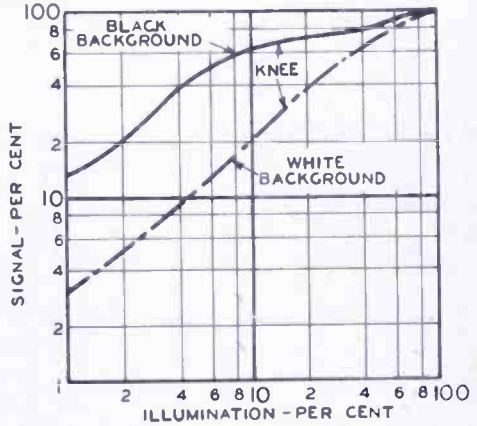
(b) Lens stop set so that highest light of the wedge is two stops above the approximate knee of the curve.
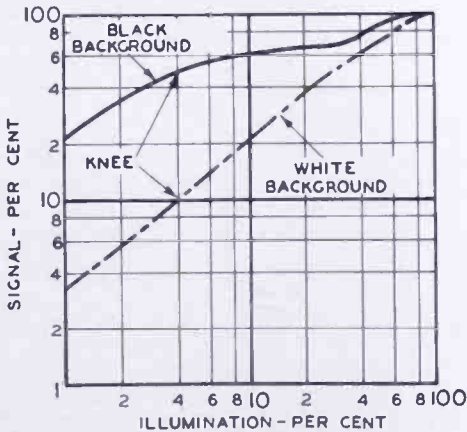
(c) Lens stop set so that highest light of the wedge is four stops above the approximate knee of the curve.

Fig. 9 — Transfer characteristic for tubes having mesh-target spacing of 3 mils and target voltage of 1.5 volts. Ghost is defocused.

secondaries are collected by the mesh due to the spread of initial velocities. With the mesh at two volts, far fewer electrons get through. At a 1-volt target voltage (Figures 11 and 12), the condition of compression is still more evident because more secondary electrons get through the mesh. This large compression near black and even for lighter greys does straighten out the transfer curve but it does so at the expense of pushing the blacks down into the noise level so that a

black and white picture with few intermediate greys is obtained. In the case of low target voltages and white backgrounds, the points near black are doubtful because they are so little above the noise. The shape of the curves under these conditions, therefore, may not be as shown.

(a) Lens stop set so that highest light of the wedge is at the approximate knee of the curve.

(b) Lens stop set so that highest light of the wedge is two stops above the approximate knee of the curve.
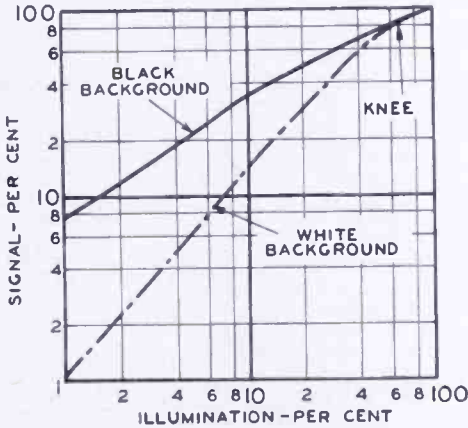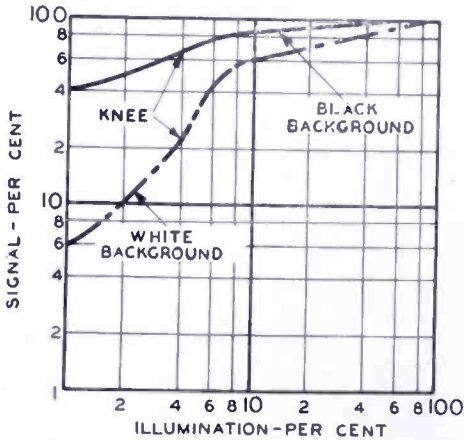

(c) Lens stop set so that highest light of the wedge is four stops above the approximate knee of the curve.

Fig. 10 — Transfer characteristic for tubes having mesh-target spacing of 1 mil and target voltage of 1.5 volts. Ghost is defocused.

Many suggestions for obtaining the best operation conditions for image orthicons can be drawn from these curves. Certainly, the target voltage should be kept in the neighborhood of two volts to prevent bad compression in the low lights. With this value of target voltage it is noted that wide spaced and close spaced tubes have about the same general transfer characteristic. However, it is still difficult to match tubes that differ widely in target spacing because of the presence of white edges and the lower signal-to-noise level of wide-spaced tubes.

The curves also bring out the danger of operating too far over the knee. The use of a lens opening that is too wide will give a picture with a narrower tonal range because of the black compression. Also, the white halo and eventually the black border will appear. For best results about one or two stops over the knee is a good compromise. *The curves also clearly show that in order to match pictures from the same scene on two or more cameras, the same target voltage should be used and the lens set on each camera to bring the same high light say two stops above the knee.* This last item, of course, corrects for any variation in photosensitivity from one tube to another.
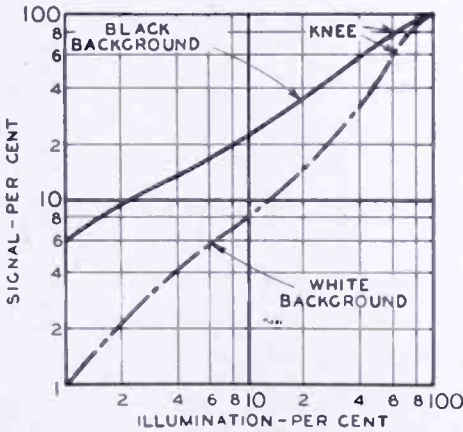
(a) Lens stop set so that highest light of the wedge is at the approximate knee of the curve.

(b) Lens stop set so that highest light of the wedge is two stops above the approximate knee of the curve.
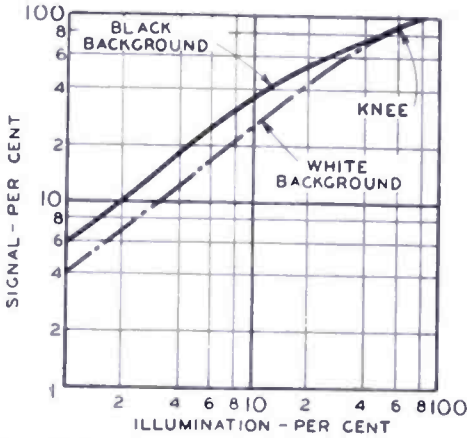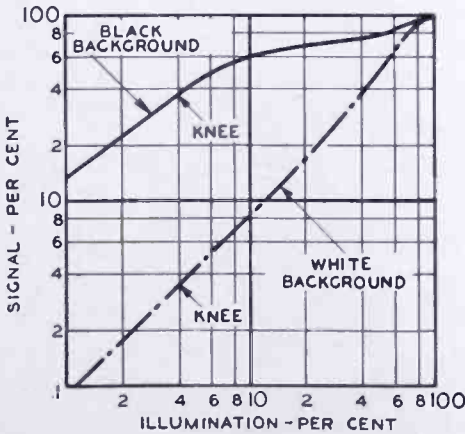

(c) Lens stop set so that highest light of the wedge is four stops above the approximate knee of the curve.
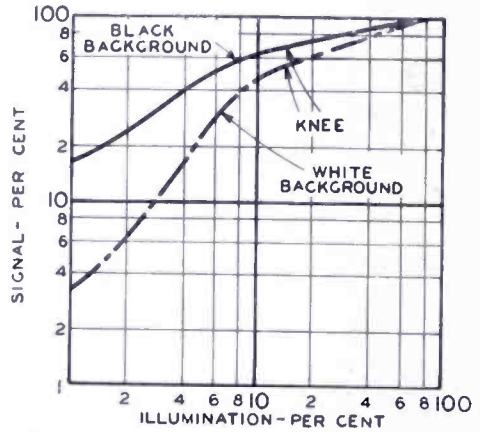
Fig. 11 — Transfer characteristic for tubes having mesh-target spacing of 3 mils and target voltage of 1 volt. Ghost is defocused.

The use of a log-log scale for the transfer curves has an advantage for those working with kinescope recordings in that transfer characteristics for photographic film are plotted the same way. The various

transfer characteristics can, therefore, be followed through the complete system in order to find out the best combination. The image orthicon curves clearly indicate that when properly used in kinescope recording the image orthicon tends to compress the whites and to expand the grays. Although this characteristic may not give a result
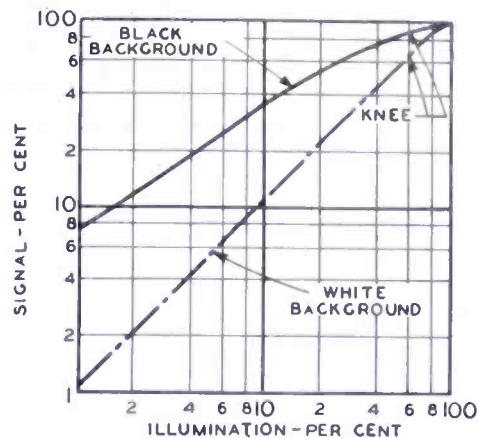
(a) Lens stop set so that highest light of the wedge is at the approximate knee of the curve.
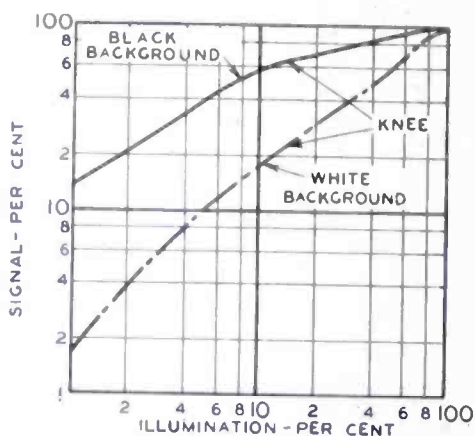
(b) Lens stop set so that highest light of the wedge is two stops above the approximate knee of the curve.
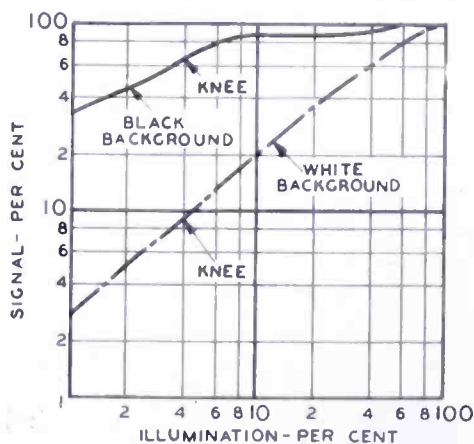
(c) Lens stop set so that highest light of the wedge is four stops above the approximate knee of the curve.

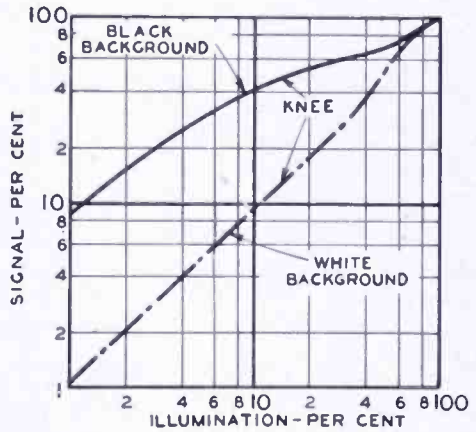Fig. 12 — Transfer characteristic for tubes having mesh-target spacing of 1 mil and target voltage of 1 volt. Ghost is defocused.

like that of a photograph, it does give a pleasing picture. Results closer to those obtained in photography can be obtained by running the highlights just at the knee. This method of operation, however, is only possible with close-spaced tubes (RCA 5826) and even here the user may not like the somewhat lower resolution and signal-to-noise ratio of the intermediate grays.

Under operating conditions the user may see the transfer characteristic as a linear plot or, if he looks at a photographic step wedge, as a semi-log plot with the ordinates as seen on his oscilloscope as

linear and the abscissa as a log. Plotting on semi-log paper has the advantage that if the dc level is changed, the shape of the curve remains the same with the whole curve being shifted up and down. On a log-log plot the shape of the curve will change since a constant signal is being either added or subtracted. The dc signal may be due to many causes and can be changed by changing the blanking level. Because the log-log plots as drawn in the figures do not include any dc signal, they may be changed over into semi-log plots.

ANTI-GHOST TUBES

As has been shown, the ghosts as seen near highlights in the final picture are due to reflected secondary electrons from the parts of the target corresponding to the highlights being focused back onto other parts of the target. In commercial tubes these ghosts can be minimized by defocusing the tube by means of the photocathode voltage or by using two loops of focus in the image section.* The first method leads to a definite loss of resolution; the second requires a photocathode voltage one fourth of the normal value so that resolution will also be lost unless a much higher magnetic field is used at the image section. The displacement of the ghost relative to the original image is the integrated result of the nonparallelism of the electric and magnetic fields throughout the distance between target and photocathode. This nonparallelism is small in the center, but large near the edges. If these fields in some way can be kept more parallel over the entire

Fig. 13—Photocathode, target, and mesh assembly of anti-ghost tube having extra mesh.

target area, the image due to reflected electrons should focus back onto its original position.

The first type of anti-ghost tube tried has an extra mesh (Figure 13) mounted about ¼ inch in front of the regular target mesh. The effect of this extra mesh is to straighten the electric field so that it is parallel to the magnetic field at all parts of the target. After several trials a spacing for this extra mesh was found that almost completely eliminates the ghost in all parts of the target. However, some loss of sensitivity results because even with a 200-mesh screen the transmission is down to about 75 per cent. Attempts to use a woven mesh of very high transmission were unsuccessful because the crossovers in

---

* This method was used by Schade in his measurements of transfer characteristics. See reference (1).

the mesh could be seen in the transmitted picture. With 200-mesh electroplated screens the screen is not visible.

A second type of tube has been designed in which a mesh is not used. It was found that if accelerator grid No. 6 is brought closer to the target, the ghost registered better with its original position. Several tubes have been made up in which the target cup has been made shorter and grid No. 6 correspondingly longer. At the same time the spacing between the target cup and grid No. 6 was reduced. In tubes with optimum parts length and spacing the ghost registers quite well except for its appearance when close to the edges of the target. Even here it is only slightly separated from the highlight which causes it. Figure 14 shows a comparison of the image structure of a standard and an anti-ghost tube.

During the work on the second type of anti-ghost tube a study was also made of the effect of varying the spacing between photocathode and grid No. 6. This spacing was varied from about 0.05 to 0.3 inch. For the wider spacings the "S"-type distortion is greater and the photocathode voltage required to obtain corner focus may differ from that required for center focus by as much as 25 volts. For spacings of 0.1 inch or less the "S"-distortion is much less and the difference between center and corner focus only about 5 volts. The need for close grid-No. 6-to-photocathode spacings is especially great in anti-ghost tubes because registration of the ghost is so closely dependent on photocathode voltage.

(a) Standard tube.

(b) Anti-ghost tube having grid-No. 6 closer to target.
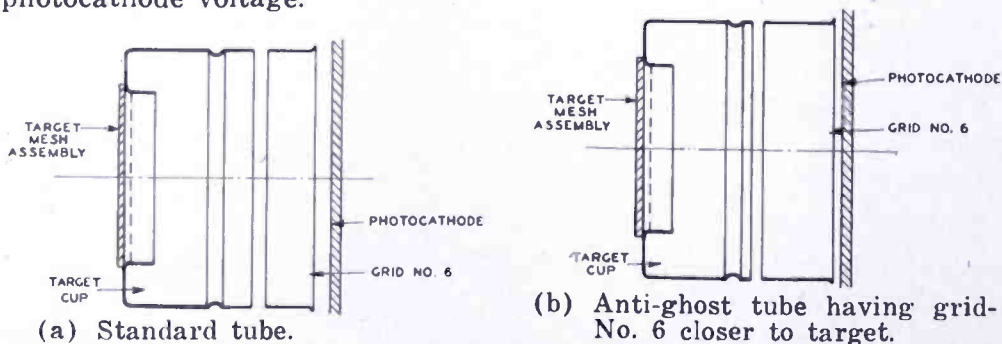
Fig. 14—Photocathode, target, and mesh assembly.

ACKNOWLEDGMENT

SOME DESIGN CONSIDERATIONS OF ULTRA-HIGH-FREQUENCY CONVERTERS*

BY

WEN YUAN PAN

Home Instrument Department, RCA Victor Division,
Camden. N. J.

Summary—A commercially good ultra-high-frequency converter must involve an optimum engineering compromise between many factors, such as cost, oscillator stability, oscillator radiation, freedom from spurious responses, low thermal noise introduced by the converter, etc. These design factors can be modified by the type of tuned circuits, the choice of tubes and crystals and the intermediate frequency used in the converter. The oscillator injection is also an important factor affecting the converter performance when a crystal rectifier is employed as a mixer. These considerations apply equally well to the design of ultra-high-frequency receivers.

Measurements and field observations have indicated that at frequencies between 500 and 890 megacycles, about the same general performance can be obtained by a crystal mixer followed by a low-noise intermediate-frequency amplifier as with a tuned radio-frequency amplifier using commercial tubes. The crystal mixer is favored because of lower cost and a simpler circuit.

The characteristics of the Model "P" experimental ultra-high-frequency converter are described with particular reference to its use in connection with the ultra-high-frequency test which has been taking place at Bridgeport, Connecticut†. This test is being made to investigate the factors governing commercial television broadcasting at ultra-high frequencies.

INTRODUCTION

IT has been proposed that that portion of the frequency spectrum between 500 and 890 megacycles be allocated for commercial television broadcasting in order to satisfy the demand for additional channels. This would add 65 channels to the present 12-channel very-high-frequency (VHF) band. If such a plan is adopted, television receivers will have to tune to both the VHF and the ultra-high-frequency (UHF) channels. The existing television receivers, covering only the VHF channels, can be adapted to receive UHF programs by means of a UHF converter which operates on a double superheterodyne principle and uses one of the VHF channels as the converter intermediate fre-

---

* Decimal Classification: R 583.6 × R 310.

† This test is being conducted by the National Broadcasting Company and the Radio Corporation of America; see R. F. Guy, J. L. Seibert and F. W. Smith, "Experimental Ultra-High-Frequency Television Station in the Bridgeport, Connecticut Area", *RCA Review*, Vol. XI, No. 1, p. 55, March, 1950.

quency. The converter oscillator, in this case, must be tuned to frequencies below the corresponding signal frequencies, to maintain the proper relation between the picture and sound carriers, unless the VHF receiver has a symmetrical intermediate-frequency (i-f) response and intercarrier sound.

The performance requirements of UHF converters differ in many respects from those of VHF receivers due to the fact that the propagation properties of the UHF and VHF waves are different, and also because the UHF converter is operated at much higher frequencies. The work at ultra-high frequencies is still in the exploratory stage and the exact propagation properties of UHF waves are not well known. Early experiments have indicated that a great deal more transmitted power is required to give the same area coverage as obtained on a VHF station.[1,2] An important characteristic of a UHF converter is, therefore, its ability to amplify weak signals to a usable level with a good output signal-to-noise ratio. The output signal-to-noise ratio is generally specified in terms of noise factor which is a measure of how nearly a receiving apparatus approaches the theoretical minimum of residual noise. Since the UHF converter is operated at much higher frequencies, the oscillator frequency drift has to be held within a much closer percentage tolerance. Unless a high intermediate frequency is used in the converter, the radio-frequency (r-f) tuned circuit becomes less effective in rejecting the image and spurious responses as the signal frequency is increased. Consequently, the performance characteristics of converters used for UHF reception would require new design techniques.

Two Basic Converter Designs

1. The first basic design, as shown in the block diagram of Figure 1, consists of an r-f amplifier, a mixer-oscillator, an i-f amplifier and a power supply. The noise factor of the r-f amplifier, using commercial tubes such as the 6J4, 2C43, pencil triode, etc., increases with frequency. The noise factor is increased about 6 decibels when the frequency is increased from 100 to 500 megacycles and 10 decibels from 100 to 890 megacycles. A tuner has been constructed according to the block diagram of Figure 1, using a 6J4 r-f amplifier, a 6J6 mixer-oscillator and two 6AG5 i-f amplifiers, with a 132-138 megacycle

[1] G. H. Brown, J. Epstein and D. W. Peterson, "Comparative Propagation Measurements; Television Transmitters at 67.25, 288, 510 and 910 Megacycles", *RCA Review*, Vol. IX, No. 2, p. 177, June, 1948.

[2] G. H. Brown, "Field Test of Ultra-High-Frequency Television in the Washington Area", *RCA Review*, Vol. IX, No. 4, December, 1948.
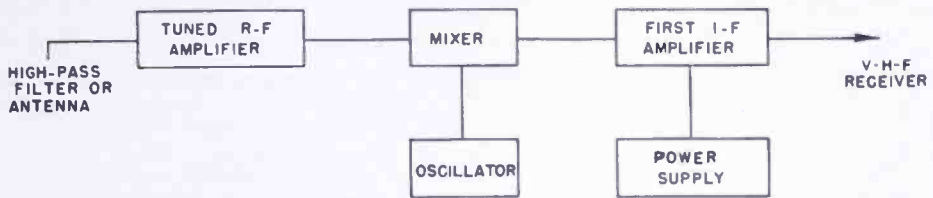
Fig. 1—Block diagram of UHF converter using r-f amplifier.

first intermediate frequency. The tuned r-f amplifier may be fed directly from the antenna or through a high pass filter.

2. The block diagram of Figure 2 illustrates an alternate converter design. It is noted that the r-f amplifier and the mixer are replaced with a crystal mixer. A driven grounded grid i-f amplifier, also known as grounded cathode and grounded grid amplifier, follows the crystal mixer. The noise factor of this type of converter design is determined primarily by the intermediate frequency, because an average crystal mixer introduces a loss of about 8.5 decibels at all frequencies up to 1000 megacycles. When an i-f of 100 megacycles or less is used, the noise factor of the converter with a crystal mixer is approximately the same as with a tuned r-f amplifier. The Model "P" experimental UHF converter uses a G-7 crystal rectifier, and an intermediate frequency centered at 210 megacycles.

The favorable noise factor of a UHF converter with a crystal mixer, compared to that with a tuned r-f amplifier, marks only one of many differences between UHF and VHF reception. The r-f tube effectively suppresses the oscillator radiation through the receiving antenna in VHF receivers, but it is far less effective at UHF. In an oscillator radiation test, the tuner and the Model "P" converter were each connected to a dual-Vee antenna with a gain of 5.7 decibels above that of a ½λ dipole at 530 megacycles. The antenna was 32 feet above ground, and connected to the tuner or converter by a 30-foot, type RG-59/U transmission line. The field intensity meter used was a radar receiver Model APR-4 together with a pencil-triode preamplifier. The receiving antenna used to pick up the oscillator radiation was also of a dual-Vee type 20 feet above the ground, located 100 feet away from the radiating antenna. A 30-foot, type RG-9A/U transmission line was used between the field intensity meter and the receiv-
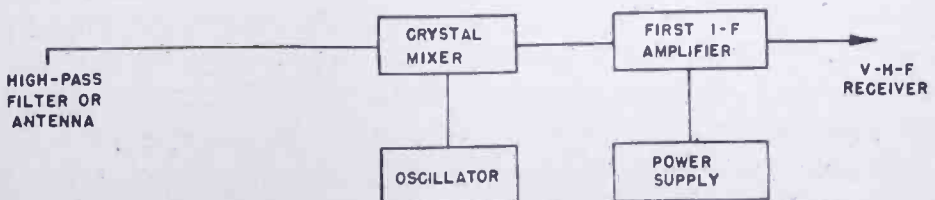
Fig. 2—Block diagram of UHF converter using crystal mixer.

ing antenna. The measured results are as follows:

	r-f Amplifier Tuner		Model "P" Converter	
UHF dial setting	600 Mc.	700 Mc.	600 Mc.	700 Mc.
Oscillator frequency	465 Mc.	565 Mc.	396 Mc.	496 Mc.
Osc. volts at rec. ant.	3000 μv.	37000 μv.	low	low
Osc. power into 72 ohm load	.125 μw.	.19 μw.	low	low
Osc. volts at F.I. meter	9 μv.	70 μv.	low	low
Field intensity at 100 ft.	60 μv/m.	450 μv/m.	low	low

The oscillator radiation from the Model "P" converter was so low that the field intensity meter was not sensitive enough to measure it, whereas the tuner established a field intensity at 100 feet of 60 and 450 microvolts per meter at oscillator frequencies of 465 and 565 megacycles, respectively, in spite of the fact that the tuner has a tuned r-f amplifier. Apparently there are various ways to minimize the oscillator radiation at UHF; the use of a tuned r-f amplifier may not be a principal remedy.

Aside from the favorable performance of a converter with a crystal mixer followed by a driven grounded-grid i-f amplifier, as shown in Figure 2, compared to that with a tuned r-f amplifier of Figure 1, the crystal mixer type of converter is commercially preferred because of its low cost and simplicity in circuit arrangement. It is worthwhile mentioning at this point that the lowest-priced tube acceptable for r-f amplifier operation currently costs several times as much as a germanium crystal rectifier. Therefore, the use of crystal mixers in UHF receiving apparatus seems to be the logical trend for the Industry to follow until better and less expensive UHF tubes are available commercially.

IMPORTANT FACTORS TO BE CONSIDERED IN DESIGNING A UHF CONVERTER WITH CRYSTAL MIXER FOLLOWED BY A DRIVEN GROUNDED GRID I-F AMPLIFIER

From early experiments and previous tests, and from the UHF tests conducted at Bridgeport, Connecticut since the beginning of this year, it has been learned that UHF converters must be designed to have, among other things, a low noise factor, low oscillator radiation, high rejection of spurious responses and a stable local oscillator. To fulfill these major requirements, certain design factors of the converter should be given special attention.

Converter Intermediate Frequency

The converter performance characteristics which are greatly influenced by the choice of the intermediate frequency are, in particular, the noise factor, oscillator radiation and spurious responses. The best intermediate frequency to use in a UHF converter must involve a good engineering compromise between these factors.

Effect on noise factor: The converter noise factor is principally determined by the choice of intermediate frequency inasmuch as the noise factor of an i-f amplifier is a function of frequency but the losses introduced by the crystal mixer and the r-f tuned circuits are approximately constant throughout the entire proposed UHF television band. Under normal operating conditions, the optimum intermediate frequency from the standpoint of noise factor is in the neighborhood of 30 to 40 megacycles. At a higher i-f, the converter noise factor is increased due to the characteristics of the i-f tubes; and at a lower i-f it is also increased due to the characteristics of the crystal mixer. In a practical converter design, the lowest possible converter i-f is 54 to 60 megacycles (channel 2); therefore, some sacrifice in noise factor seems unavoidable.

Effect on oscillator radiation: In contrast to the consideration of noise factor, a higher converter i-f lowers the oscillator radiation.

$$\text{Radiated power through the converter antenna} \propto \left(\frac{\text{r-f band width}}{\text{converter i-f}} \right)^2$$

With the same r-f band width, the oscillator radiation is reduced to one-fourth by doubling the converter i-f. This relation takes into account only the oscillator radiation through the antenna of a converter with one r-f tuned circuit. Direct radiation from the converter chassis is a separate factor and can be minimized by proper shielding of the oscillator.

Effect on spurious responses: A high converter i-f also increases the rejections of image response, cross modulation and other spurious responses. However, when the converter i-f is greater than one-third of the lowest signal frequency, 167 megacycles in this particular case, a new spurious response is introduced at a frequency which heterodynes with the second harmonic of the oscillator to produce a signal at the converter i-f. This interference frequency is inside the proposed UHF television band, therefore, the converter may offer very little discrimination against it, as the r-f tuned circuits may not be sufficiently selective. This new spurious response is called the "osc-2nd-

harmonic image response," the rejection and frequency of which, as measured in a Model "P" converter, are indicated in Figure 3. At a frequency of 630 megacycles, the signal heterodynes with either the fundamental or the second harmonic of the local oscillator to produce a 210-megacycle difference frequency. The amplitude of the i-f signal which is produced by heterodyning the UHF signal with the fundamental of the oscillator frequency is only a few decibels above that of the other i-f signal, which is produced by heterodyning the UHF signal with the second harmonic of the oscillator frequency. To avoid this "osc-2nd-harm. image response," VHF television channels 7 to 13 inclusive are not recommended for use as converter intermediate frequency.
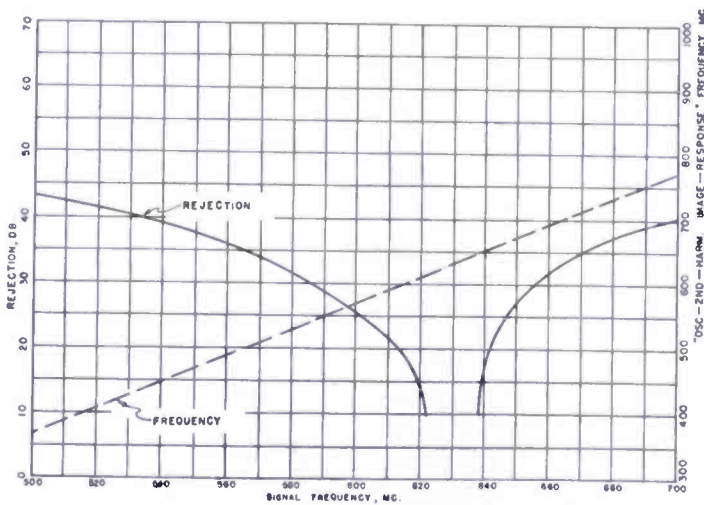
Fig. 3—The rejection and frequency of the "osc-2nd-harm. image-response" of a converter using one r-f tuned circuit and an intermediate frequency centered at 210 Megacycles.

For the best compromise between noise factor, oscillator radiation and spurious responses, an intermediate frequency in the order of 135 megacycles should be employed by UHF converters. A converter i-f outside the VHF television band would, however, require wiring changes and circuit alterations of the VHF receiver upon installation of the converter. Therefore, a converter i-f of 76 to 88 megacycles seems to be the next best choice. A band width of 12 megacycles, covering two adjacent VHF channels, is desirable so that an alternate channel may be used for UHF reception if the other VHF channel happens to be assigned to the location where the converter is installed.

Tuned Circuits

The portion of the frequency spectrum proposed for UHF television service is too high to deal with lumped constants but is too low to be treated with microwave practices. The tuned circuit governs, to a great extent, the stability of the converter oscillator and the rejection

of spurious responses. In extreme cases, when the initial Q of the r-f tuned circuit is very low, the converter noise factor is slightly degraded.

Conventional tuned circuits: Lumped constants, coils and capacitors, work well in the VHF band. At UHF the lead inductance of a capacitor becomes so significant that designers have found it difficult to reproduce results.

The butterfly circuit has a wide frequency coverage and is usable throughout the proposed band. Its application, however, is limited because of the pronounced spurious modes and the difficulty in ganging.
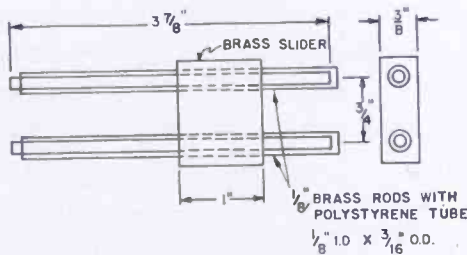
Fig. 4—A constant-C variable-L type of UHF tuned circuit.

A tuned circuit in the form of a coaxial line works well to frequencies above 1000 megacycles. It is a high Q circuit and may be tuned to cover a wide frequency range. The possibility of harmonic generation, and the necessity of using a sliding contact or a non-contacting plunger, are the main objections to its applications at UHF.

Some special tuned circuits: Besides these conventional tuned circuits, numerous special tuning devices have been developed during the past several years, primarily for frequencies from 500 to 1000 megacycles. An early circuit,[3] shown in Figure 4, consists of two silver plated brass rods and a tuning block made of brass. The block is insulated from the rods by a dielectric material and in such a manner that the capacitance between the block and the rods remains constant at any tuning position. This circuit is capable of covering a fairly wide frequency range and works satisfactorily over a substantial portion of the proposed band. At the extreme tuning position, however, the free length of the rods is no longer negligible compared to one wave length. Some loss occurs in the tuned circuit due to the presence of the free length of the rods. Extreme care must also be exercised in making the tuned circuit assembly, as the alignment of the rods relative to the block has to be mechanically exact. A somewhat simpler tuned circuit, which employs two shaped copper foils cemented to a bakelite tubing, is used in the Model "M" tuner[4] and is illustrated in Figure 5. The effective inductance and the capacitance between the conductors are varied by means of a brass core. By properly shaping

---

[3] This form of tuned circuit was developed by V. D. Landon and J. E. Eckert, and described in an unpublished report dated September 20, 1948.
[4] T. Murakami: "An Experimental Ultra-High-Frequency Television Tuner", *RCA Review*, Vol. XI, No. 1, p. 68, March, 1950.

Fig. 5—A variable-C and variable-L type of UHF tuned circuit.

the copper foil, the r-f and the oscillator can be tracked without much difficulty even with an intermediate frequency as high as 210 megacycles. According to field reports from Bridgeport, this circuit, when it is operated without special modifications, seems to have a long time frequency drift which is probably caused by the moisture absorption of the bakelite tubing. Since it is necessary to limit the tubing dimensions to a size that is small compared to a wave length at UHF, the frequency coverage is limited. The constructional details of a later device[5] developed by the writer is indicated in Figure 6. This takes advantage of the well known series resonant property of the circuit inductance and capacitance to tune through the proposed band. The circuit is comprised of a fixed effective inductance element and a variable capacitor. The tube constants such as the grid to plate capacitance and the electrode lead inductances constitute a part of the tuned circuit. To cover the band, the circuit employs a pair of brass or silver plated brass or kovar wires 1/16 inch in diameter, separated by 1/4 inch, and a specially constructed capacitor which is variable from .5 to 5.0 micromicrofarads by means of a ceramic tubing and a brass core. Low-loss dielectric material is essential for stable oscillator
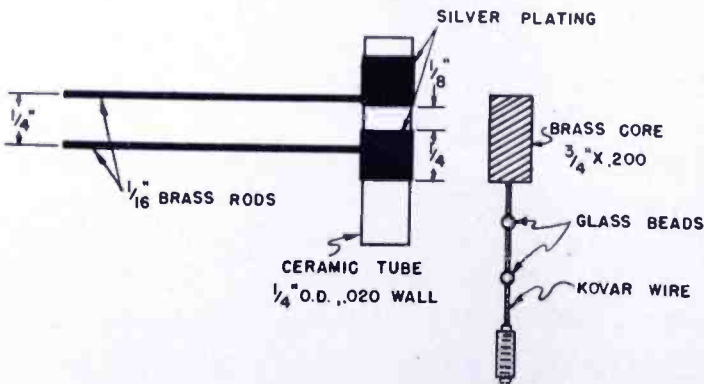
Fig. 6—A series-resonant type of UHF tuned circuit.

[5] A similar oscillator circuit was simultaneously but independently worked out by J. M. Pettit of Stanford University. See "Ultra-High-Frequency Triode Oscillator Using a Series-Tuned Circuit", *Proc. I.R.E.*, Vol. 38, No. 6, pp. 633-635, June, 1950.

operation as the negative resistance of the oscillator tube is generally low, especially at the higher frequency end of the band. This circuit can readily be shielded to suppress direct oscillator radiation from the chassis.

Oscillator Injection

The performance of a crystal-mixer converter relies, to a great extent, on the uniformity and the amplitude of oscillator injection, as it affects the matching in the r-f and i-f tuned circuits, the conversion loss and excess temperature noise of the crystal and the oscillator radiation.

Impedance matching: The crystal sees a certain impedance from the r-f circuit and sees another impedance from the i-f circuit. The impedances of the r-f and i-f tuned circuits must be designed to match
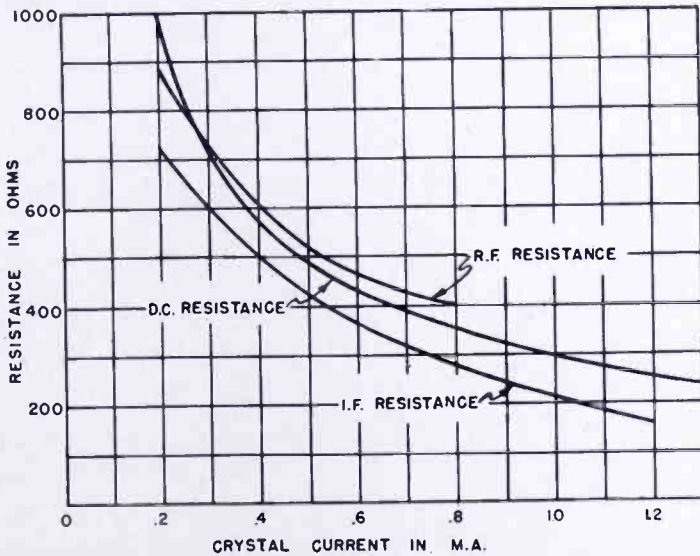
Fig. 7—The variations of r-f, i-f and d-c resistance of a typical G-7 crystal rectifier with oscillator injection.

the corresponding impedances of the crystal mixer under operating conditions. At a given crystal excitation power, the crystal presents one impedance to the r-f circuit and another impedance to the i-f circuit. These r-f and i-f impedances of the crystal mixer vary greatly with its excitation power. Such variations for an average G-7 germanium crystal are illustrated in Figure 7, from which it may be seen that the r-f crystal resistance varies from 900 ohms with an excitation power corresponding to a crystal current of .2 milliampere to 400 ohms with that corresponding to a crystal current of .8 milliampere. Similarly, the i-f resistances under these conditions are 700 ohms and 300 ohms respectively. With conventional methods of oscillator coupling, the oscillator injection, and hence the crystal excitation power, may vary over wide limits which would introduce severe losses due to mismatching in the r-f and i-f tuned circuits.

Conversion loss and excess temperature noise: Uniform oscillator injection not only minimizes the r-f and i-f impedance mismatch, it also improves the efficiency of the mixer performance. In general, the loss of a crystal mixer consists of the conversion loss and the loss due to the excess temperature noise. In the frequency-conversion process not all of the available power in the r-f signal is converted into power at the intermediate frequency. Some power is lost during the conversion process. This conversion loss is high with insufficient oscillator injection, but it becomes practically independent of oscillator injection if more than sufficient excitation power is provided. For crystals such as the 1N21B silicon and G-7 germanium, an excitation power of 500 microwatts, corresponding to a crystal current of approximately .5 milliampere, is considered as sufficient oscillator injection. In addition to the conversion loss, the crystal, when driven by a local oscillator, generates more noise than the noise produced by an equivalent resistor. This excess temperature noise of a crystal mixer is inversely proportional to the intermediate frequency but it increases with the amount of crystal excitation power. For a given intermediate frequency, there is an optimum level of oscillator injection where the combined conversion loss and the excess temperature noise of the crystal is a minimum.

It appears to be possible to improve the mixer efficiency by applying a direct-current voltage to the crystal in the proper polarity together with a low oscillator injection, on the theory that the crystal might present a conversion loss equivalent to that with sufficient oscillator injection because of the direct-current voltage, and at the same time the excess temperature noise might be lowered. However, results from measurements made on two types of converters having i-f's at 210 and 60 megacycles respectively showed very little improvement in mixer efficiency with this arrangement over that of normal operation. On the other hand, this arrangement may be helpful from the standpoint of oscillator radiation.

Oscillator radiation: One of the major advantages of the crystal mixer is the possibility of supplying a lower excitation power from the local oscillator for efficient mixer operation. A lower excitation power leads to a lower oscillator power being radiated through the converter antenna. Direct chassis radiation depends largely upon the shielding of the oscillator circuit, the oscillator frequency, the type of oscillator circuit and the chassis dimensions. Measurements made in accordance with the RMA specifications for oscillator radiation revealed the fact that the chassis radiation from a 340-megacycle unshielded oscillator in a $8 \times 7 \times 2\frac{1}{2}$ inch chassis was as much as 2000 microvolts per meter from a $\frac{1}{2}\lambda$ dipole at a distance of 100 feet. The

field strength was reduced to 200 microvolts per meter with a partial shield. When the oscillator was set at 450 megacycles, however, the chassis radiation was too low to be measured with or without the shield. When the oscillator circuit is well shielded and chassis dimensions properly proportioned, the oscillator radiation through the converter antenna is more or less under the designer's control and the amount is roughly computable. With a fixed amount of crystal excitation power, the radiated power varies directly with the square of the r-f band width and inversely with the square of the intermediate frequency. The narrower the r-f band width, or the higher the intermediate frequency, the less the radiated power will be. By knowing the radiated power, then the

$$
\begin{matrix} \text{Field strength, in volts per meter,} \\ \text{from } \frac{1}{2}\lambda \text{ dipole at a distance } d \text{ in} \\ \text{the direction of maximum radiation} \end{matrix} = \frac{23 \sqrt{\text{Radiated power in watts}}}{\text{Distance in feet}}
$$

To keep the field strength, at a distance of 100 feet, less than 15 microvolts per meter, which is the suggested limit on oscillator radiation, the radiated power must be kept below .004 microwatt. A field strength of 15 microvolts per meter corresponds to a signal of 1.5 microvolts from a $\frac{1}{2}\lambda$ dipole across a matched load of 75 ohms at 500 megacycles. Such a signal may not cause trouble to other services or interference to neighboring reception. The ratio of field strength, E_f, at the $\frac{1}{2}\lambda$ dipole to the signal strength, E_s, from a $\frac{1}{2}\lambda$ dipole across a matched resistance R_0, is a function of R_0 and frequency f.

$$
\frac{E_s}{E_f} = \frac{5.58 \sqrt{R_0 \text{ (ohms)}}}{f \text{ (mc)}}
$$

It is seen that the corresponding signal strength from a $\frac{1}{2}\lambda$ dipole across a matched load of 75 ohms is 3.7 microvolts at 210 megacycles or 12.5 microvolts at 60 megacycles.

Types of Crystals and Tubes

There are many types of commercial crystal rectifiers available at the present time which may be used as mixers at frequencies up to 1000 megacycles. The 1N21B (silicon), G-7 (germanium) and CK-710 (germanium) are the logical choices on the basis of mixer performance and cost. The frequency response of these crystals is practically uniform from 5 to 500 megacycles and is down about 1 decibel at 1000 megacycles. The germanium crystals are far less expensive, generally

capable of withstanding a higher inverse voltage, and have the peculiar ability of self-healing in cases where the crystals have been electrically broken down. On the other hand, the 1N21B silicon crystal has less conversion loss. Measurements have been made on fairly large quantities of 1N21B, G-7 and CK-710 crystals and it has been found that the average mixer loss of the 1N21B crystal is about 6.5 decibels while that of the germanium crystals, G-7 and CK-710, is about 8.5 decibels at 600 megacycles. Some selected germanium crystals performed just as efficiently as the 1N21B silicon crystals however.

The G-7 crystal stands the highest peak inverse voltage, in the order of 5 volts compared to about 2 volts for the 1N21B and the CK-710 crystals, and its average direct-current characteristic approximates the relation

$$I = 55 \times 10^{-6} \left[\epsilon^{10(V-RI)} - 1 \right]$$

where I is the current in amperes and V the voltage in volts applied across the crystal and R is the spreading resistance. The spreading resistance of the G-7 crystal, which is a linear resistance in the semi-conductor resulting from the constriction of the current-flow lines in the semi-conductor near the contact, is about 10 ohms. The measurements also indicated that the conversion loss of G-7 crystals correlates, to a certain degree of consistency, with their direct-current characteristics. This fact, however, might be incidental to the particular samples being measured. If this correlation holds true for a large quantity of production units, it may be possible to preselect the G-7 crystal rectifiers by a relatively simple means.

The proposed opening of the UHF television band reveals the need of further advances in the technique of making electron tubes — tubes for UHF applications with lower noise factor, higher transconductance, etc. Several new types of UHF tubes are now under development. Up to the present time commercial tubes such as the 12AT7, 2C51, 6J4, 5703, etc., may be used as oscillators for frequencies below 700 or 800 megacycles. The pencil triode (RCA 5876) oscillates at frequencies up to and beyond 1700 megacycles; the 6F4, 1200 megacycles; and an RCA developmental tube having a 6F4 mount housed in a miniature bulb, at about 1000 megacycles. These tubes have great possibilities for use as UHF oscillators. The choice of tubes for driven grounded grid i-f amplifier operation is not as limited as in the case of UHF oscillators. For an intermediate frequency of 100 megacycles or less, the 12AT7 or the 2C51 is probably satisfactory. At higher i-f's the capacitance between the anodes or between the anode and cathode of the twin triodes unavoidably degrades the ampli-

fier performance. In this case, two triodes in separate envelopes are recommended. Recently RCA has been developing a new twin-triode with special precaution to minimize the inter-anode capacitance and to improve other factors essential to driven grounded grid operation.

The factors thus far considered, namely the choice of the intermediate frequency, the type of tuned cricuit, the oscillator injection and the types of crystal and tubes, are important for the design of a UHF converter with a crystal mixer followed by a driven grounded grid i-f amplifier. It is noted that each factor involves a compromise between the various performance requirements or between cost and performance. There are also cases where a converter is designed for special purposes. Under these conditions, certain performance requirements are to be given special weight. To illustrate the various converter characteristics more specifically, and present the measured and observed results, the Model "P" experimental UHF converter will be described.

Model "P" Experimental UHF Converter

The Model "P" experimental UHF converter was developed for use in conjunction with the demonstration of the dot-sequential color television system before the Federal Communications Commission in Washington, D.C., and also for the UHF tests in Bridgeport, Connecticut. The Washington and the Bridgeport transmitters are operating at frequencies of 523-529 and 529-535 megacycles respectively. The Model "P" converter was, therefore, designed to be continuously tunable through the range of 500 to 700 megacycles. The converter is self-contained and requires no wiring changes upon installation. The complete circuit diagram is shown in Figure 8, and a top view and a bottom view of the converter chassis in Figures 9 and 10 respectively.

Intermediate Frequency

An i-f band from 204 to 216 megacycles was chosen so as to enable the VHF receiver to use either channel 12 or 13 for UHF reception. The relatively high i-f made it possible to obtain high rejections of image and spurious responses and low oscillator radiation with only one r-f tuned circuit. The oscillator tuned from 290 to 490 megacycles and a 6J6 was selected as the oscillator tube on the basis of cost and attainment of the necessary frequency range within the ratings of the tube. The lower oscillator frequency, because of the high i-f, made the microphonic tendency and oscillator drift less accentuated. These advantages were obtained, however, at the expense of about 3 decibels higher noise factor due to the choice of 210 megacycles instead of 60
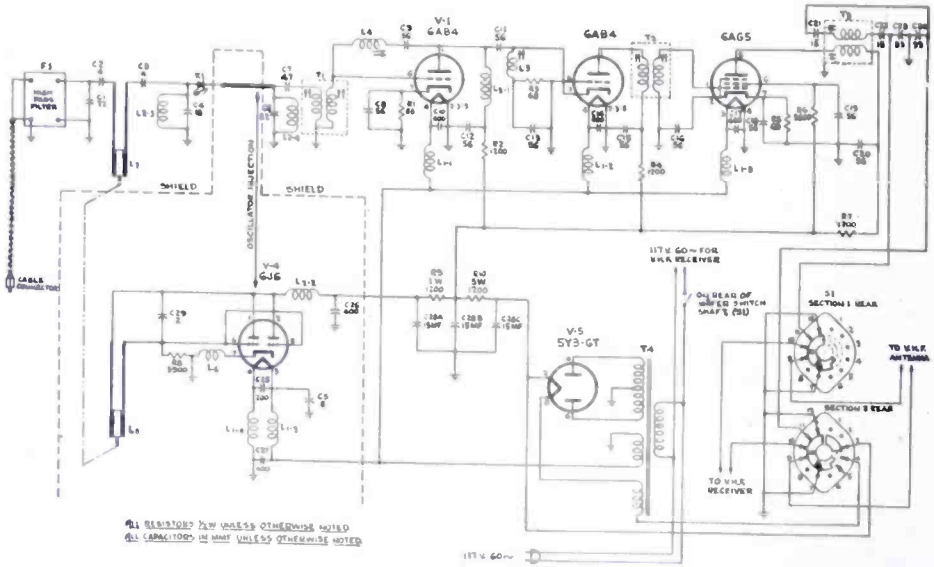
Fig. 8—Schematic diagram of the Model "P" experimental UHF converter.

megacycles i-f, which also introduces the "osc-2nd-harmonic image response." The rejection of this response at frequencies in the neighborhood of 630 megacycles is extremely low as indicated in Figure 3. For the purpose for which this converter was designed, the "osc-2nd-harmonic image response" is not objectionable.

R-F and Oscillator Tuned Circuits

The UHF input signal is fed to a high-pass filter through a 75-
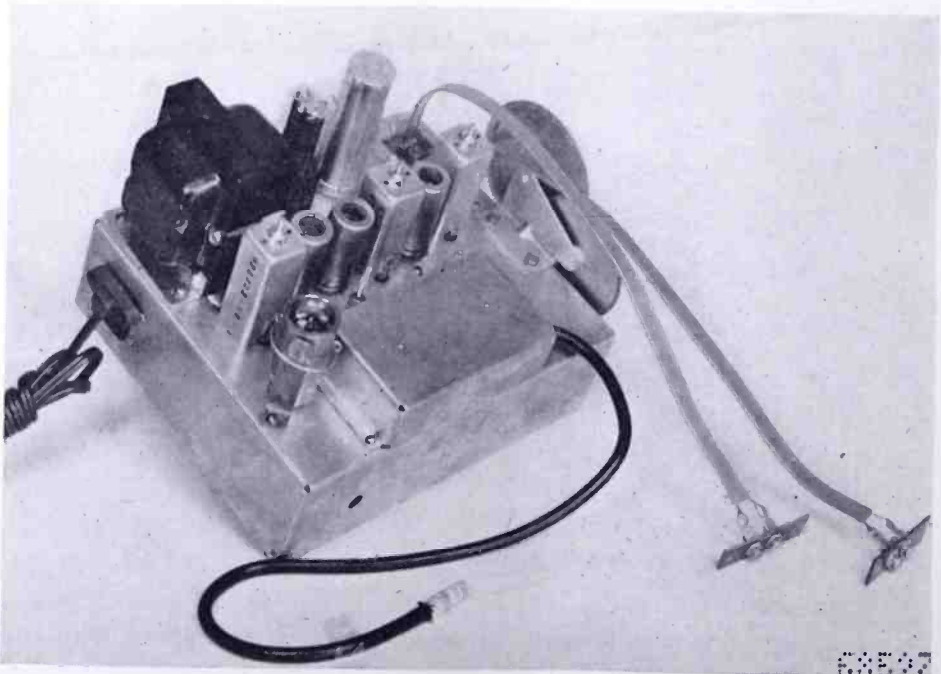
Fig. 9—Converter chassis, top view.

ohm coaxial cable. The filter cuts off at about 485 megacycles and it has an insertion loss of about 2 decibels in the pass band. The r-f tuned circuit, shown by Figure 5, consists of two shaped copper foils of .0025 inch thickness cemented on a bakelite tubing .251 $\times$ 3 inches and a brass core .249 $\times$ 1¼ inches. This circuit, together with impedance transformation networks to maintain proper matching, serves as a selective coupling device between the filter and the crystal mixer. Under these conditions, the r-f band width is approximately 18 megacycles which corresponds to an operating Q of the tuned circuit of 35; and a fairly low and uniform standing-wave-ratio is observed
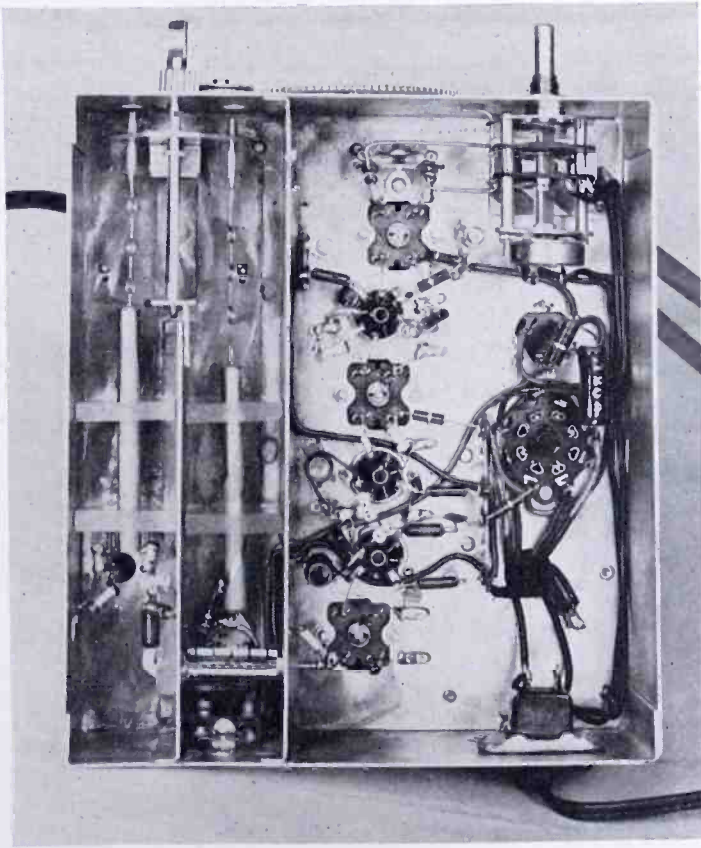
Fig. 10 — Converter chassis, bottom view.

throughout the entire tuning range. The selectivity of the r-f tuned circuit, with the aid of the high-pass filter, effectively rejects the image and other spurious responses such as the direct i-f feed-through, ½ i-f and ⅓ i-f responses. The ½ i-f and ⅓ i-f responses are formed by the generation of second and third harmonics respectively, during the conversion process in the G-7 germanium crystal mixer. Curves representing the rejections of image, direct i-f, ½ i-f and ⅓ i-f responses are shown in Figure 11. It is noted that all such responses are considerably more than 60 decibels below the response of the desired

signal. The construction of the oscillator tuned circuit is similar to that of the r-f tuned circuit except for the shape of the copper foils. The copper foils of the oscillator tuned circuit are shaped in the form of a bifilar winding for tracking purposes, thus also reducing the oscillator radiation to some extent as the fields produced in the oscillator circuit are partially cancelled.

Oscillator Injection

As shown by Figure 8, the crystal mixer is connected to the driven grounded grid i-f amplifier, which uses two 6AB4 tubes, through a $3\frac{1}{4}$-inch length of #16 copper wire and an effective terminating capacitance of about 12 micromicrofarads. The inductance of this wire is in series resonance with the terminating capacitor approximately
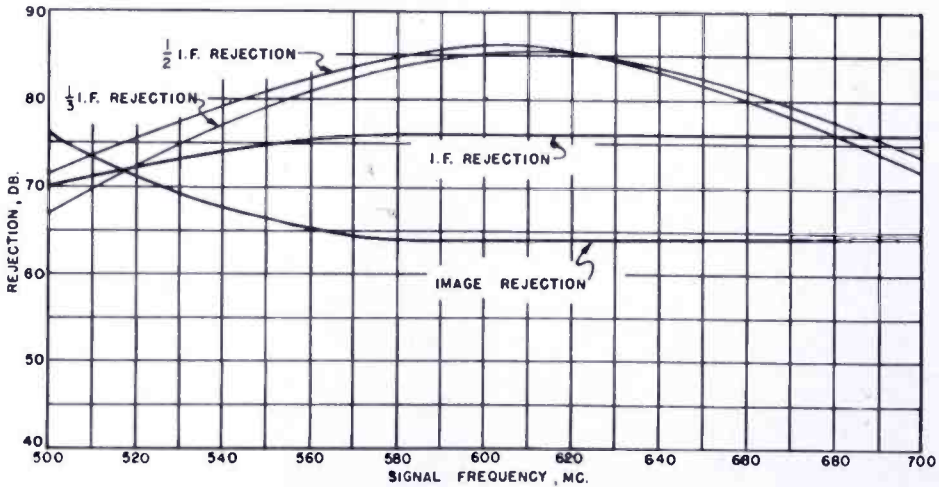
Fig. 11—Rejection of spurious responses.

at the intermediate frequency. The wire and the terminating capacitor also serve as a pick up circuit for oscillator injection to the crystal mixer. The oscillator signal being picked up under these conditions varies considerably with frequency. These variations alter the crystal impedances presented to the r-f and i-f circuits. Wide variation of oscillator injection also degrades the mixer performance as the optimum operating range of most crystal rectifiers is limited. The 1N21B, for instance, will perform most efficiently if the oscillator injection is such that the rectified direct current is within the range .5 to 1.0 milliampere. The optimum operating range for the G-7 crystal is .5 to 1.5 milliamperes. The higher operating limits of both crystals may be extended if the intermediate frequency is higher than 167 megacycles; however, strong oscillator injection is always undesirable from the standpoint of oscillator radiation.

Oscillator-Injection Equalizer

In this experimental converter, an oscillator-injection equalizer is used which, insofar as oscillator injection is concerned, is a band-pass filter of broad cut-off characteristic. The pass band occurs at frequencies where the amplitude of the normal oscillator injection, without the equalizer, is a minimum, thus producing a far more uniform injection throughout the entire tuning range. A picture showing the construction of the equalizer and how it is connected in place, in a Model "P" converter, is given in Figure 12. The equalizer is in the form of a hollow brass cylinder with a number of narrow slots and a large opening. The equalizer is soldered to the oscillator shields and encloses the wire which connects the crystal mixer to the i-f amplifier.
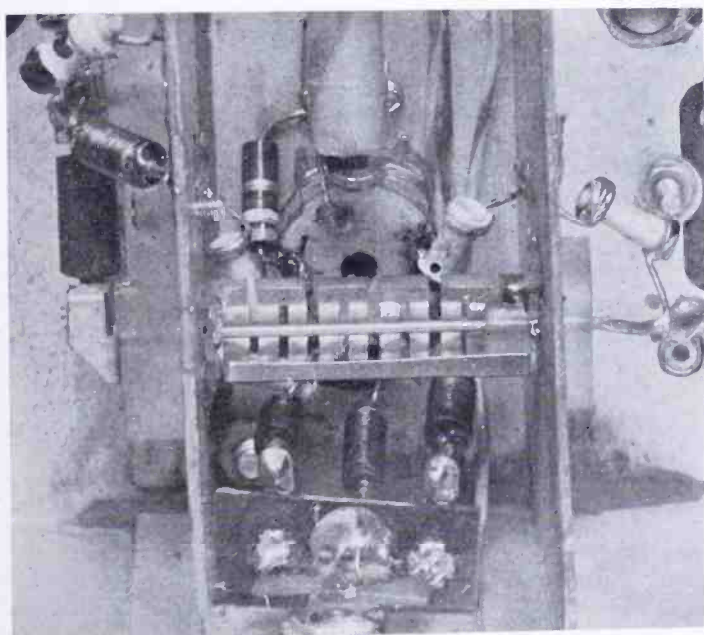
Fig. 12—An oscillator-injection equalizer connected in place in a model "P" converter.

The equalizer also operates as a shield to regulate the amplitude of oscillator injection at all frequencies. By varying the constructional details of the equalizer, the optimum oscillator injection may be obtained without changing its band pass characteristics. The broad cut-off characteristic is caused by the fact that current is flowing through the slotted elements in both directions. This characteristic is desirable in order to widen its useful operating range.

Typical curves indicating the variations of r-f resistance and i-f resistance of the G-7 crystal due to the change in oscillator injection are plotted in Figure 13 for the Model "P" converter without the equalizer. The improvement brought about by use of the oscillator-
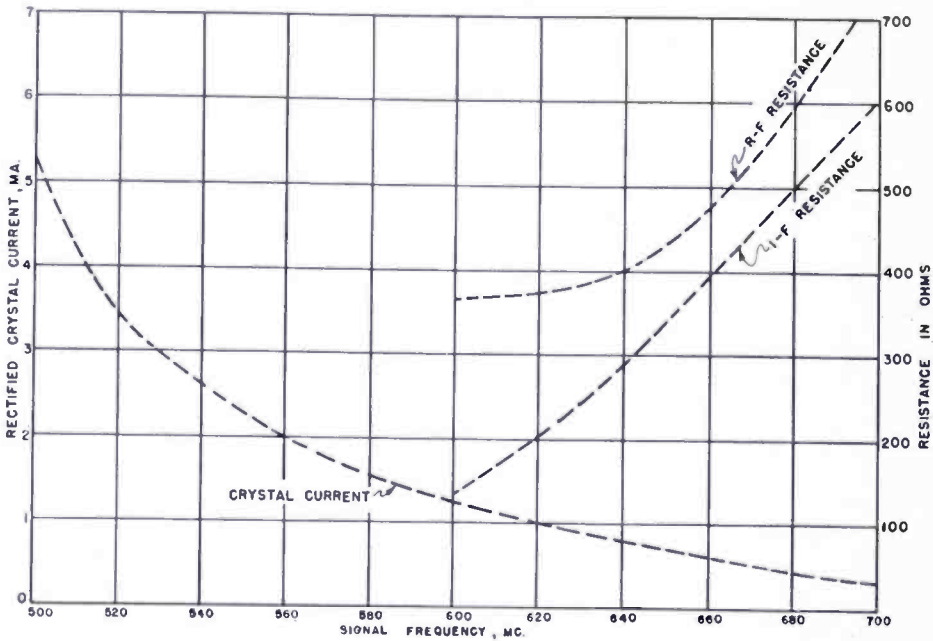
Fig. 13—The variations of crystal r-f and i-f resistance of the model "P" converter without the oscillator-injection equalizer.

injection equalizer can readily be seen by comparing Figures 13 and 14. With the equalizer, the maximum variation of the r-f resistance throughout the entire frequency range varies from 410 ohms at the low frequency end to 380 ohms at the high frequency end. The corresponding variation in i-f resistance is 330 to 150 ohms. Further-
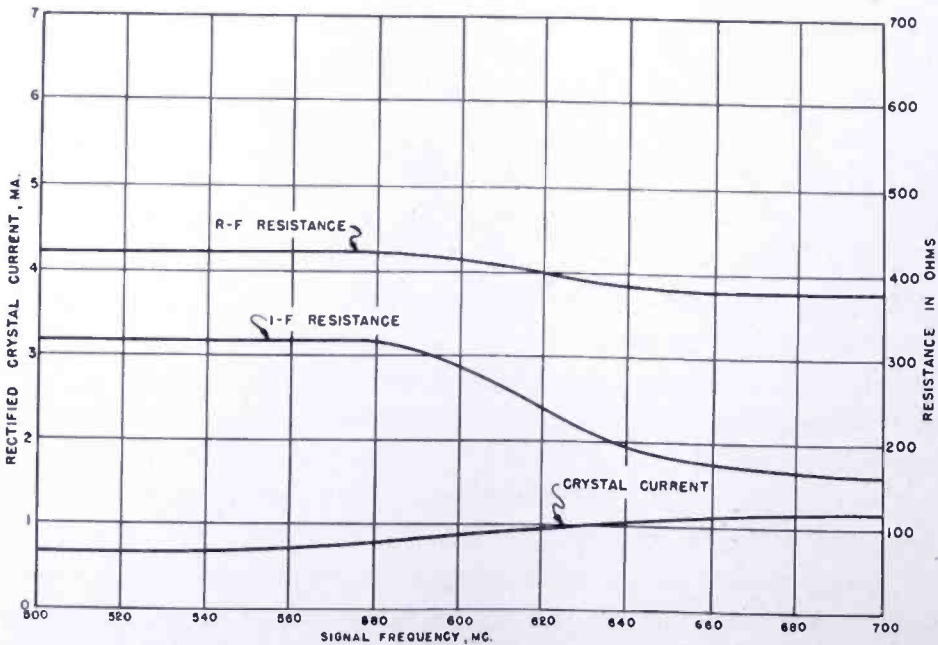
Fig. 14—The variations of crystal r-f and i-f resistance of the model "P" converter with the oscillator-injection equalizer.

more, the oscillator injection always falls within the optimum operating range of the G-7 crystal.

Oscillator Stability

The oscillator frequency drifts as much as 1000 kilocycles over a period of $\frac{1}{2}$ hour from a cold start. The long time drift is probably caused by the moisture absorption in the bakelite tubing. In actual operation, the heaters of the oscillator and the i-f tubes are kept hot even during the standby periods. This arrangement may shorten the life of the tubes, but the power dissipated from the heaters raises the temperature of the oscillator to such a point that the oscillator does not drift too much thereafter. The heater power also helps dry the bakelite tubing so that the oscillator frequency becomes fairly stable within a relatively short period of time. Under actual operating conditions, the maximum drift at 530 megacycles is 100 kilocycles and it becomes stable in a period of three minutes. According to reports from Bridgeport, the frequency stability of this experimental converter is quite satisfactory. Curves showing the oscillator warm-up drift as a function of time at 500, 600 and 700 megacycles from a cold start and with the heaters on, are plotted in Figure 15. In this converter, the frequency drift is improved by a ratio of approximately 10 to 1 by leaving the heaters on.

Oscillator Radiation

Since the cut-off frequency of the high-pass filter is at about 485 megacycles, it helps attenuate the oscillator radiation through the converter antenna except at frequencies close to 700 megacycles. The filter together with a relatively narrow r-f band width, a high intermediate frequency and a uniform oscillator injection, limits the radiation to less than 20 microvolts per meter from a $\frac{1}{2}\lambda$ dipole at a distance of 100 feet at frequencies from 500 to 650 megacycles; and 50 microvolts per meter at 700 megacycles. Direct chassis radiation is small at frequencies above 600 megacycles; but it is quite high at 544 megacycles, the amount being dependent upon how well the oscillator is shielded. With a partial shield, a field strength of 200 microvolts per meter at 100 feet was observed. If a better shield is used, the amount of radiation will be reduced.

I-F Amplifier

The i-f amplifier, shown in Figure 8, consists of a driven grounded grid stage, using two 6AB4 tubes, and a pentode stage, using a 6AG5 tube. The i-f transformers are more or less conventionally constructed; a typical production sample is shown in Figure 16, with 4 turns of

#19 wire on the primary and 3 turns of #19 wire on the secondary. The complete i-f system has six tuned circuits which effectively prevent any interactions between the harmonics of the local oscillator in the VHF receiver and the converter oscillator. The converter i-f selectivity is shown in Figure 17A; the response is uniform within 1 decibel from 204 to 216 megacycles. A typical i-f response curve of a VHF receiver is given in Figure 17B. The pentode i-f stage raises the converter gain, thus lowering the operating sensitivity of the VHF
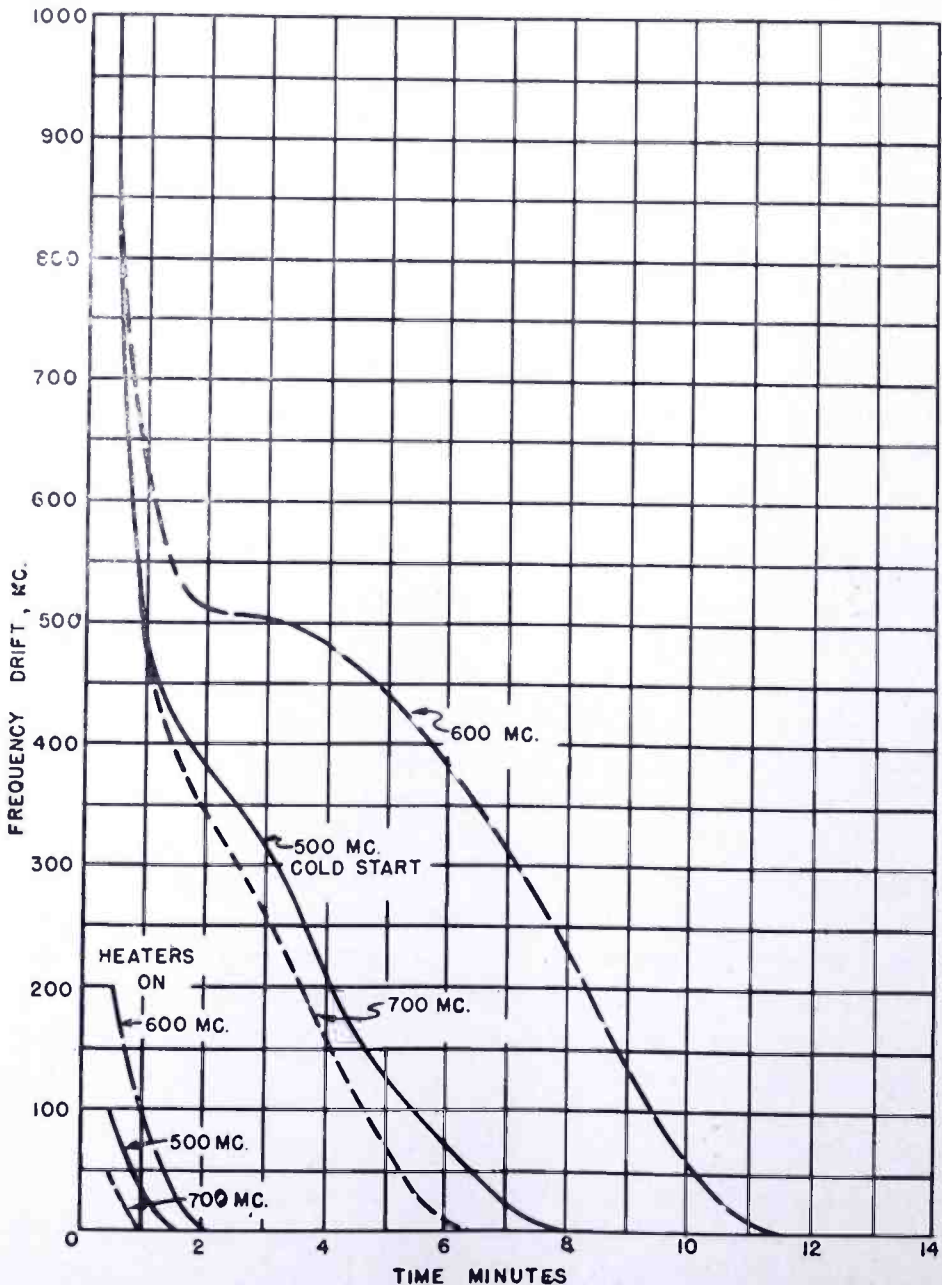
Fig. 15—Oscillator warm-up drift of the model "P" converter.

receiver. Consequently, the possibility of picking up VHF signals is minimized and the noise present in the VHF receiver would not appreciably influence the noise factor of the converter.

Noise Factor

The i-f amplifier has an average noise factor of 6.5 decibels and a gain of 26 decibels. Since the noise factor of an average VHF receiver is about 13 decibels on channels 12 or 13, the converter i-f amplifier will have a combined noise factor according to the following relation:

$$\begin{matrix} \text{combined N.F.} \\ \text{(converter i-f} \\ \text{and VHF receiver)} \end{matrix} = \text{(converter i-f)} \frac{\text{N.F.}}{} + \frac{\text{VHF receiver N.F.} - 1}{\text{gain of converter i-f}}$$

$$= 4.47 + \frac{19.9 - 1}{400} = 4.52 \text{ or } 6.55 \text{ decibels.}$$

Fig. 16—Production sample of a 210-megacycle i-f transformer.

With 8.5 decibels mixer loss and about 3 decibels loss in the high pass filter and the r-f tuned circuit, the overall converter noise factor is in the order of 18 decibels, and remains fairly constant throughout the entire frequency range.

Bridgeport Test

Up to May 22, 1950, over thirty installations of the Model "P" experimental UHF converters had been completed. These converters are scattered over a large area, under widely different terrain conditions. The report on these tests will be made by the National Broadcasting Company when completed.

CONCLUSION

The design considerations of UHF converters apply equally well to UHF receivers. A UHF receiver functions as a combined UHF converter and a VHF receiver. The tuner of a UHF receiver which is similar to UHF converter both in function and in design is an integral part of the receiver instead of being a separate unit. The only
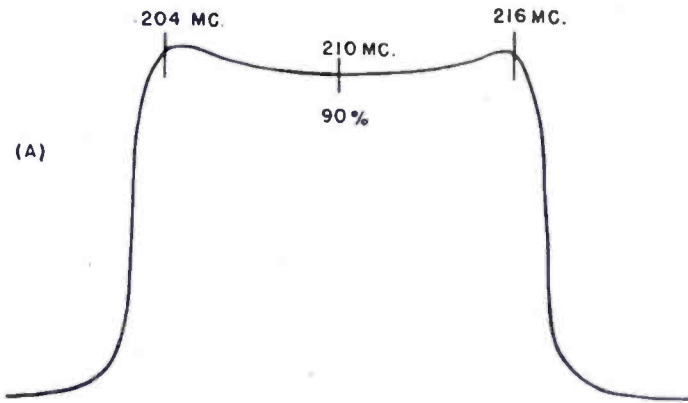
Fig. 17—Selectivity curves; (A) model "P" converter, (B) a typical i-f response of a VHF television receiver.
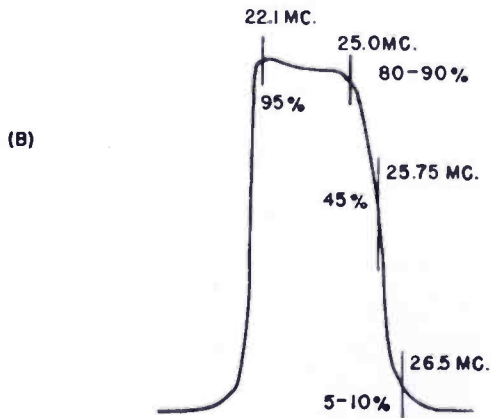
important difference between the design of a UHF receiver and a converter is the fact that it is possible to use only one intermediate frequency in a receiver for both UHF and VHF reception. An intermediate-frequency band from 41 to 47 megacycles has been proposed for such receivers.

ACKNOWLEDGMENT

THE ORTHOGAM AMPLIFIER*

By

C. L. Townsend and E. D. Goodale

Engineering Department. National Broadcasting Co., Inc.,
New York

Summary — *The problem of gradient correction in the television film transmission system is analyzed and the system transfer characteristic, as determined experimentally, is presented — correction amplifiers having adjustable amounts of compensating non-linearity in the light gray and white portions of the picture signal are described.*

General Considerations

PRIOR to World War II it was conceded generally that the technical quality of television film transmission was superior to that of direct pickups, due in large measure to the compromise that was necessary in live studio operation between scene brightness required for best results by the relatively insensitive studio cameras then in use, and the brightness which could actually be provided without serious discomfort to performers caused by heat and glare. However, with the development of the image orthicon camera for direct pickup, and its rapid improvement following the war, the situation has changed, so that today the technical quality obtainable from direct pickup is actually somewhat superior to that generally obtained from film reproduction.

The introduction of kinescope recordings as a means of television program syndication put further demands on film reproducing systems. To fill this new need, a complete recording and reproducing system having very low total picture degradation is required since the original signal is already restricted in range and resolution by its first passage through the television system.

The experience of several years' operation showed that most criticism of film picture reproduction concerned blank (saturated) or chalky faces, and flare. With an average good iconoscope, during its normal service life, the flare problem could be reduced substantially by edge-light techniques and by controlling film maximum densities. The problem of white compression, however, was not amenable to any generally known treatment. In photographing motion pictures for television use, faces could be made to "go dark" on the film, with some desirable results, but usually that method was difficult to use, and

---

* Decimal Classification: R583.14.

often increased flare. In kinescope recording the problem could be even worse, since in some cases it was not possible to control the original pickup conditions for best kinescope recording results, with the consequent possibility that some white compression would be present in the incoming video voltages in the recording channel. A method of minimizing these additive compressions was needed.

BASIS FOR GRADIENT CORRECTION

For some time it has been known that iconoscope film pickup tubes[1, 2] do not produce video voltages ideally suited for reproduction by a normal kinescope unless gradient correction is applied. A re-evaluation of the transfer characteristic required in the television transmission system for optimim picture quality was undertaken, to include conditions actually encountered in normal commercial broadcast operation.

A series of slides was produced, each having an "average gray" background (density about 1.2) and, centered in that area, a rectangular "window". Each slide was made with a different window density, to cover the range normally encountered in practice. The slides were projected in succession, and in such a way that the same portion of the mosaic was used for each window. Oscilloscope amplitude readings produced the curve of Figure 1. This curve closely approximates that given for the average iconoscope gradient characteristic[*] over the actual operating range. From Figure 1 it can be seen that, under the best conditions, the iconoscope output voltage is a fairly linear function of film image density. Of course, other iconoscopes may have somewhat different characteristics, and a survey of all tubes in NBC service throughout the country shows this to be true. However, the reproduced curve appears to be a reasonable average, and constitutes a fair basis for initial design work if the limits of variation are borne in mind.

If a film pickup device produces an output voltage which is a linear function of film density, then, by definition, that voltage is a linear function of the logarithm of the input light energy. To recreate those original energies on the face of a kinescope, the logarithm of its light output energy must be linearly related to its control grid voltage. Thus a logarithmically responsive system would be created, with essentially complementary transductions occurring at its input and output.

---

[1] O. H. Schade, "Electro-Optical Characteristics of Television Systems", *RCA Review*, Vol. IX, Nos. 1, 2, 3, 4, March, June, September, December, 1948.

[2] D. G. Fink, "Brightness Distortion in Television", *Proc. I.R.E.*, Vol. 29, No. 6, June, 1941.

[*] RCA Tube Handbook, sheet 92 CM-6581.

Reference is made to the standard characteristics curve of a 10BP4 kinescope. In this chart*, grid volts are plotted against output in foot-lamberts, on a linear basis. However, the eye does not respond to output energy linearly, but rather logarithmically. Consequently, to obtain a more useful visualization of the effective kinescope transfer characteristic, the indicated values are replotted in Figure 2. Here, a semi-log plot of the characteristic shows severe white compression which, in fact, is realized in operation. In other words, this typical kinescope, without gradient correction, does not meet the ideal requirement postulated in the preceding paragraphs.
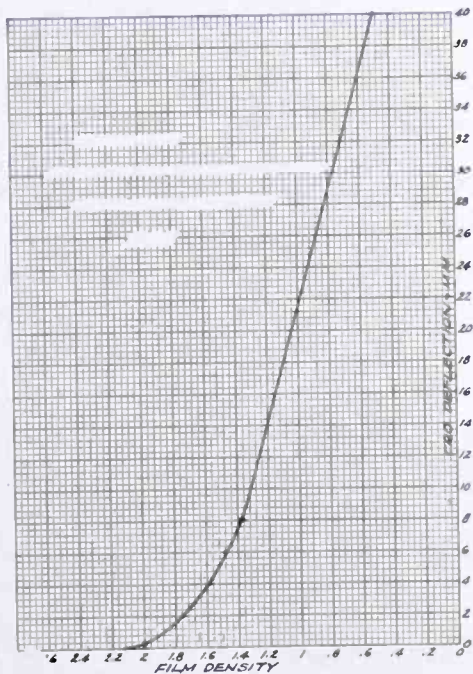
Fig. 1—Film density versus output voltage of an iconoscope with normal illumination.
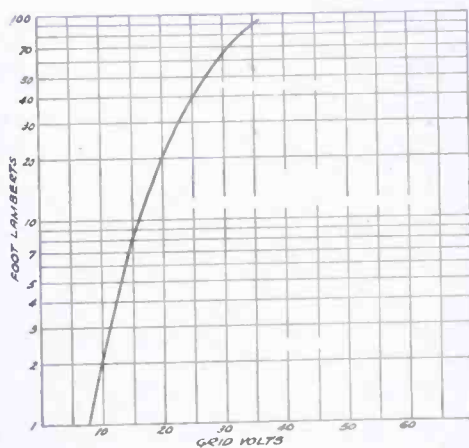
Fig. 2—Semi-log plot of light output versus grid volts of 10BP4 kinescope.

The kinescope recording portion of this study was begun by adopting a somewhat novel viewpoint on the process. Much had been written on tone-rendition in kinescope recordings, but that concept was discarded in favor of the idea that the overall recording-reproducing system was intended to accept a given voltage range on its input terminals, and was required to deliver that same voltage range at its output terminals, with minimum electrical distortion — in other words, to be as nearly "transparent" as possible. The desirable transfer-characteristic is, then, a straight line when input volts are plotted against output volts, on linear coordinates.

To determine the characteristic which is actually obtained in the existing recording-reproducing system, a "window" test was again used. A video voltage, representing the window and an appropriate back-

* RCA Tube Handbook, sheet 92 CM-6675.

ground, was fed to the recording system. The amplitude of the voltage of the window proper could be precisely controlled to produce any value within the normal recording range, plus some excess into overload values, if desired. A recording was made of this signal, and the film processed normally. That film was then reproduced on an iconoscope system, and the output voltage values noted. The resulting plot is shown in Figure 3, and includes a wider range than is normally used. Again a serious compression of white-range voltages is present. All transfer characteristics of the intermediate recording and reproduction steps also were plotted, with significant information produced at each point. Exposure and processing methods were altered in an effort to reduce the undesirable effects shown in Figure 3, but the general characteristic remained.
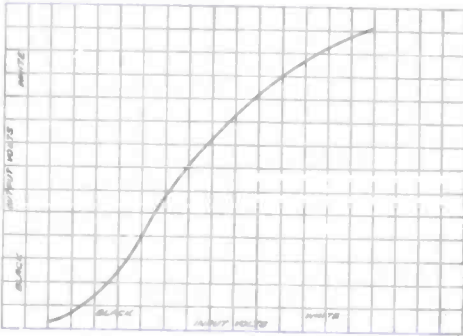
Fig. 3—Volts input to kinescope recording versus volts output from film reproducer.

An analysis of Figures 2 and 3 indicates that some non-linear compensation is needed for both direct film and kinescope recording reproduction. The two cases differ as to amount required, but are otherwise generally similar. Both are simple curves, and compensation should be feasible.

Model "A" Orthogam Amplifier

Many times in the past "gamma correction" amplifiers have been built which had variously shaped transfer characteristics. Most of these actually compressed one part of the characteristic in order to get a relative expansion of another. Figures 2 and 3 indicate that the "black" half of the characteristic should not be altered, but rather an expansion in the "white" range is required. No *gradient* change should be permitted in the near-black signals, even though their relative amplitude is reduced to permit white expansion.

With the above requirements in mind, the Model "A" orthogam amplifier was designed with two parallel amplifiers, as indicated in Figure 4. The upper branch path provides a completely linear output voltage, to which the lower branch adds expanded white voltages. Large video voltages can be fed to V5, and its bias can be controlled to allow only the highlight tips of those voltages to be passed by the tube. Thus both amount and gradient of the correction can be controlled, without causing non-linear operation in the black region. The smoothly-rounded grid cut-off characteristic of V5 was found to pro-

vide reasonably accurate compensation for the effects noted, when the two gain controls and the compensator bias were adjusted for optimum visual effect on a good monitor. As predicted by Figures 2 and 3, the largest improvement occurred when kinescope recordings were reproduced, but direct film transmission also was bettered appreciably.

Results — Model "A"

Six orthogam Model "A" amplifiers were put into operational service as an extended performance check. "In-Out" tests immediately gained the cooperation of the operating personnel. Noticeable improvement in film transmission quality was commented on by observers not familiar with the tests. As an unexpected dividend in many cases the effect of flare was reduced, since in normal operation most of it occurs at low amplitude in dark areas, and the orthogam reduces the relative amplitude of such voltages. However, it shortly became apparent that some changes in the method were required. Operating crews found
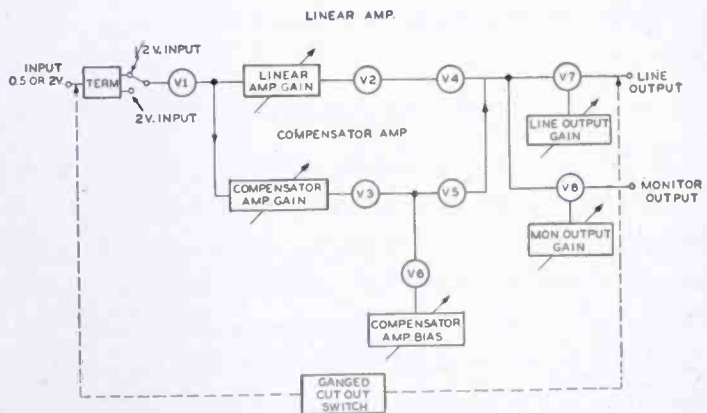
Fig. 4—Block diagram of Model "B" orthogam amplifier.

the units were "wild" — that is, they made video level riding difficult. This was found to be due to the fact that once a correct gradient was chosen for the normal maximum voltage level, much steeper gradients existed above that point, in the nominally unused region of overload. Frequently a video voltage peak would rise into that region and the additional amplification there would drive it far higher than it would otherwise have gone. Subsequent reduction of system gain corrected the matter, but only after a troublesome transition period. With close attention during rehearsal, and constant vigilance during broadcast, these effects could be acceptably minimized, but final judgment was that the Model "A" was not an operationally desirable tool.

Model "B" Orthogam Amplifier

Based on the above results, a new attack on the problem was made.

Using the same basic philosophy of correction, it was decided that the major additional requirement was that the top desired gradient must be the greatest actually encountered in the system under operating conditions. Thus, instead of a continuously rising gradient in the overload-voltage region, the new orthogam must be linear at the steepest desired slope. This objective has been achieved in the Model "B" orthogam amplifier.

The unit consists of a 6-tube amplifier as shown in Figure 5 mounted on a chassis approximately 5 inches high, 15 inches wide and 9 inches deep, complete with a self-contained power supply. It requires 110 volts alternating current at approximately 1.2 amperes when operating from its internal power supply, or approximately 110 volts alternating current at 0.6 ampere and $+285$ volts regulated at 130 milliamperes when operating from an external power supply. The input video voltage level should be .5 volt peak to peak or greater. It will deliver from .5 to 2.0 volts peak to peak into a 75-ohm load. The overall frequency response is flat to 7 megacycles. Figures 7, 8 and 9 show photographs of the completed unit.

CIRCUIT ARRANGEMENT — MODEL "B"

Referring to Figure 5, the first tube, VI, is a 6AH6 used as a conventional video amplifier and having a gain of about 12. A potentiometer, P1, is included in the imput circuit to control the level of the video voltage reaching the grid of the first tube. This should always be adjusted to give approximately .5 volt peak-to-peak signal as measured at the pin jack adjacent to the input gain potentiometer on the rear of the chassis. The first half of the second tube, V2, a dual triode type 12AT7, is a unity gain inverter stage and the second half is connected as a diode dc restorer across the grid of the third stage, V3, to insure that blacks in the picture always occur at the same point on the tube characteristic. The third tube, V3, is a type 6AH6 used in a nonlinear amplifier stage having high degeneration in its cathode circuit. The germanium crystals shunted across its cathode impedance determine the non-linear amplifying characteristics of this tube. The polarity of the video signal on the grid of the tube is such as to have whites in the positive direction, and the crystals are connected so that increasing voltage at the cathode will cause them to conduct. The stage, therefore, causes high degeneration of black and near-black signals, and as the signal approaches the white amplitude, the amount of degeneration will be reduced by the shunting action of the crystals which start to conduct. The point at which conduction takes place

Fig. 5—Circuit diagram of Model "B" orthogam amplifier.

depends upon the voltage settings of the potentiometers P2 and P3 controlling the voltages supplied to the crystals.

The remaining stages of the amplifier V4, V5 and V6, are straight-forward video amplifiers. V4 has a potentiometer, P5, in its cathode circuit to control the gain of the stage. The two output stages, V5 and V6, are driven from the same signal source, namely the plate of V4, thus giving two outputs, a regular and a monitor, each having gain control circuits in their cathodes. They are capacitively con-nected to the load circuits.

OPERATION

In using the Model "B" orthogam amplifier, the level of the in-coming video signal should first be determined, and an appropriate setting of P1, made such that under normal conditions of operation the peak-to-peak voltage on the grid of V1 will be approximately .5 volt as measured at the pinjack adjacent to the input gain potentiom-eter. With the potentiometers P2 and P3 in the most counterclock-wise position, the crystal diodes will be biased open and the amplifier will have a linear characteristic. As the potentiometers P2 and P3 are turned clockwise the crystal diodes will start to conduct on white peaks and thereby give increased amplification to the white end of the video signal due to the reduction in degeneration in the third stage and the resultant increase in gain. As shown in the schematic there are two shunt crystal circuits, one consisting of two IN-54 crystals and a variable resistance, P4; the other consisting of a single crystal having a fixed resistance of 220 ohms in series with it. The potentiometer P2 controls the dc potentials applied to the two series crystals and de-termines the so-called lower breakpoint. Having two crystals in series smooths out the abrupt break in the resultant non-linear amplifying characteristic of the stage, and the series resistance of P4 (slope control) limits the gain of the stage in the stretched condition due to conduction by these crystals. Normally P4 is turned to its maximum clockwise position where it is out of the circuit, permitting maximum gain for the stage. For certain types of film it may be desirable to in-crease the separation in the extreme white portion of the signal and to accomplish this a second diode circuit is included, the conduction point of which is controlled by the dc potential applied to the single crystal via potentiometer P3. The action of this circuit is to give a second, or upper breakpoint in the overall characteristic in the region of the extreme white portion of the signal. There is some interaction between the two, so in actual practice they have to be adjusted simul-taneously. In operation the resultant effect is to increase the gradient

of the white portions of the video signal relative to the black portions and thus give greater separation between the tones in the white end of the signal. A variety of transfer characteristics can be obtained by careful adjustment of the potentiometers P2, P3 and P4. The use of the two crystal circuits gives a fairly good approximation to a power function characteristic for this stage of the amplifier.

In the normal adjustment of the amplifier, the peak-to-peak video voltage on the grid of V1 is set as previously specified and, with the diodes in a nonconducting state (P2 and P3 counterclockwise and P4 clockwise), the gain of V4 is set to maximum by turning the gain potentiometer P5, in the cathode of V4, all the way clockwise. The output level then is adjusted to the desired value by setting the output potentiometers P6 and P7, located at the center rear of the chassis, to the appropriate setting to give the required output peak-to-peak voltage. This can be checked by switching from position 1 to position 2 on the characteristic selector and adjusting P6 and P7 until the same peak-to-peak voltage is obtained in either position. If there appears to be a slight stretching action taking place with P2, P3 and P4 set as indicated, the input potentiometer P1 should be turned counterclockwise slightly until the stretching disappears. After adjusting P1, P6 and P7 as above, the procedure would be to reduce the gain of the amplifier, with the characteristic selector in position 2, to about one half of its previous value by turning P5 counterclockwise and then adjusting P2, P3 and P4 until the desired shape of transfer curve is obtained for the particular film in question. If, when the desired characteristic is obtained, the output level is not at the desired value, it can be adjusted by controlling the gain of V4.

The characteristic selector knob on the front panel has five separate positions which may be chosen by the operator. Position 1 simply connects the input of the amplifier to the output, removing the amplifier completely from the circuit. Position 2 is associated with the variable controls P2, P3 and P4 and may be adjusted to suit the individual's wishes. Positions 3, 4 and 5 are fixed degrees of compensation which are determined by the potentials associated with those circuits on the switch and may be suitable for some particular types of operation. These particular characteristics are entirely arbitrary and may be changed by making appropriate changes within the unit. When using positions 3, 4 or 5, suitable adjustment of the gain of V4 will have to be made to maintain the same overall peak-to-peak volts. The single diode circuit potentiometer, P3, is effective for positions 3, 4 and 5 as well as for position 2. Likewise the slope control, P4, is in the circuit for all positions of the characteristic selector except position 1.

The left hand toggle switch labeled "Emergency Cutout" is merely an arrangement whereby the shunting diode crystal may be made inoperative and the non-linear action of the amplifier thereby removed without the necessity of switching the characteristic selector knob back to position 1. It is intended to be used only in case of trouble and should always be turned "on" if the unit is in service. When the emergency cutout is switched to the "off" position a readjustment of the linear gain control P5 will be required to increase the overall gain of the amplifier.

In some instances it may be desirable to use a regulated $+B$ supply which can be accomplished by feeding $+285$ and ground into the two-terminal plug arrangement at the rear of the chassis. When so operating, the snap switch labeled *INT*, *EXT* inside the unit should be thrown to the *EXT* position. This disconnects the high voltage rectifier circuit of the internal power supply but leaves the heaters con-
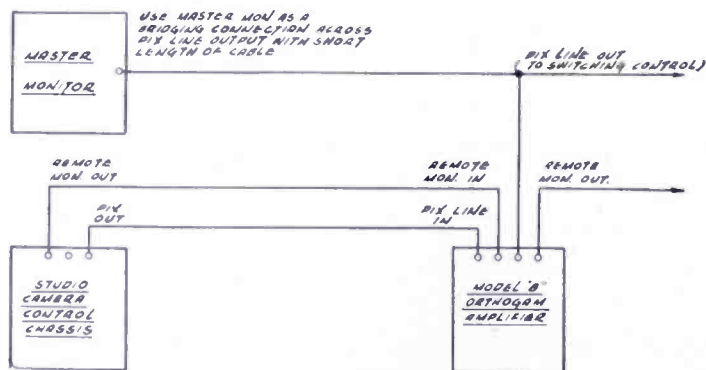
Fig. 6—Connections for Model "B" orthogam amplifier.

nected. For some types of operation it may be desirable to use external regulated $+B$ if a high degree of stability is required, or if the primary power supply is unstable. For most normal operations the internal power supply will be adequate. When the unit is used in conjunction with standard studio type iconoscope film reproducing equipment, it should be connected directly in the output of the camera control unit of the film chain as shown in Figure 6.

RESULTS — MODEL "B"

Several NBC film studios now have been equipped with Model "B" units, and considerable operational experience indicates that the gain-riding difficulties experienced with the "A" model has been largely overcome, and substantial improvement provided in the transfer characteristic of the overall system. This is evidenced in the viewed picture by a reduction in the chalkiness of faces and an improvement in the separation between other white and near-white portions of the reproduced image. The average brightness of the picture is reduced

Fig. 7—Model "B" orthogam amplifier — front view.
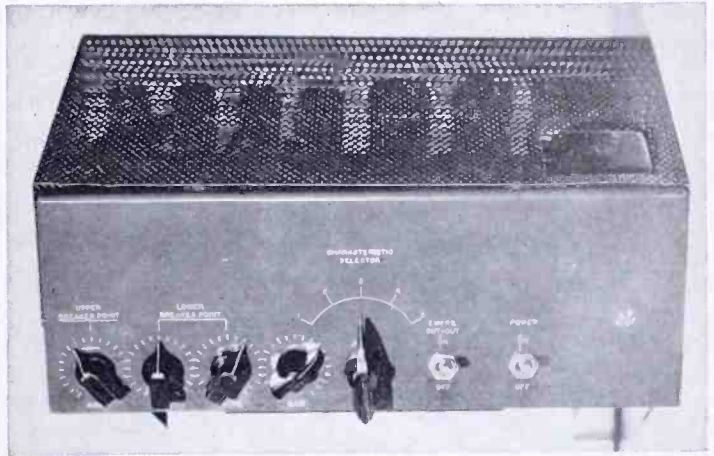
Fig. 8—Model "B" orthogam amplifier — rear view.
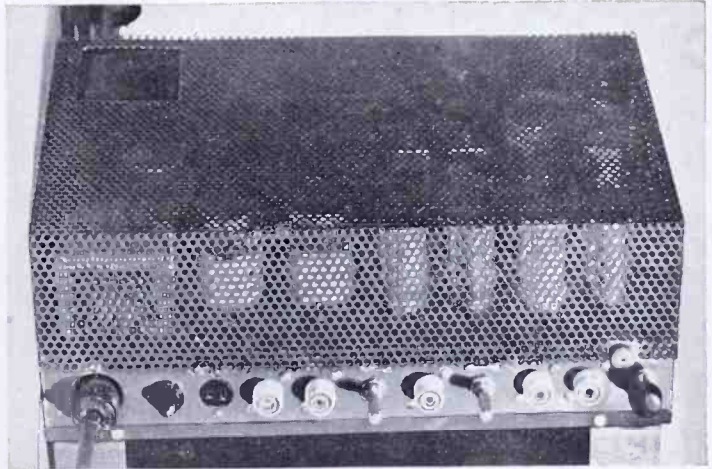
Fig. 9—Model "B" orthogam amplifier — top view of chassis.
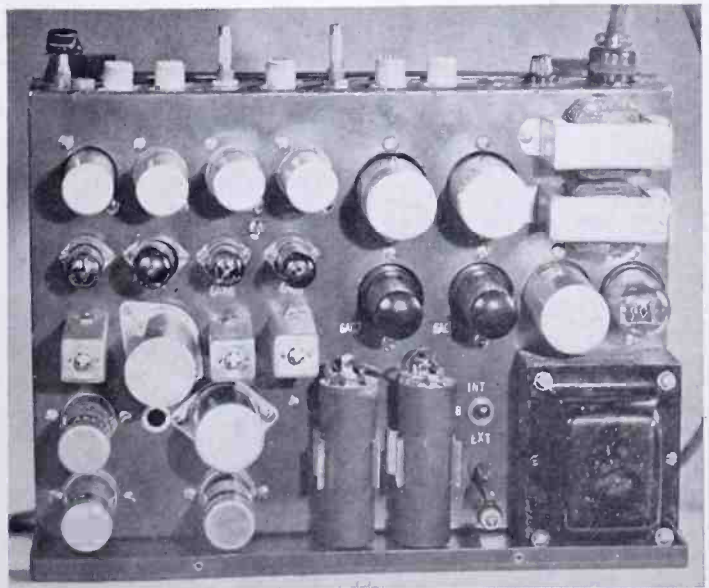
somewhat due to the fact that the alternating-current axis has been pushed towards the blacks. The end result is a more natural and pleasing reproduction.

ACKNOWLEDGMENT

THE BRIEF CASE AMPLIFIER*

BY

J. L. HATHAWAY AND RALPH C. KENNEDY

Engineering Department, National Broadcasting Company, Inc.,
New York, N. Y.

Summary—A highly effective and versatile miniature field amplifier for sound broadcast pickup is described. Although small enough to be transported in a standard brief case together with necessary accessories, it incorporates features not ordinarily found in conventional size units, including a line equalizing oscillator and an automatic audio gain control. Necessary operating adjustments have been minimized in order to reduce operating errors and setup time.

Considerations leading to the present design are outlined together with a description of amplifier facilities and measured performance characteristics. General applications and field test results are described.

APPLICATION

FOR some years the broadcasting industry has felt the need of miniature sound pickup field amplifiers. Consequently, various special units were constructed which could be quickly transported to locations of remote program origination and connected to telephone lines with a minimum of effort. These were for emergency type broadcasts such as disasters and other short-notice special events, but although useful, their fields of application were extremely limited. It was felt that more versatile miniature amplifiers should be developed and that they should handle not only the "flash" jobs but many of the ordinary remote broadcasts as well. Thus, transportation would be facilitated and engineering broadcasting and storage space requirements reduced while setup and equalization time would be minimized. Such equipment should possess the necessary facilities found in conventional amplifiers plus certain additional features for improved and simplified operation.

DESIGN CONSIDERATIONS

One of the most important requirements, and a difficult one to meet in miniature equipment, was the achievement of optimum signal-to-noise ratio. This dictated the use of balanced input circuits and high level mixing.

---

* Decimal Classification: R363.2.

In order to avoid the use of a special carrying case, the present amplifiers were designed to be contained in standard type brief cases. This arrangement offered several advantages, including ruggedness, replaceability and appearance. A man loaded down with cumbersome broadcast apparatus frequently had difficulty entering certain scheduled public or private affairs, and in fact sometimes found it too late by the time he gained entrance through the rear door. However, a man with a neat appearing brief case in hand is not likely to find the front door much of an obstacle nor is he likely to be mistaken for a furniture mover.
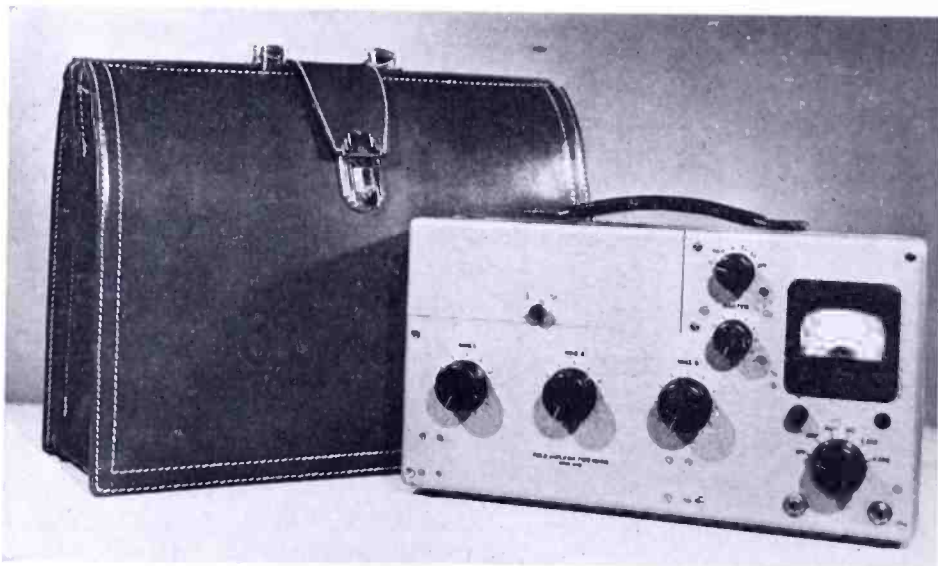
Fig. 1—Amplifier and brief case.

Experience indicated that power for a field amplifier should be self-contained. Even in cities having alternating-current power, occasions arose requiring self-powered units. Certain of the larger field amplifiers were arranged to operate normally on alternating-current power, but to shift automatically to batteries during power failures or when used at non-alternating-current locations. This excellent arrangement, however, required extra size and weight and consequently could not be incorporated in the miniature design. Self-contained 1.5-volt A and 135-volt B batteries power the new brief case amplifier, which has extremely low drain. A complete set of batteries costs $3.15 and is good for 25 hours of operation at 3 hours per day— only 12½ cents per hour of operation.

Questionnaires, circulated among operating personnel, indicated the advantage of some degree of automatic audio gain control (AAGC), so this feature was included in the unit.

MECHANICAL DETAILS

The present remote equipment, including brief case housing, is pictured in Figure 1. The amplifier rests on 4 rubber bumper feet. Figure 2 pictures the battery arrangement while Figure 3 is a bottom view of the amplifier chassis. The case measures 15 inches wide by 3 inches deep by 7 inches high and the complete unit including batteries weighs only 13 pounds, 5 ounces. The brief case accounts for 4 additional pounds and is so arranged that after insertion of the amplifier for transportation, an internal flap folds over the amplifier top leaving the entire upper portion of the case available for microphone cords
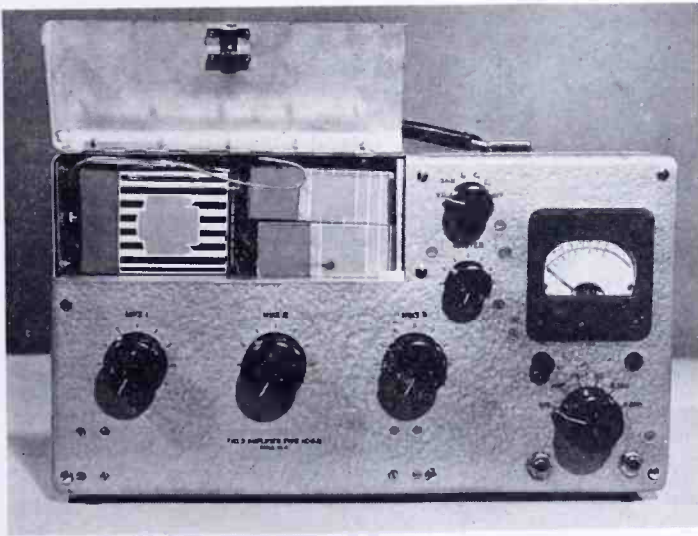
Fig. 2—Amplifier with battery compartment open.

and earphones. Actually, it will accommodate 3 type KB-2C microphones with cables plus at least one monitor set, spare cable, batteries, and tubes.

One of the most important and difficult problems in the design of a low-drain, low-level amplifier is that of microphonics. Consequently, the entire electronic chassis is shock mounted from the case, front panel, and battery compartment by means of rubber isolators. Furthermore, except for the output stage, all tubes are shock mounted or capped with special loaded shields. For maintenance, the chassis may be slid from its case by removing the front "binderhead" screws and pulling it forward along drawerlike guides. Only a few parts are not readily accessible, and these may be reached by removal of adjacent components.

FACILITIES

The amplifier accommodates three low impedance microphones through separate high-level faders, with filters to prevent radio-frequency pickup reaching the pre-amplifier tubes even in strong radio-frequency fields. A single 600-ohm padded output circuit is provided for telephone line feed. Means are available for paralleling an additional amplifier mixer, whereby up to 6 microphone positions may be employed. In this arrangement, two complete amplifiers are employed, and are interconnected at pin jacks through a plug-in shielded lead. Plate and filament potentials as well as plate current and VU level may be metered. A built-in four-frequency oscillator is provided for telephone line equalization, and an AAGC is incorporated for improved signal to noise as well as to aid in maintenance of correct output level. The AAGC is so adjusted that it has little effect on sub-normal peaks but acts only as a check valve for high passages. This
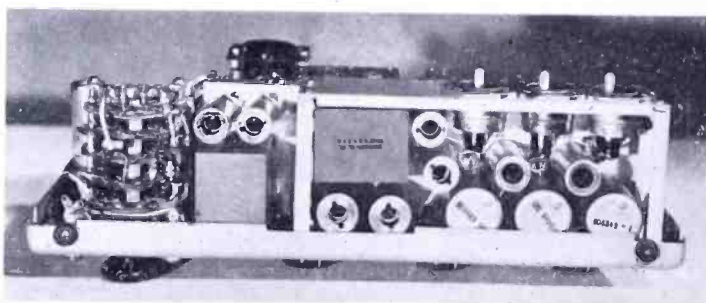
Fig. 3—Bottom view of amplifier chassis.

action permits safe operation of the amplifier at several decibels higher average level than could be otherwise maintained. Two low impedance monitoring jacks are provided at the output. Overall gain is sufficient for conventional high-quality microphones. Normal output level after padding corresponds to +8 VU, the presently accepted telephone line standard.

CIRCUIT

As shown in schematic diagram Figure 4, the three microphone circuits are balanced to ground and signals stepped up in voltage to the pre-amplifier grids through mu-metal shielded input transformers. This results in optimum signal-to-noise ratio. During development, tests were conducted on more than a dozen different types of miniature and subminiature tubes until a satisfactory one was found. This, the CK512AX, generated approximately 15 decibels lower microphonic

Fig. 4—Schematic diagram of brief case amplifier.

noise under given conditions than the next best, and furthermore, its tone characteristic rendered it inaudible in broadcast receivers cutting off audio response above 5 kilocycles.

Fading is accomplished after pre-amplification by means of audio-taper carbon potentiometers. These were utilized only after a test of 50,000 mechanical rotations without excessive wear or noticeable noise. The fader outputs are combined in the main gain control and thence are fed into the second amplifier stage, also of the CK512AX type. The main gain control is not generally considered an operating adjustment unless 6 microphone circuits are utilized. When a single brief case amplifier is used, the main gain is generally set at the beginning of a program and thereafter not readjusted.

Following the second stage, an interstage transformer couples to the push-pull grids of 1T4 controlled amplification tubes. These in turn drive push-pull 1S4 output tubes, incorporating a negative feedback loop. AAGC action is achieved through balanced and voltage-delayed rectification of a portion of the output potential. The resultant negative rectified potential is applied to the grids of the controlled amplifier tubes in order to reduce gain during abnormally high-level passages.

A 4-decibel isolation pad is used in feeding the telephone line. This small pad would not be sufficient for correct line equalization with the more conventional methods employed in most field amplifiers; however, in this unit a means is provided for exact equalization. In it, a 600-ohm resistor is substituted for the line by depressing a button during adjustment of the transmitted equalizing tone. Thereafter, the button is released without further tone level adjustment. The equalizing oscillator is activated and set to frequency through the main power switch—an arrangement for minimizing controls. The oscillator itself is of the phase shift type with tapered resistor and capacitor values for optimum waveform and uniform output. Its voltage is injected into the number 3 fader for exact level adjustment.

CHARACTERISTICS

Measured characteristics averaged from 17 units are as follows:
(1)   Gain, faders and main gain open—90 decibels
(2)   Frequency response, 40 to 12,000 cycles per second—± ½ decibel
(3)   Maximum output distortion, +18 dbm, 100 through 4000 cycles per second—2 per cent
(4)   Normal output distortion, +8 dbm, 100 through 4000 cycles per second—1 per cent

(5) Input impedance-bridging for 150-ohm microphones

(6) Output impedance—530 ohms

(7) Gain variation, 2 unused faders full on to full off—3 decibels

(8) Equalizing oscillator frequencies—100, 1000, 2500 and 4500 cycles per second

(9) AAGC attack time—30 milliseconds

(10) AAGC recovery time—0.3 second

(11) A drain—380 milliamperes plus 50 milliamperes when equalizing

(12) B drain—16.5 milliamperes plus 1 milliampere when equalizing

FIELD USE

Brief case amplifiers have been field tested throughout the country with gratifying results. To date the only seriously adverse comment came from an operation where a unit was located beside a regulated power supply. Hum pickup was encountered due to the interstage transformer not having a mu-metal shield. After addition of such a shield, the hum level dropped by 25 decibels and results were satisfactory. Consequently, all of the units were treated to the same improvement.

These amplifiers have been used to pick up dance bands, news roundups, night clubs, horse races, etc. Comments of operating personnel have been extremely favorable.

Equalization has been found to be accurate and rapid. The process generally requires less than 30 seconds compared to the usual 15 minutes for an amplifier without built-in oscillator, where tone must be sent over a spare telephone line from the studio transmission room. The extremely low background noise has been found to contrast with the high hiss, plop, and microphonics found in many conventional size amplifiers utilizing low-level fading, or worse, low-level unbalanced fading. Even in miniature equipment the advantages of balanced microphone circuits and high-level faders are evident and far outweigh the disadvantages of size, weight, and cost.

The excellent performance, versatility and convenience of the brief case amplifier combine to render it a valuable addition to sound pickup apparatus.

LINEAR PHASE SHIFT VIDEO FILTERS*

By

G. L. Fredendall† and Ralph C. Kennedy‡

Summary—This paper is intended primarily to guide the designer through the necessary steps in the calculation of the values of capacitances and inductances in the Bode linear phase shift filter which approximates the desired requirements on attenuation through cutoff and in the attenuation region.

Application of the linear phase shift filter in the production of "mixed highs" in dot-sequential color television is given.

Band-pass and band-elimination filters with linear phase shifts are also described briefly.

INTRODUCTION

IN some television circuits requiring low-pass filters, unusual requirements are imposed on the phase shift characteristic; namely, that the phase shift shall closely approach a linear function of frequency in the pass band and through the cutoff region. Such a demand is made to insure that the filter shall respond to a step function with the minimum rise time and minimum amplitude of ringing consistent with the sharpness of cutoff.

The optimum transient response for an abrupt cutoff filter is the response of the idealized low-pass filter depicted in Figure 1. Distinctive features of this response are equal ringing before and after the transition and minimum rise time.

Sharp cutoff, minimum phase shift filters respond with a greater rise time and a high amplitude of ringing on the trailing edge of the transition. Ringing is absent from the leading edge. Hence when such filters are used to restrict the video bandwidth, television pictures exhibit noticeable ringing following sharp transitions between half tones, which occur at or near an angle of 90 degrees to the direction of scanning. Such ringing may be minimized by the substitution of a linear phase shift filter which acts effectively to diminish the amplitude of trailing ringing by a factor of approximately 2.

Anticipatory ringing is added to the transition equal in magnitude and waveshape to the trailing ringing. In general, a television picture

restricted by a linear phase shift filter exhibits greater resolution and apparent freedom from ringing than is possible with the ordinary minimum phase shift filter.

Linear phase shift filters may take the form of the well-known constant-K type followed by all-pass filters for phase equalization of the attenuating filter. However a more systematic approach to the linear phase shift filter was devised by H. W. Bode and is known as Bode's parameter determination.[1]

BODE PARAMETER DETERMINATION

The lattice configuration is the most convenient form for design purposes. In fact, the linear phase shift filter cannot be placed in ladder form at all. Even the bridged-T equivalent may not be available.
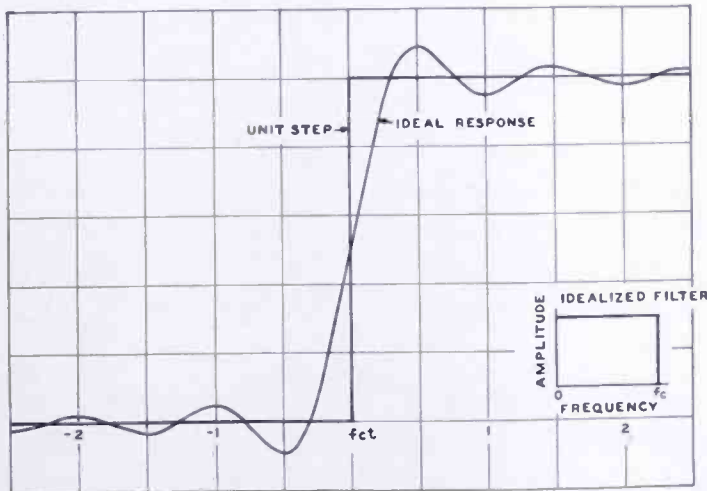
Fig. 1—Response of an idealized low-pass filter to a step function.
Rise time (10%-90% response) = $0.45/f_c$.
Frequency of damped oscillation $= f_c$.

In Figure 2 the arms of the lattice are represented by Z_x and Z_y which are cascaded, simple parallel-tuned circuits. The number of circuits is determined by the requirements of the particular design. Z_x and Z_y viewed as two terminal networks present reactance-frequency characteristics which pass alternately through zero and infinite reactance as the frequency is increased. Values of infinite reactance occur at the "poles" of the arm and values of zero reactance occur at the "zeros". Frequencies corresponding to poles and zeros are located on the critical frequency diagrams as indicated in Figures 2-b, d. For convenience in working with the diagrams, the frequency scale is in terms of a parameter α. An amplitude-frequency characteristic of the filter (Figure 2c) is also sketched on the same frequency scale as

[1] H. W. Bode and R. L. Dietzold, "Ideal Wave Filters", *Bell. Sys. Tech. Jour.*, Vol. XIV, pp. 215-252, April, 1935.

an aid in identifying the three regions of the filter, the transmission, cutoff, and attenuation regions.

It is well known that certain correspondence must exist between the critical frequencies of Z_x and Z_y if the lattice network is to exhibit filter characteristics at all. In the transmission region, the critical frequencies representing poles of Z_x must coincide with those representing zeros of Z_y. Similarly, the zeros of Z_x must coincide with the poles of Z_y. Either Z_x or Z_y may have a zero at the origin.[2]
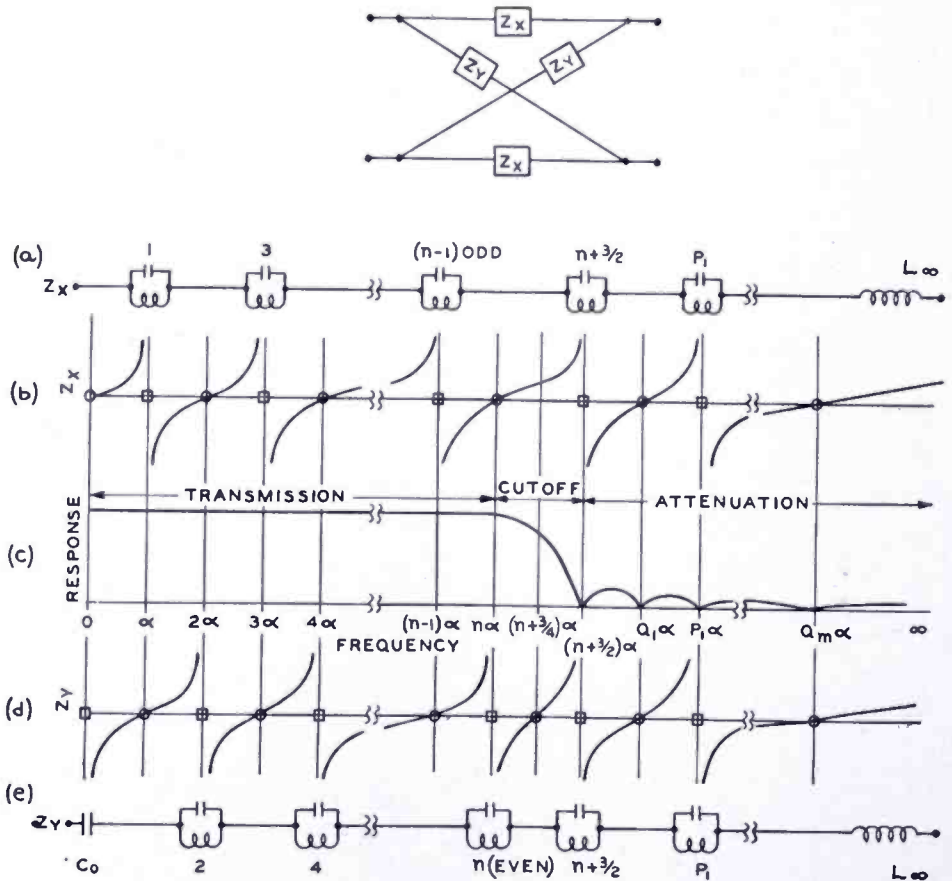
Fig. 2—(a) Z_x arm.
   (b) Critical frequency diagram for Z_x, □ poles, ○ zeros.
   (c) General form of amplitude response.
   (d) Critical frequency diagram for Z_y.
   (e) Z_y arm.

In the attenuation region, however, poles coincide with poles and zeros with zeros. A different situation arises in the interior of the cutoff region in which either Z_x or Z_y must have a zero unmatched by a pole of the opposite arm.

---

[2] In this discussion Z_x is assigned a zero at the origin. The case of a zero of Z_y at the origin amounts merely to a reversal of polarity of the filter.

The foregoing principles apply to all filters. In addition, the requirement of substantially linear phase shift in the transmission and cutoff regions requires that:

(1)   The zeros and poles shall be equally spaced in the transmission region by an interval denoted by α in Figure 2-c.

(2)   The length of the cutoff region shall equal $3/2\ \alpha$ and contain only a zero at the center of the interval contributed by one arm. The other arm shall have no critical frequencies. End points of the cutoff region are excepted.

(3)   That one or more critical frequencies be placed in the attenuation region spaced at equal intervals $(=\alpha)$ as in the transmission region depending upon the degree of phase linearity required in the cutoff region. Considerations of attenuation may also modify the spacings of critical frequencies. Critical frequencies in the attenuation region that are more remote from the cutoff region may depart from the equal spacing rule without appreciable effect on the linearity of phase in the cutoff region.

From the foregoing discussion it is clear that many critical frequencies closely spaced in the transmission region correspond to small values for α and, therefore, lead to a short cutoff interval. If the ratio of cutoff interval to transmission band is r, the number of critical frequencies in the transmission band is $3/2r$.

CALCULATION OF CIRCUIT ELEMENTS

Let it be assumed for the moment that the number and locations of the zeros and poles of the lattice arms Z_x and Z_y have been established by requirements of a specific design. Resort would then be made to Foster's Reactance Theorem for the solution of the circuit elements.[3] The constant coefficient in the reactance theorem is supplied from a knowledge of the propagation and impedance functions of the lattice.[4] The details of the solutions are omitted here since the designer will be concerned only with the formulas for the circuit elements. Four cases must be distinguished.

In case (I), Z_x and Z_y have poles at infinite frequency and Z_y has a zero in the center of the cutoff region. This arrangement corresponds to Figure 2-b, d. Circuit elements for the K'th parallel tuned circuit of Z_x are given in terms of α by the following formulas:

[3] F. E. Terman, RADIO ENGINEERS' HANDBOOK, p. 200, McGraw-Hill Book Co., New York, N. Y., 1943.

[4] H. W. Bode and R. L. Dietzold, loc. cit., p. 250.

$$C_K = \frac{1}{L_K \omega^2_K} = \frac{1}{4H\pi^2\alpha^2} \frac{(K^2-1^2)(K^2-3^2)\cdots(K^2-P^2)\cdots}{(K^2-2^2)(K^2-4^2)\cdots(K^2-Q^2)\cdots}$$

$$\frac{\text{over all internal poles of } Z_x \text{ except the K'th}}{\text{over all internal zeros of } Z_x}, \quad (1)$$

$$L_\infty = H, \quad (2)$$

$$H = \frac{R}{4\alpha} \frac{1^2 \cdot 3^2 \cdot 5^2 \cdots P^2 \cdots \text{over all internal poles of } Z_x}{2^2 \cdot 4^2 \cdot 6^2 \cdots Q^2 \cdots \text{over all internal zeros of } Z_x}, \quad (3)$$

in which

$P\alpha =$ frequency corresponding to the P'th pole of Z_x.

$Q\alpha =$ frequency corresponding to the Q'th zero of Z_x,

$R =$ load resistor,

$\omega_K = 2\pi K\alpha$.

The circuit elements for the K'th parallel tuned circuit of Z_y are given by the following formulas:

$$C_K = \frac{1}{L_K\omega^2_K} = \frac{K^2}{H4\pi^2\alpha^2} \frac{(K^2-2^2)(K^2-4^2)\cdots(K^2-P^2)\cdots}{(K^2-1^2)(K^2-3^2)\cdots(K^2-Q^2)\cdots}$$

$$\frac{\text{over all internal poles of } Z_y \text{ except the K'th}}{\text{over all internal zeros of } Z_y}, \quad (4)$$

$$C_0 = \frac{1}{H4\pi^2\alpha^2} \frac{2^2 \cdot 4^2 \cdots P^2 \cdots \text{over all internal poles of } Z_y}{1^2 \cdot 3^2 \cdots Q^2 \cdots \text{over all internal zeros of } Z_y}, \quad (5)$$

$$L_\infty = H, \quad (6)$$

$$H = \frac{R}{\alpha\pi^2} \frac{2^2 \cdot 4^2 \cdots P^2 \cdots \text{over all internal poles of } Z_y}{1^2 \cdot 3^2 \cdots Q^2 \cdots \text{over all internal zeros of } Z_y}. \quad (7)$$

In case (II), Z_x and Z_y have poles at infinite frequency and Z_x has a zero in the center of the cut-off region as illustrated in Figure 3-a. The formulas for the elements are also given by Equations (1)-(7).

In case (III), Z_x and Z_y have zeros at infinite frequency and Z_x has a zero in the center of the cut-off region. Figure 3-b illustrates this

arrangement of critical frequencies. The formulas for the elements are given by Equations (8)-(12).

Case (IV), which is shown in Figure 3-c, corresponds to zeros for Z_x and Z_y at infinity and a zero for Z_y in the center of the cut-off region. Equations (8)-(12) apply to Case (IV).

In case (III), Z_x and Z_y have zeros as infinite frequency. The corresponding formulas are:
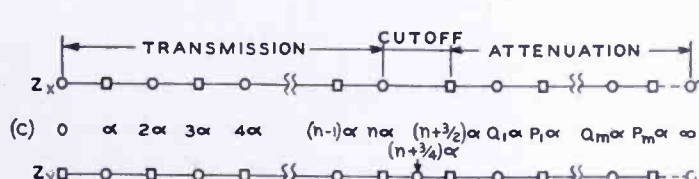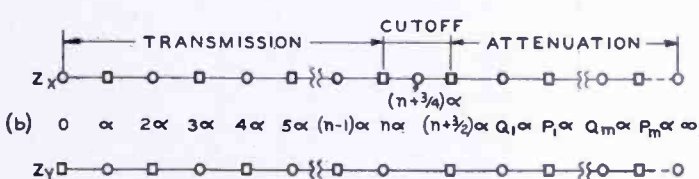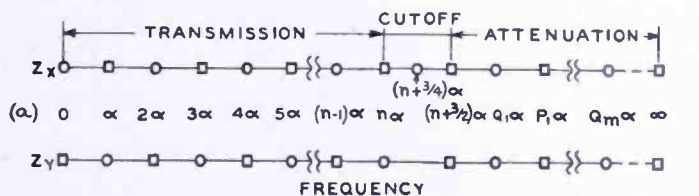
Fig. 3—Possible arrangements of critical frequencies in the linear phase shift filter.

for Z_x,

$$C_K = \frac{1}{L_K \omega^2{}_K} = \frac{1}{H} \frac{(K^2-1^2)(K^2-3^2) \cdots (K^2-P^2) \cdots}{(K^2-2^2)(K^2-4^2) \cdots (K^2-Q^2) \cdots}$$

$$\frac{\cdot \text{ over all internal poles of } Z_x \text{ except the K'th}}{\cdot \text{ over all internal zeros of } Z_x}, \qquad (8)$$

$$H = R\pi^2\alpha \frac{1^2 \cdot 3^2 \cdot 5^2 \cdots P^2 \cdots \text{all internal poles of } Z_x}{2^2 \cdot 4^2 \cdot 6^2 \cdots Q^2 \cdots \text{all internal zeros of } Z_x}; \qquad (9)$$

for Z_y,

$$C_K = \frac{1}{L_K \omega^2{}_K} = \frac{K^2}{H} \frac{(K^2-2^2)(K^2-4^2) \cdots (K^2-P^2) \cdot}{(K^2-1^2)(K^2-3^2) \cdots (K^2-Q^2) \cdots}$$

$$\frac{\cdot \text{ over all internal poles of } Z_y \text{ except the K'th}}{\cdot \text{ over all internal zeros of } Z_y}, \qquad (10)$$

$$C_0 = \frac{1}{H} \frac{2^2 \cdot 4^2 \cdot 6^2 \cdots P^2 \cdots \text{over all internal poles of } Z_y}{1^2 \cdot 3^2 \cdot 5^2 \cdots Q^2 \cdots \text{over all internal zeros of } Z_y}, \tag{11}$$

$$H = 4R\alpha \frac{2^2 \cdot 4^2 \cdots P^2 \cdots \text{over all internal poles of } Z_y}{1^2 \cdot 3^2 \cdots Q^2 \cdots \text{over all internal zeros of } Z_y}. \tag{12}$$

EXAMPLES OF A LINEAR PHASE SHIFT FILTER

The use of the above formulas will be illustrated by a specific example.[5] It will be assumed that the ratio r of the cutoff interval to the transmission interval is to be approximately 0.4, leading to $n = 3.75$. Since n must be an integral number, the value 4 is taken.
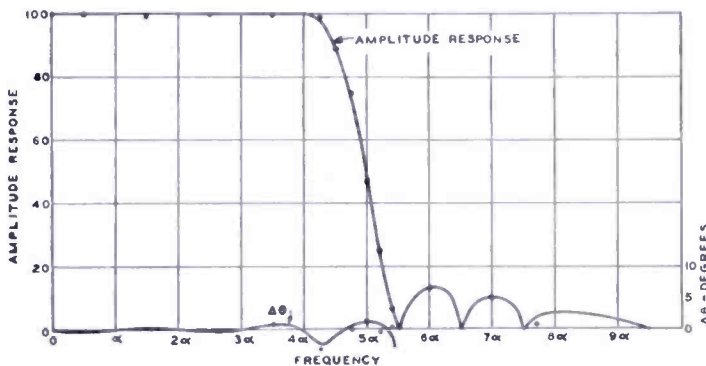
Fig. 4 — Amplitude and phase responses of a linear phase shift filter. Response calculated at data points.

With this choice of n, the transmission region will extend to 4α and the first frequency of theoretically infinite attenuation will occur at 5.5α according to the $3\alpha/2$ rule for the width of the cutoff region.

Poles in the attenuation region will be located at 5.5α, 7.5α and infinity. Zeros will be located at 6.5α and 9.5α.

With the above arrangement of poles and zeros, the critical frequency diagram for Z_x and Z_y is as illustrated in Figure 2 for case (I). The values of circuit elements in terms of α and the load resistance R appear in the first line of Table I. Specific values for filters having 71 per cent response at 2, 4, 6 and 8 megacycles are included in the table. The load R is 150 ohms.

The amplitude-frequency and phase-frequency characteristics of the filter tabulated in Table I are shown in Figure 4. For the purpose of pointing out the small deviations from linearity present in the actual phase characteristic, a linear phase variation $\theta = \frac{\pi}{\alpha} f$, is subtracted and the difference characteristic plotted as $\Delta\theta$ in Figure 4. It should be noted that the maximum deviation throughout the frequency interval $0 - 5.4\alpha$ is about 4 degrees.

[5] H. W. Bode and R. L. Dietzold, loc. cit., p. 249.
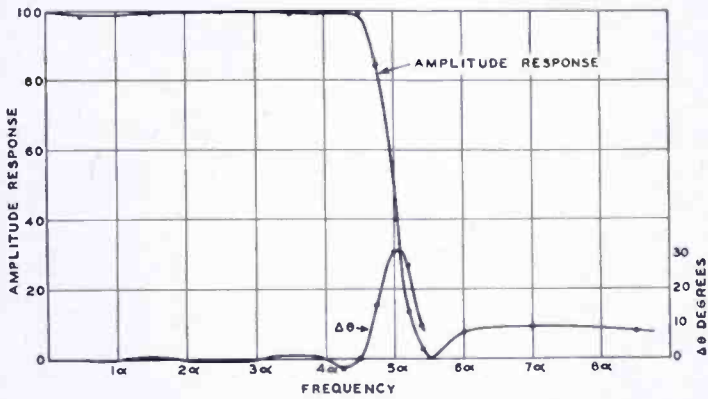
Fig. 5 — Amplitude and phase responses of the simplified filter. Response calculated at data points.

The transient response of an experimental model of this filter is given in Figure 6. Symmetry of the response is a result of the high degree of phase linearity exhibited in Figure 4.

The response of a minimum phase shift filter having similar cut-off characteristics would ring at the trailing edge with approximately two times the amplitude of the ringing shown in Figure 6. No ringing would be present at the leading edge of the transition for a minimum phase shift filter.

The importance of critical frequencies in the attenuation region is made apparent by an examination of the phase characteristic of a simplified filter which has the same critical frequencies in the transmission and cutoff regions as the preceding filter but includes no critical frequencies in the interior of the attenuation region beyond 5.5α. This arrangement is case (IV) for which Equations (8)-(12) apply. The elements of the filter are listed in Table II.

Inspection of Figure 5 reveals that good phase linearity no longer exists in the cutoff region of the simplified filter, although linearity
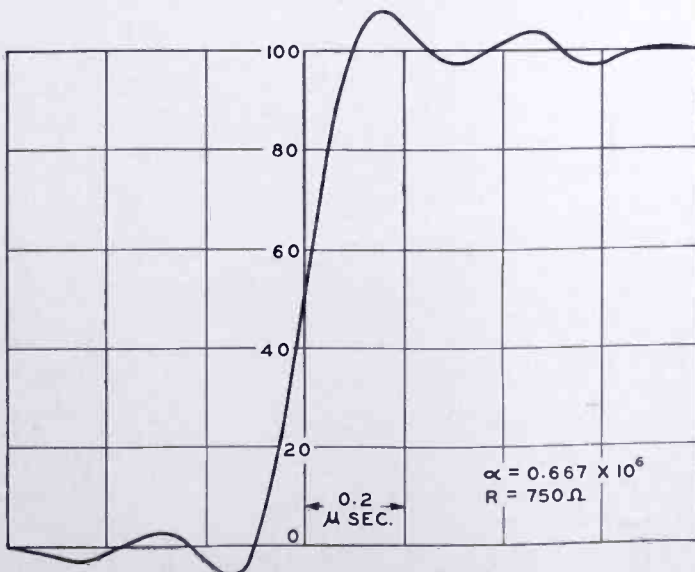
Fig. 6 — Transient response of linear phase shift filter (experimental).

Table I—Linear Phase Shift Filter.

Cutoff Frequency	Rise Time	First Frequency of High Attenuation
cycles/sec	sec	cycles/sec
4.75α	0.094/α	5.5α
mc	μ sec	mc
2	0.22	2.32
4	0.11	4.64
6	0.07	6.96
8	0.05	9.28

load R = 150 ohms

Z_x

	L_1	L_3	L_5	L_7	L_∞	C_1	C_3	C_5	C_7
	henries					farads			
	.2010R	.0205R	.0086R	.0041R	.0157R	.1260	.1372	.0970	.1095
α	α	α	α	α	α	Rα	Rα	Rα	Rα
	microhenries					micromicrofarads			
mc									
2	71.3	7.30	3.06	1.46	5.59	1990	2170	1540	1730
4	35.8	3.65	1.53	0.73	2.80	999	1090	768	868
6	23.9	2.44	1.02	0.49	1.87	665	724	512	578
8	17.9	1.83	0.77	0.36	1.40	499	544	384	434

Z_y

	L_2	L_4	L_6	L_8	L_∞	C_2	C_4	C_6	C_8	C_0
	henries					farads				
	.0495R	.0108R	.0055R	.0034R	.0142R	.1280	.1457	.1520	.1318	.2500
α	α	α	α	α	α	Rα	Rα	Rα	Rα	Rα
	microhenries					micromicrofarads				
mc										
2	17.6	3.85	1.96	1.21	5.06	2010	2310	2410	2090	3960
4	8.82	1.92	0.98	0.61	2.53	1010	1150	1200	1040	1980
6	5.88	1.28	0.65	0.40	1.69	676	769	802	696	1320
8	4.42	0.96	0.49	0.30	1.27	507	577	602	522	990

Z_x — L1 (α) C1, L3 (3α) C3, L5 (5.5α) C5, L7 (7.5α) C7, L∞

Z_y — L2 (2α) C2, L4 (4α) C4, L6 (5.5α) C6, L8 (7.5α) C8, L∞, C0

Table II—Simplified Filter.

Cut-off Frequency	First Frequency of High Attenuation	L_1	L_3	L_5	C_1	C_3	C_5
4.75α/sec	5.5α/sec	henries			farads		
mc	mc	$.2042R/α$	$.0243R/α$	$.0211R/α$	$.1239/Rα$	$.1157/Rα$	$.0396/Rα$
		microhenries			micromicrofarads		
2	2.32	72.7	8.64	7.50	1960	1830	625
4	4.64	36.4	4.32	3.76	979	915	315
6	6.96	24.2	2.88	2.50	653	609	208
8	9.28	18.2	2.16	1.87	490	457	156

(bracketed Z_x)

L_2	L_4	L_6	C_2	C_4	C_6	C_0
henries			farads			
$.0535R/α$	$.0153R/α$	$.0135R/α$	$.1187/Rα$	$.1039/Rα$	$.0622/Rα$	$.2500/Rα$
microhenries			micromicrofarads			
19.02	5.42	4.79	1870	1640	983	3950
9.52	2.71	2.39	938	822	492	1970
6.34	1.81	1.59	625	547	328	1320
4.75	1.35	1.19	469	411	246	989

(bracketed Z_y)

z_x — L1 $α$ — L3 $3α$ — L5 $5.5α$ — C1, C3, C5

z_y — L2 $2α$ — L4 $4α$ — L6 $5.5α$ — C2, C4, C6, C0
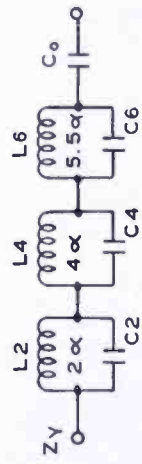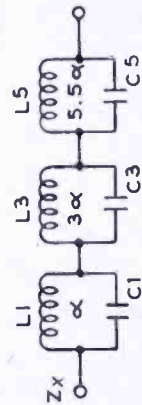
load R = 150 ohms

in the transmission region is as good as that shown in Figure 4. A zero placed at 6.5α would probably improve the linearity of phase in the cut-off region.

Construction of the Linear Phase Shift Filter

Since the lattice filter is a balanced structure, a balanced source must be used. The load likewise must be balanced, but if the midpoint of the load resistor is grounded, an unbalanced output from either output terminal to ground may be taken depending upon the polarity desired.

A convenient balanced source is two cathode followers fed push-pull from the plate and cathode of a driver tube. Unwanted incidental reflections within the lattice structure will be avoided if the source impedance equals the load impedance.

Since the filter cannot absorb the capacitance of tubes and wiring, the value of the load resistor should be chosen so that the characteristics of the filter are not unduly modified by capacitance loading.
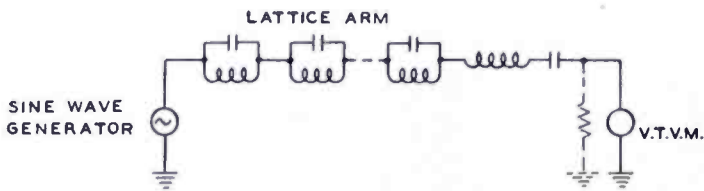

Fig. 7—Line-up of a lattice arm.

The filter cannot be expeditiously lined up by frequency sweep methods as with simple video amplifiers. A satisfactory procedure is to select all capacitors by accurate measurement and adjust the inductances in parallel with the respective capacitors for the known anti-resonant frequency of the parallel circuit. Distributed capacitance of coils may be allowed for in the capacitance measurement except in the case of the inductances L_∞.

One arm of the lattice is tuned at a time by means of a signal generator and vacuum tube voltmeter as shown in Figure 7. Each tuned circuit is adjusted independently for a minimum reading of the voltmeter at the appropriate resonant frequency. When all tuned circuits are adjusted, a suitable resistor may be shunted across the voltmeter and a complete frequency run of the arm taken. Peaks of the voltmeter reading occur at the series resonances of the arm, and dips occur at the anti-resonances. If the series resonances check, the arm has been correctly set up. Figure 8 shows an arrangement of the filter elements which is both convenient and satisfactory. One Z_x and one Z_y arm are laid out on the lower panel in a parallel manner from input to output. The upper panel also carries Z_x and Z_y arms. All arms are interconnected at the ends of the panels.

APPLICATIONS OF THE LINEAR PHASE SHIFT FILTER

1. *Mixed Highs in a Dot-Sequential Color System*

In the dot-sequential color system, the frequency spectrum corresponding to each of the primary colors is divided into two ranges. One range extends from 0 to approximately 2 megacycles and is responsible for conveying color information; the second range extends from approximately 2 to 4 megacycles and is used for the production of mixed-highs.
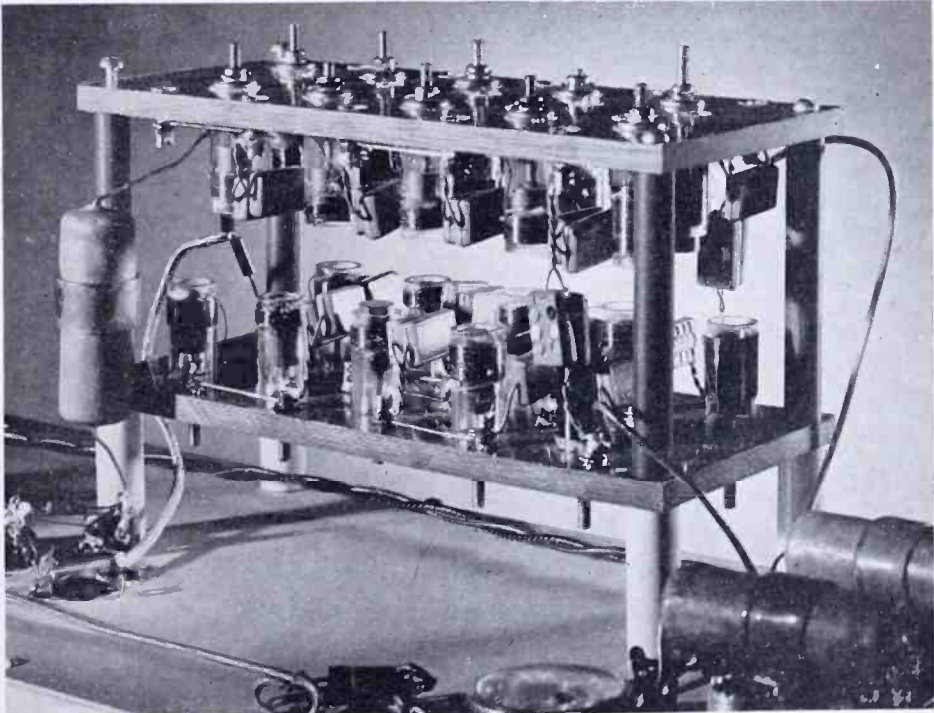

Fig. 8—Arrangement of elements in the linear phase shift filter.

It is desirable that the division of the video spectrum be carried out without objectionable phase distortion in either range. If minimum phase shift filters are employed for the separation, excessive phase distortion is likely in the cutoff regions of the filters. In this instance, the linear phase shift filter in the arrangement shown in Figure 9a provides a practical solution. The upper range of frequencies is isolated by adding to the output of a linear phase shift filter the output of equal magnitude but opposite polarity of a delay line or all-pass circuit having uniform delay equal to the delay of the filter. The lower range of frequencies is available directly at the output of the filter.

2. *Band-pass and Band-elimination Filters with Linear Phase*

Band-pass filters with excellent phase characteristics result when
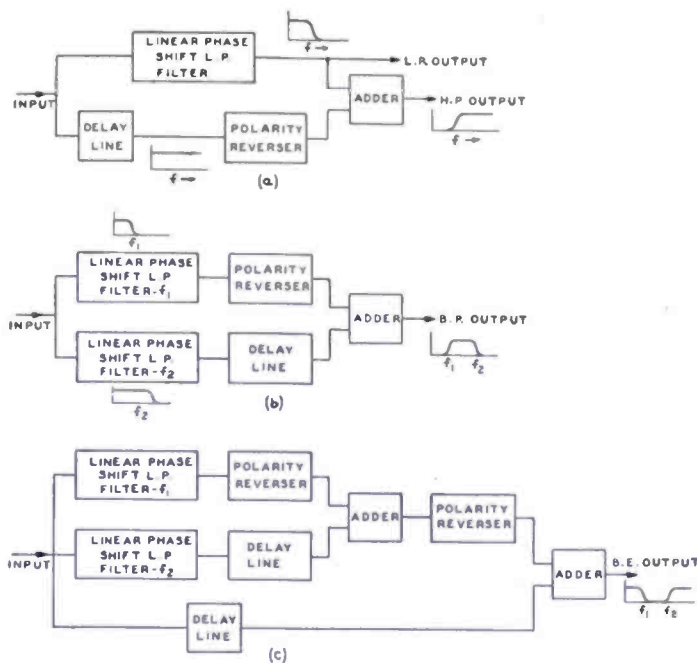
Fig. 9—(a) Mixed-
highs circuit.
(b) Linear phase
shift band-pass filter.
(c) Linear phase
shift band-elimina-
tion filter.

two low-pass linear phase shift filters are connected as illustrated in
Figure 9b. Here the delays of the two branch circuits are made equal
by the insertion of a delay line in the filter of video bandwidth. A
band-pass characteristic results when the output of one filter is added
with reverse polarity to the output of the other.

The circuit of Figure 9b suggests the logical development of the
linear phase shift band-elimination filter in Figure 9c by arranging
for the subtraction of the band pass characteristic obtained in Figure
9b from the output of a delay line transmitting the entire spectrum.
The delays of the three branches should be equal and uniform.

AN ANALYSIS OF THE SAMPLING PRINCIPLES OF THE DOT-SEQUENTIAL COLOR TELEVISION SYSTEM*

A Report

BY

RCA LABORATORIES DIVISION, PRINCETON, N. J.

Summary—This paper consists of three appendixes to the paper of the same title which appeared in the June 1950 issue of RCA Review, pages 255-286. These appendixes are: I—Reproduction of High-Frequency Detail with a Low Sampling Rate; II—Transmission of the Dot-Sequential Color Television Signal on Coaxial Cables of Restricted Bandwidth; and III—The Action of the Dot-Sequential Color Television System in the Presence of an Abrupt Red-Green Transition.

APPENDIX I

REPRODUCTION OF HIGH-FREQUENCY DETAIL WITH A LOW SAMPLING RATE

T̶HE previous analysis illustrated by Figure† 10 showed the manner in which high-frequency detail was reproduced when the high-frequency component of the signal had a frequency in the mixed-high region. Specifically, in Figure 10, the frequency of the picture component was chosen to be 3.4 megacycles, while the sampling frequency was 3.8 megacycles. Figure 10(g) was noted to be a rather good reproduction of the original function shown in Figure 10(a). However, it was realized that since the sampling frequency was only ten per cent greater than the signal frequency, the construction of Figure 10 did not fully establish the fact that the high frequency detail was produced by a multiplication of the input signal and the gating function. Accordingly, the calculations have been repeated in this appendix, but this time using a sampling frequency of 2.4 megacycles and a picture signal component of 4.0 megacycles. Here, the picture signal component is sixty-seven per cent *higher* than the sampling frequency, so the phenomenon is well illustrated.

The signal from the green camera tube is $G + g \cdot \sin(\omega t)$. For purposes of this illustration, f has been chosen as 4.0 megacycles,

---

$G = 1$ and $g = 1/2$. Figure 30 (a) shows this signal $1 + 1/2 \sin(\omega t)$.

The dc signal G goes through the transmitter sampler, but since the ac term is of a frequency lying in the region committed to "mixed-highs," this latter signal goes through Adder No. 2 and the appropriate band-pass filter into Adder No. 1 of Figure 1. Hence the signal into the transmitter modulator is

$$\frac{G}{3} [1 \pm 2 \cos(\omega_0 t)] + g \cdot \sin \omega t. \tag{37}$$

Expression (37) also applies to the voltage on the kinescope grid of a black-and-white receiver. The background term is sampled while the mixed-high signal, unsampled, is superimposed to supply fine detail. The positive polarity sign applies to the first scan of a line, while the negative sign applies to the second scan of the same line.

The signal out of the second detector of a color receiver also has the same form as Expression (37). Sampling in the receiver results in a signal on the grid of the green kinescope of the form

$$\frac{1}{3} [G + g \cdot \sin(\omega t)] [1 \pm 2 \cos(\omega_0 t)]. \tag{38}$$

A plot of this expression is shown in Figure 30 (b) with a sampling frequency of 2.4 megacycles.

The output of the blue sampler (the voltage on the grid of the blue kinescope) is

$$\frac{g}{3} \sin(\omega t) [1 \pm 2 \cos(\omega_0 t + 120°)], \tag{39}$$

while the voltage on the grid of the red kinescope is

$$\frac{g}{3} \sin(\omega t) [1 \pm 2 \cos(\omega_0 t - 120°)]. \tag{40}$$

The voltage on the blue kinescope is shown in Figure 30 (c), while the voltage on the red kinescope is given by Figure 30 (d).

Following the procedure of Figure 10, the positive values of Figures 30 (c) and 30 (d) have been combined with the positive values of Figure 30 (b) to show the effect of the combined light intensities for
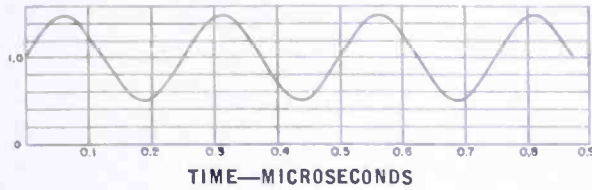
Fig. 30—(a) Signal out of green camera tube; $f = 4.0$ megacycles,
$G + g \cdot \sin(\omega t) = 1 + \frac{1}{2} \sin(\omega t)$.
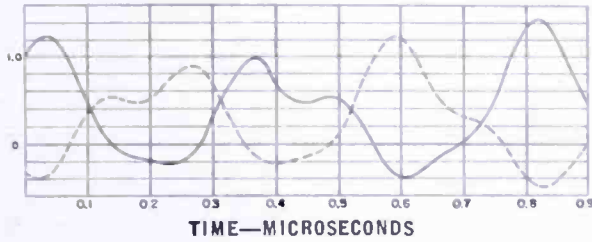
(b) Signal on the green kinescope grid of a color television receiver.
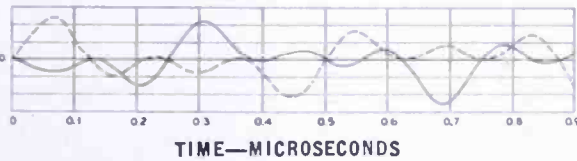
(c) Voltage on the blue kinescope grid.
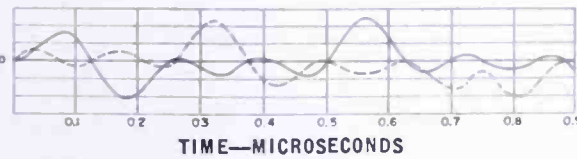
(d) Voltage on the red kinescope grid.
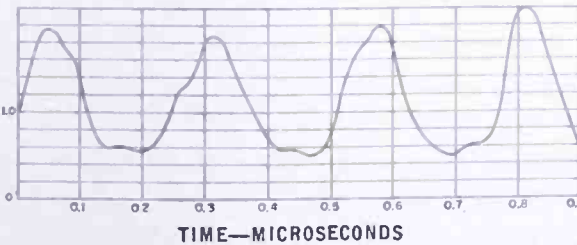
(e) Combined light intensity of two successive scans of the same line, obtained by adding light intensities of the green, red and blue tubes.
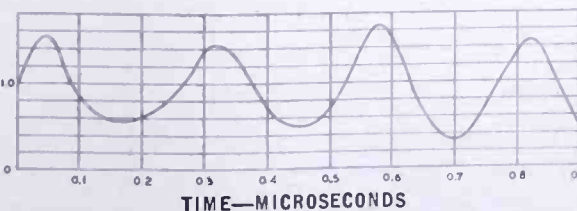
(f) Combined light intensity of two successive scans of the same line, obtained by adding light intensities of the green and red tubes. The sampling frequency is 2.4 megacycles.

two successive scans of the same line. The result of this combination is shown in Figure 30(e).

Inspection shows that Figure 30(e) is a satisfactory reproduction of Figure 30(a). However, it is well known that the resolution of the eye is very poor in blue, so it seems better to combine only Figure 30(d) with Figure 30(b), with Figure 30(f) resulting. This latter curve is an excellent reproduction of Figure 30(a). It should be noted that the periodicity of the curve of Figure 30(f) corresponds to a frequency of 4.0 megacycles, and bears no relation to the periodicity of the sampling function.

The construction leading to Figure 30(f), and particularly Figure 30(b), emphasizes that the output of the sampler is the *product* of the input signal and the gating function. This fact, together with the

TIME—MICROSECONDS
GREEN RESPONSE TO BAND LIMITED STEP FUNCTION
$f_0 = 2.4$ Mc., $f_B = 4.1$ Mc.
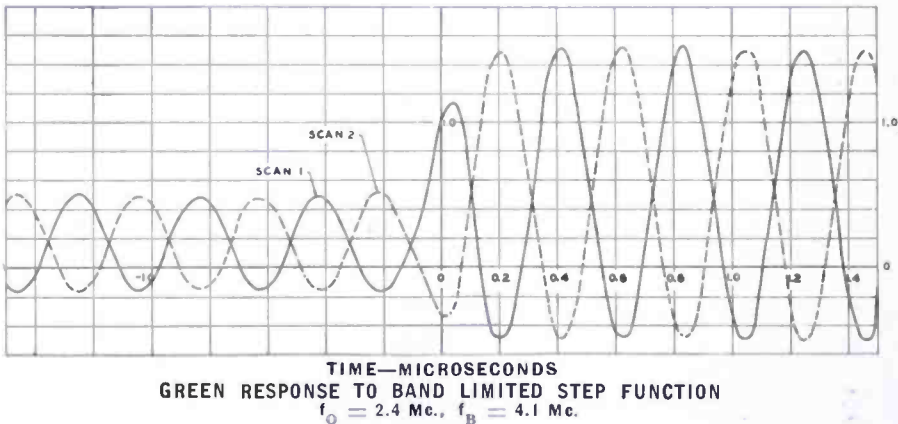
Fig. 31—Response to step function. Signal on the green kinescope grid of a color television receiver. Sampling frequency is 2.4 megacycles.

principle of mixed highs, produces full detail limited only by total bandwidth available. This conclusion is further strengthened by examining the response of the system to a step function.

Figure 31 has been constructed from Equation (31) to show the signal on the green kinescope when the initial signal is a step function as shown in Figure 11, with $M = 1/2$, and with a sampling frequency of 2.4 megacycles. The transmission band has been limited to 4.1 megacycles. Figure 31 corresponds to Figure 15, except for the choice of sampling frequency.

Figure 32 shows the combined light intensity of two successive scans of the same line on the green kinescope of a color television receiver, obtained by adding the positive values of the two curves of Figure 31. The dashed line in Figure 32 is taken from Figure 12 to show the best response possible in a frequency band limited to video frequencies less than 4.1 megacycles.

The mixed-high signal on the red kinescope grid due to the step
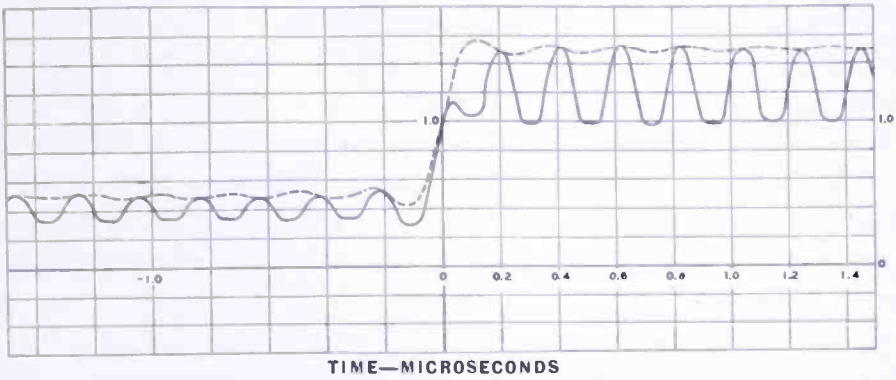
TIME—MICROSECONDS
GREEN RESPONSE TO BAND LIMITED STEP FUNCTION SUMS OF SCANS
$f_0 = 2.4$ Mc., $f_B = 4.1$ Mc., $f_A = 2.0$ Mc.

Fig. 32—Response to step function. Combined light intensity of two successive scans of the same line on the green kinescope of a color television receiver. Sampling frequency is 2.4 megacycles.

function in the green channel is given by Equation (35). The positive values of this function, when added to the curve of Figure 32, result in Figure 33. It should be noted that Figure 32 corresponds to Figure 16 and Figure 33 corresponds to Figure 24, except that in Figures 16 and 24 the sampling frequency is 3.8 megacycles, and in Figures 32 and 33 the sampling frequency is 2.4 megacycles.

APPENDIX II

TRANSMISSION OF THE DOT-SEQUENTIAL COLOR TELEVISION SIGNAL ON COAXIAL CABLES OF RESTRICTED BANDWIDTH

Presently available coaxial cables used in networking of monochrome television signals will pass no signals of frequencies greater than approximately 2.7 megacycles. Since the sampling frequency in the dot-sequential color television system as used experimentally in
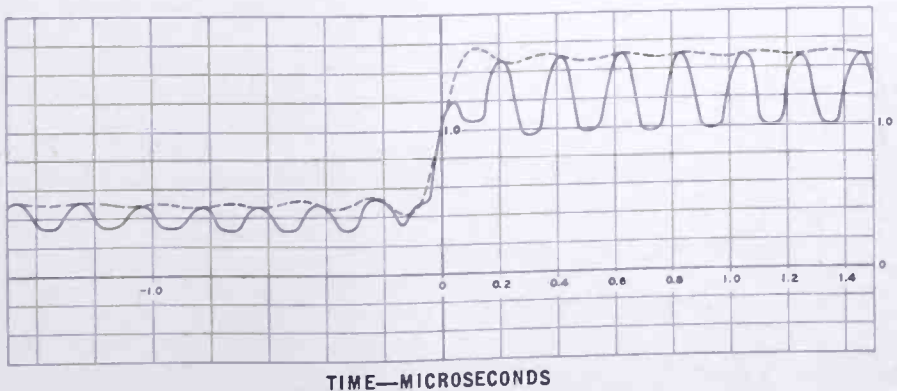
TIME—MICROSECONDS
GREEN RESPONSE WITH CROSS TALK ADDED
$f_0 = 2.4$ Mc., $f_B = 4.1$ Mc., $f_A = 2.0$ Mc.

Fig. 33—Response to step function. Combined light intensities from the red and the green kinescopes. Sampling frequency is 2.4 megacycles.

Washington is approximately 3.6 megacycles,* color information is lost when the composite signal usually used to modulate the transmitter is transmitted over the coaxial cable.

While it is anticipated that coaxial cables of at least four-megacycle bandwidth will be made available by the time that such cables are needed for commercial color television transmission, it is desirable to make use of the present cables for experimental purposes in the interim period.

When a standard monochrome television signal containing information out to four megacycles is passed over the 2.7-megacycle cable, the picture definition is reduced accordingly. It is the purpose of this appendix to describe two versions of a method of transmitting dot-sequential color television signals over the present coaxial cables, retaining color information and accepting loss of resolution corresponding to that suffered by a monochrome signal over the same transmission medium.

Figure 34 shows a diagram of the first method of transmission. The normal color system components are shown with dashed lines at the left. The components added for the low frequency cable transmission are shown with solid lines at the right.

The crystal oscillator which provides the normal sampling signal feeds into a regenerative multiplier which produces a sampling signal which is exactly two-thirds the frequency of the normal sampling signal, namely, 2,388,750 cycles. This latter signal, together with the synchronizing signals and the simultaneous green, red and blue signals from the camera, are fed to a transmitter type sampler especially provided at the originating station. The output of this sampler then feeds into the coaxial cable. A color synchronizing burst with a frequency of 2,388,750 cycles is placed on the back porch of the horizontal synchronizing pedestal for transmission over the cable. At the receiving end of the cable, a receiver type sampler is provided, with sampling of each color taking place at a rate of 2,388,750 times per second. Low-pass filters, with cut-off below this sampling frequency, are placed in the green, red and blue outputs of this sampler. These

---

* In the above report, the sampling frequency was assumed to be 3.8 megacycles. Since November, 1949, the sampling frequency used at the WNBW transmitter in Washington has been 3,583,125 cycles per second. The ratio of this latter number to the scanning line frequency of 15,750 lines per second is 227½. This fractional relationship affords a direct means of obtaining the dot interlace. At the present time, the color synchronization is obtained by transmitting a burst, several cycles duration, of the sampling signal on the back porch of the horizontal synchronizing pedestal. This burst, as well as the sampling component in the picture signal, is removed by the bandwidth limitations of the coaxial cable.

three signals are then used to feed a normal transmitter sampler at the station which is being programmed by the coaxial cable transmission. The 2,388,750-cycle burst coming over the cable is multiplied up to 3,583,125 cycles to provide the sampling control for the latter station.

The method shown in Figure 34 is a direct approach to the problem of transmitting the color information over the limited bandwidth coaxial cable. A second method is shown by the block diagram of Figure 35. This version applies mixed-highs to more effectively utilize the bandwidth available for transmission. Color information is transmitted with detail up to 0.3 megacycle, with signal mixing to apply mixed highs extending upward from 0.3 megacycle.
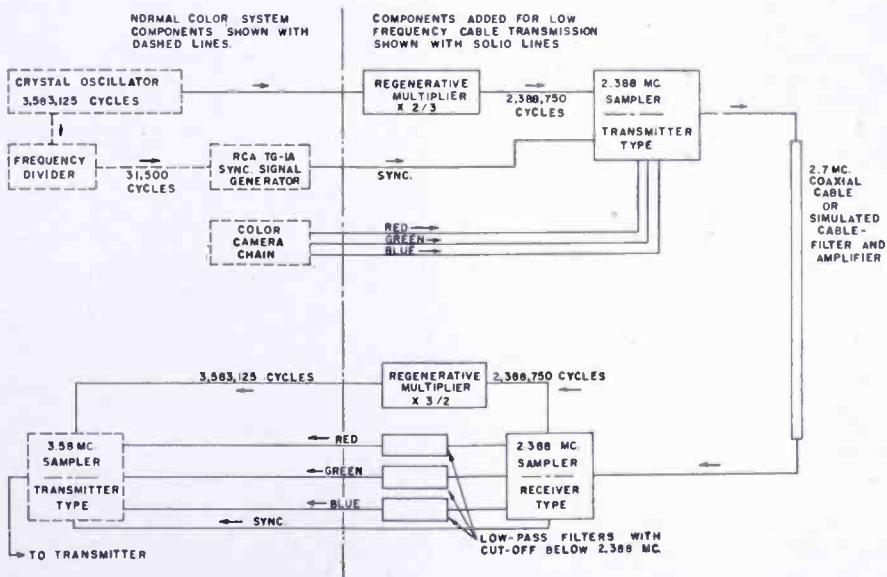
Fig. 34—Block diagram of the equipment used to transmit color television signals over coaxial cables of restricted bandwidth.

To illustrate the principles of operation, assume that the signal from the green camera tube is

$$G.C.S. = G + g \cdot \sin \omega_1 t + g_2 \sin \omega_2 t, \tag{41}$$

where $f_1 < 0.3$ megacycle,

and $0.3 < f_2 < 2.1$.

The signal into the 2.4-megacycle sampler at the sending end of the cable is simply

$$G + g_1 \sin \omega_1 t \tag{42}$$

since the low-pass (0-0.3 megacycle) filters remove the last term of (41).

When the signal of (42) is sampled in the usual fashion,

$$K_1 [G + g_1 \sin \omega_1 t] \left[\frac{1 + 2 \cos(\omega_s t)}{3} \right]$$

$$= \frac{K_1 G}{3} + \frac{K_1 g_1}{3} \sin \omega_1 t + \frac{2K_1}{3} [G + g_1 \sin \omega_1 t] \cdot \cos(\omega_s t), \quad (43)$$

where f_s is the sampling frequency of 2.4 megacycles. The band-pass
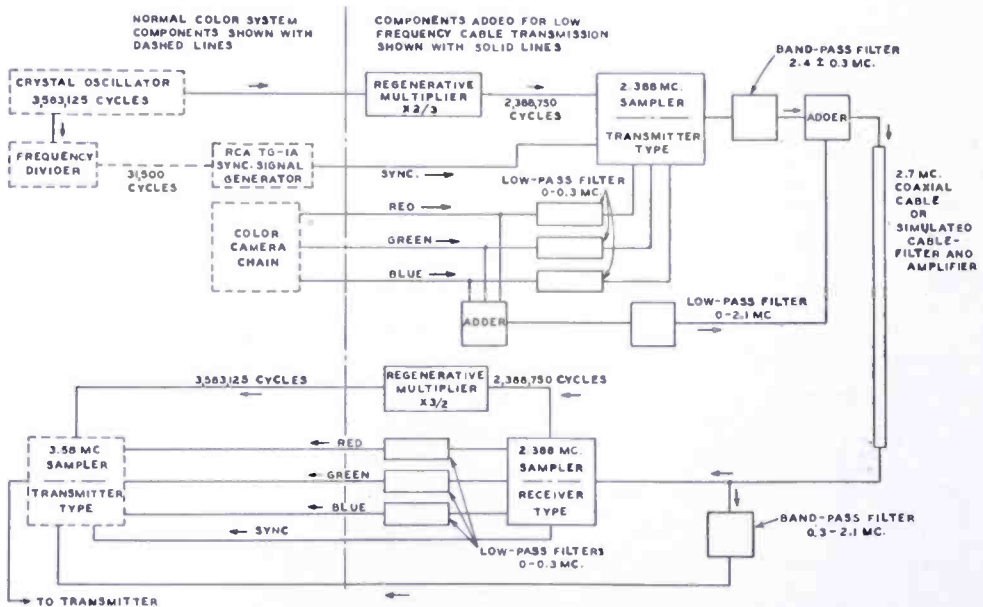
Fig. 35—A modification of the cable equipment which makes more effective use of the available band.

filter following the sampler wipes out the first two terms of (43) so the remaining signal going to the adder is simply

$$K_2 [G + g_1 \sin \omega_1 t] \cdot \cos(\omega_s t). \quad (44)$$

It should be noted that this filtering action has removed any requirement of short duty factor in sampling. In fact, the sampler can be an ordinary balanced modulator.

The entire signal given by (41) is bypassed around the sampler. The output of the adder feeding the cable is then the sum of (41) and (44),

$$\text{cable signal} = K_3 \left[G + g_1 \sin \omega_1 t + g_2 \sin \omega_2 t \right]$$

$$+ K_2 \left[G + g_1 \sin (\omega_1 t) \right] \cos (\omega_s t). \tag{45}$$

At the receiving end of the cable, the signal $K_3 g_2 \sin \omega_2 t$ goes through the band-pass filter and is used on retransmission as a regular mixed-highs signal.

Before studying the action of the sampler at the receiving end of the cable, assume that the gain controls at the transmitting end have been set so that $K_2 = 2K_3$. Then the cable signal of (45) becomes

$$K_3 \left[G + g_1 \sin \omega_1 t \right] \left[1 + 2 \cos \omega_s t \right] + K_3 g_2 \sin \omega_2 t. \tag{46}$$

Reference to Equations (14) and (15) and the adjacent text shows that when the signal of expression (46) goes through the sampler *and* low-pass filter at the receiving end of the coaxial cable, the signal on the green output is

$$K_4 \left[G + g_1 \sin \omega_1 t \right]. \tag{47}$$

This signal goes directly to the 3.6-megacycle sampler of the station which is programmed by the coaxial transmission.

This latter method provides color detail up to 0.3 megacycle, and intensity detail up to 2.1 megacycles.

APPENDIX III

The Action of the Dot-Sequential Color Television System in the Presence of an Abrupt Red-Green Transition

The analysis presented in the main body of the report, as it related to step functions, was confined to changes in a single color, that is, to intensity changes. Another effect which is encountered is that of abrupt changes in color where the colors are almost identical in intensity values.

To illustrate this effect, refer to Figure 36. Here a small patch of a scene is depicted where the scene is red on the left and green on the right. Assume that the red and green areas are of such color values that equal average electrical signals are produced by the red camera tube and the green camera tube.

The signal out of the green camera tube (with no frequency limitations) would be similar to that shown in Figure 11, with M set equal to unity. The signal out of the red camera tube would be an opposite

step, that is, the signal would have a prescribed value for t less than zero and would have zero value for t greater than zero. This would be achieved analytically by setting M equal to -1.

If the signal from each camera is limited to less than the top pass frequency, f_B, the green camera signal (G.C.S.) is obtained from Equation (28). Then (with $M = 1$)

$$\text{G.C.S.} = 1 + \frac{2}{\pi} \int_{\beta=0}^{\beta=\infty} d\beta \int_{\omega=0}^{\omega=2\pi f_B} \sin(\omega\beta)\sin(\omega t)\,d\beta$$

$$= 1 + \frac{2}{\pi} \int_{\beta=0}^{\beta=\infty} d\beta \int_{\omega=0}^{\omega=2\pi f_A} \sin(\omega\beta)\sin(\omega t)\,d\omega$$

$$+ \frac{2}{\pi} \int_{\beta=0}^{\beta=\infty} d\beta \int_{\omega=2\pi f_A}^{\omega=2\pi f_B} \sin(\omega\beta)\sin(\omega t)\,d\omega, \tag{48}$$

and the red camera signal (R.C.S.) is (with $M = -1$)

$$\text{R.C.S.} = 1 - \frac{2}{\pi} \int_{\beta=0}^{\beta=\infty} d\beta \int_{\omega=0}^{\omega=2\pi f_B} \sin(\omega\beta)\sin(\omega t)\,d\beta$$

$$= 1 - \frac{2}{\pi} \int_{\beta=0}^{\beta=\infty} d\beta \int_{\omega=0}^{\omega=2\pi f_A} \sin(\omega\beta)\sin(\omega t)\,d\beta$$

$$- \frac{2}{\pi} \int_{\beta=0}^{\beta=\infty} d\beta \int_{\omega=2\pi f_A}^{\omega=2\pi f_B} \sin(\omega\beta)\sin(\omega t)\,d\omega. \tag{49}$$
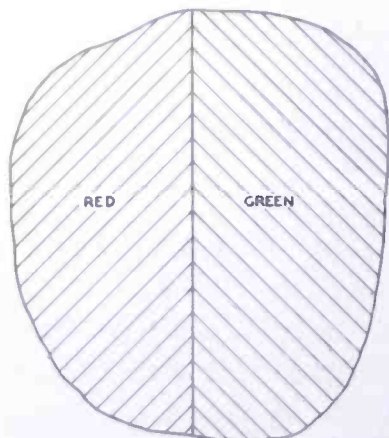
Fig. 36—An area where the transition from red to green produces constant light intensity.

The mixed-highs signal is found to be the sum of the last term in (48) and the last term in (49). This sum is seen to be zero. Physically, this result comes about from the fact that the alternating terms which make up the green step are identical, except for a reversal of polarity, to the alternating terms which make up the red step. For a standard monochrome camera viewing the patch of Figure 36, no transition would be visible.

Although it has been shown above that no mixed-high signal exists, the action of a color television receiver for this situation may still be analyzed by utilizing the principle of superposition. That is, the green step may be analyzed just as if the red step did not exist, and vice versa. Then the two solutions may be superimposed.

The signal on the green kinescope of a color television receiver, due to the green step alone, is found from Equation (31) to be

$$(\text{G.K.S.})_g = \frac{1}{3} [1 \pm 2 \cos(\omega_0 t)] \left[1 + \frac{2}{\pi} \text{Si}(2\pi f_B t) \right]. \qquad (50)$$

According to Equation (35), this green step alone produces a signal on the red kinescope grid which is

$$(\text{R.K.S.})_g = \frac{2}{3\pi} [1 \pm 2 \cos(\omega_0 t - 120°)] \, |\text{Si}(2\pi f_B t) - \text{Si}(2\pi f_A t)]. \qquad (51)$$

Conversely, the signal on the red tube from the red step alone is found from (31) by setting M equal to -1, and taking account of the fact that the red sampler lags the green sampler by 120 degrees. This latter signal is

$$(\text{R.K.S.})_r = \frac{1}{3} [1 \pm 2 \cos(\omega_0 t - 120°)] \left[1 - \frac{2}{\pi} \text{Si}(2\pi f_B t) \right]. \qquad (52)$$

The cross-talk term on the green kinescope due to the red step is likewise found from (35) to be

$$(\text{G.K.S.})_r = \frac{-2}{3\pi} [1 \pm 2 \cos(\omega_0 t)] [\text{Si}(2\pi f_B t) - \text{Si}(2\pi f_A t)]. \qquad (53)$$

The total signal on the green kinescope grid due to the color transition shown in Figure 36 is found by adding (50) and (53), yielding

$$\text{G.K.S.} = \frac{1}{3} [1 \pm 2 \cos(\omega_0 t)] \left[1 + \frac{2}{\pi} \text{Si}(2\pi f_A t) \right]. \qquad (54)$$

The total signal on the red kinescope grid due to the color transition shown in Figure 36 is found by adding (51) and (52),

$$\text{R.K.S.} = \frac{1}{3} \left[1 \pm 2 \cos(\omega_0 t - 120°) \right] \left[1 - \frac{2}{\pi} \text{Si}(2\pi f_A t) \right]. \qquad (55)$$

These last two equations show that the response to the transition in color shown in Figure 36 produces no detail greater than the frequency f_A. In other words, the mixed high-signals have cancelled to zero.

Fig. 37—Signal on the green kinescope grid of a color television receiver in the transition region of Figure 36. The sum curve may be regarded as the combined light intensity of two successive scans.

The green kinescope signal as found from Equation (54) for two successive scans of the same line is shown in Figure 37. The sum of the positive values of these two responses is also shown. This latter curve may be regarded as the light intensity, under the usual assumptions of kinescope and system linearity. The sampling frequency, f_0, has been taken as 3.8 megacycles.

Similar calculations, using Equation (55), are displayed in Figure 38. The sampling frequency, f_0, was taken to be 3.8 megacycles.

The red and green light intensity sums are shown in Figure 39, where it may be seen that the steepness of rise of the green and the steepness of fall of the red is limited to 2 megacycles, since f_A has been set at 2 megacycles in these calculations.

It is apparent that for a color transition such as shown in Figure 36, the detail at the transition is limited to frequencies no greater than f_A, the lower frequency limit of the mixed highs, and that detail between f_A and f_B is lost.

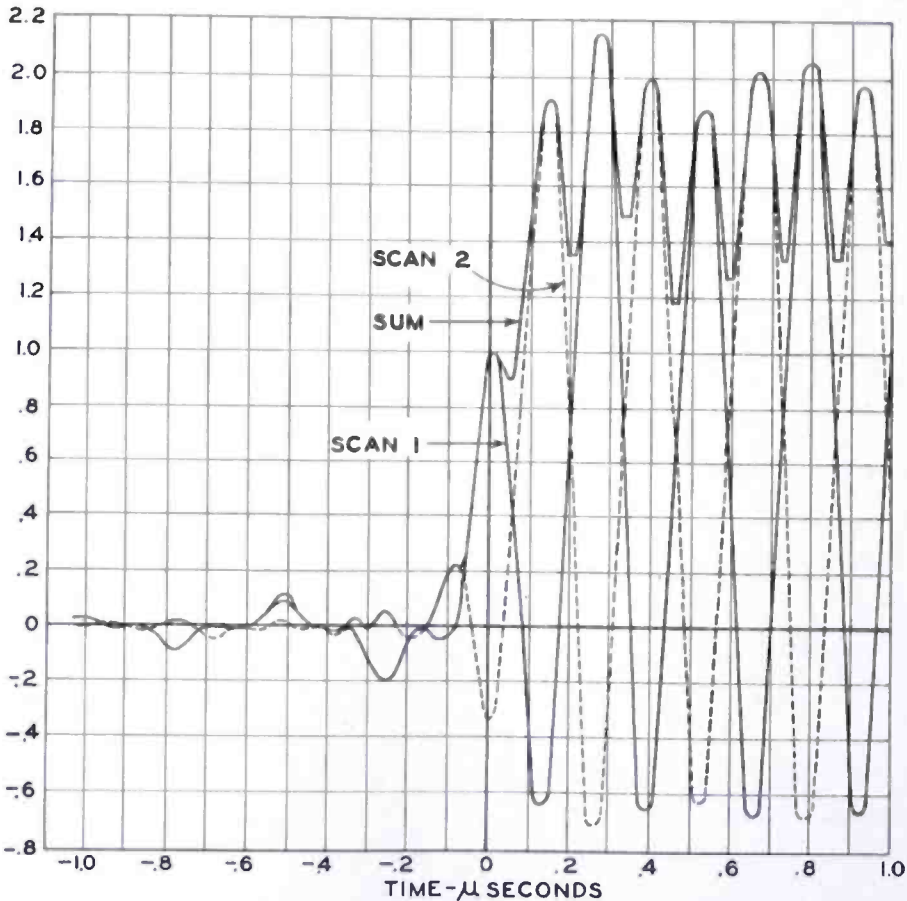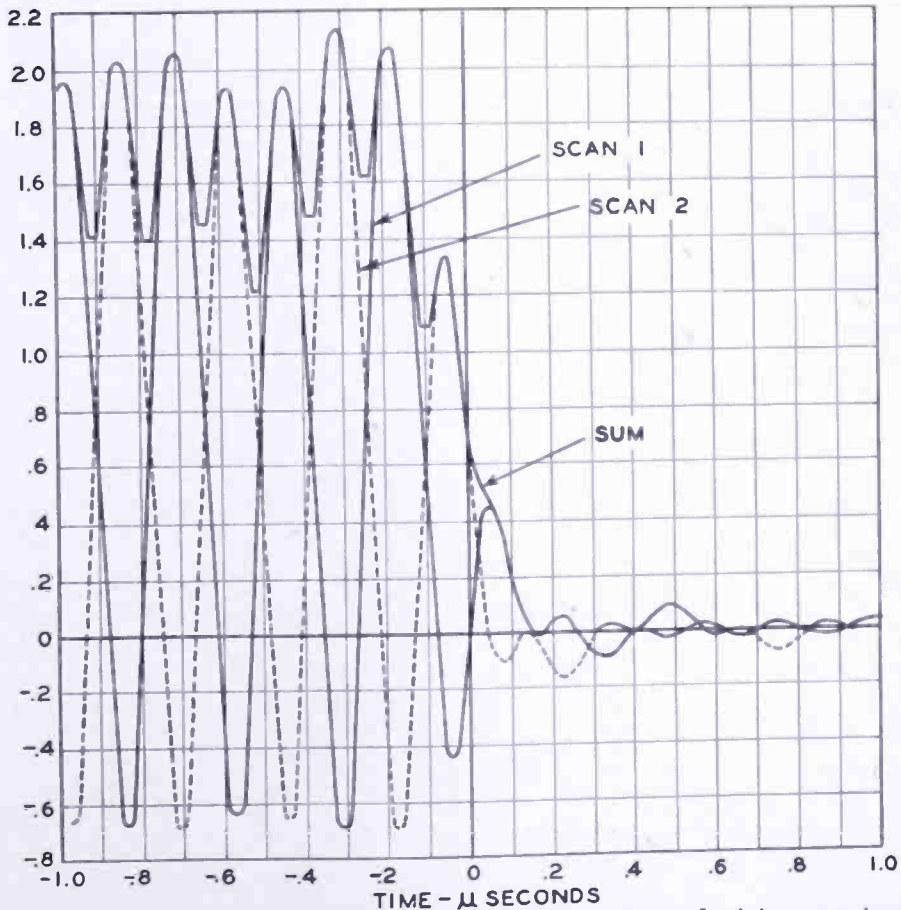Fig. 38—Signal on the red kinescope grid of a color television receiver in the transition region of Figure 36. The sum curve may be regarded as the combined light intensity of two successive scans.

This effect might at first thought be considered to be a serious defect in the dot-sequential color television system. On the contrary, it is on this point that the dot-sequential color television system again makes use of the ability of the eye to distinguish detail in brightness and the inability of the eye to see detail in color differences. Observer tests made and reported by A. V. Bedford* shows that the acuity of

---

* A. V. Bedford, "Mixed Highs in Color Television", *Proc. I.R.E.*, Vol. 38, No. 9, p. 1003, September, 1950.

the eye for detail residing in color differences is less than half as great as the acuity for detail residing in brightness. To satisfy the eye observing a color television picture at a particular distance, it is not necessary to transmit information regarding the *color* of certain tiny areas even though these areas are large enough to be distinguished by differences in brightness. Accordingly, it is not necessary in scanning from area to area of the picture to be able to change from one color to another as quickly as it is necessary to change from one bright-
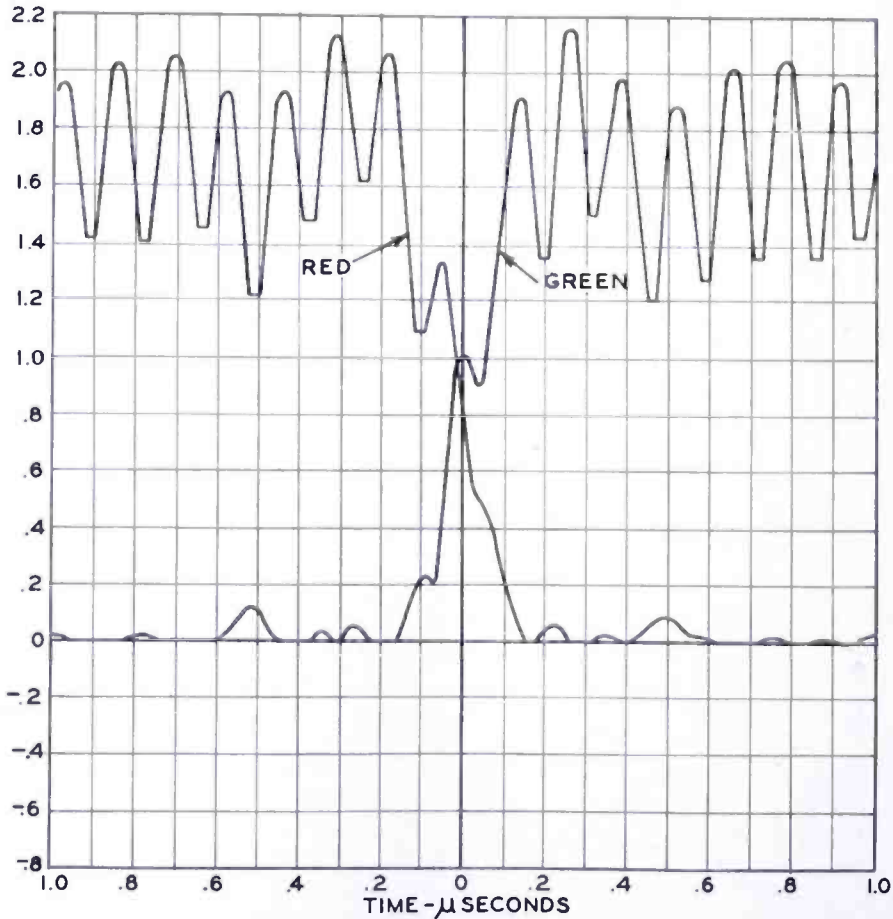
Fig. 39—Combined light intensity for two successive scans of the same line, for the transition region of Figure 36. The light intensity on the red and green tubes is shown separately.

ness to another. This report has demonstrated the ability of the dot-sequential color television system to produce brightness detail to an extent limited only by the total bandwidth allowed. Since the frequency f_A, the lower limit of the mixed-high region, has been chosen to be 2 megacycles with a 4 megacycle bandwidth, the system operates well within the limits set by physiological effects. As a matter of fact, Bedford's detailed results show that the choice of the lower limit of the mixed-highs has been a very sound one,

It is of interest to note from Figure 39 that a standard black and white receiver subjected to this color signal would show no distinction between the two areas. Likewise, a standard monochrome camera viewing the area showed in Figure 36 would not produce significant information on a black and white receiver.

RCA TECHNICAL PAPERS†

Second Quarter, 1950

Any request for copies of papers listed herein should be
addressed to the publication to which credited.

"An Analysis of the Sampling Principles of the Dot-Sequential
Color Television System", *RCA Review* June 1950

"The Apparent Source of Speech in the Mouth", M. E. Hawley
and A. H. Kettler, *Jour. Acous. Soc. Amer.* (May) 1950

"Bridgeport UHF-TV Test Results", R. F. Guy, *FM-TV* (May) 1950

"Component Considerations and Centering Adjustments for
Kinescope RCA-16GP4", *RCA Application Note AN-144*,
RCA Tube Department, Harrison, N.J. (June 15) 1950

"Determining the Tracking Capabilities of a Pickup", H. E.
Roys, *Audio Eng.* (May) 1950

"The Effect of Electrolytes on the Cathodoluminescence of Zinc
Oxide", S. Larach, *Jour. Phys. and Colloid Chemistry*
(April) 1950

"The Electron Art", J. D. Fahnestock, *Electronics* (May) 1950

"A Feedback-Controlled Calibrator for Phonograph Pickups",
J. G. Woodward, *RCA Review* (June) 1950

"A Five-Inch Television Oscilloscope", E. I. Anderson, *RCA
Licensee Bulletin LB-793* (April 20) 1950

"General Description of Receivers for the RCA Color Television
System Which Employ the RCA Direct-View Tri-Color
Kinescopes", Bulletin, RCA Laboratories Division (April).. 1950
RCA Review (June) 1950

"High-Silica Fluosilicic Acid", S. M. Thomsen, *Jour. Amer.
Chem. Soc.* (June) 1950

"An Improved Speech Inverter System", L. L. Koros, *Electronics*
(May) 1950

"The KB-3A High-Fidelity Noise-Cancelling Microphone", L. J.
Anderson and L. M. Wigington, *Audio Eng.* (April) 1950

"Maximum Tank Voltage in Class C Amplifiers", L. E. Dwork,
Proc. I.R.E. (June) 1950

"Magnetic Recording in Motion Pictures", M. Rettinger, *Audio
Eng.* (April) 1950

"A Method of Simulating Propagation Problems", Harley Iams,
Proc. I.R.E. (May) 1950

"Modifying a Horizontal Blocking Oscillator to Provide Increased
Driving Voltage for the Scanning Circuit", *RCA Applica-
tion Note AN-145*, RCA Tube Department, Harrison, N.J.
(June 15) 1950

"New Picture Tube for Color TV", *Radio-Electronics* (June) .. 1950

"New Brenkert Projection System for Drive-In Theaters", C. N.
Batsel and H. J. Benham, *Jour. S.M.P.T.E.* (April) 1950

"A New Ultra-High-Frequency Television Transmitter", J. R.
Bennett and L. S. Lappin, *RCA Review* (June) 1950

"New 'Unobtrusive' Ribbon-Pressure Microphone", H. F. Olson
and John Preston, *Broadcast News* (May-June) 1950

"Noise Generators and Measuring Technics", I. J. Melman,
Tele-Tech, part I (May), part II (June) 1950

† Report all corrections or additions to RCA Review, Radio Corporation of
America, RCA Laboratories Division, Princeton, N. J.

"Pictorial Display in Aircraft Navigation and Landing", L. F. Jones, H. J. Schrader and J. N. Marshall, *Proc. I.R.E.* (April) 1950

"The Poisoning of Cathodoluminescence in Silver-Activated Cubic Zinc Sulfide", *Jour. Chem. Phys.* (June) 1950

"Producing the 5820 Image Orthicon", R. B. Janes, R. E. Johnson and R. R. Handel, *Electronics* (June) 1950

"Program Control Console for International Program Service", S. H. Simpson, Jr., R. E. Hammond and M. P. Rehm, *RCA Review* (June) 1950

"RCA Announces new All-Electronic Color Television Employing Full-Color Tube", *Elec. Eng.* (May) 1950

"RCA Color Kinescope Demonstrated", *Tele-Tech* (May) 1950

"RCA's New Direct-View Tri-Color Kinescopes", *Radio and Tele. News* (June) 1950

"A Reflectometer for Measuring the Efficiency of Low-Reflection Films on Glass", R. F. Leinhos, *RCA Licensee Bulletin LB-796* (June 10) 1950

"The Role of International Telegraph Companies in Military Communications", Sidney Sparks, *Teleg. and Teleph. Age* (April) 1950

"Shielded Low Capacitance Video Frequency Oscilloscope Probes", J. Avins, *RCA Licensee Bulletin LB-794* (April 20) 1950

"A Simple Microwave Relay Communication System", Maurice G. Staton, *Tele-Tech* (April) 1950

"Simplified Television for Industry", J. M. Morgan and R. C. Webb, *Electronics* (June) 1950

"Stabilization of Wide Band D.C. Amplifiers for Zero and Gain", E. A. Goldberg, *RCA Review* (June) 1950

"Stainless Steel for Television", A. Rose, *Metal Progress* (June) 1950

"Servo Theory Applied to Frequency Stabilization with Spectral Lines", W. D. Hersherger and L. E. Norton, *Jour. Frank. Inst.* (May) 1950

"Studies of Thyratron Behavior, Part I — The Effect of Grid Resistance on the Recovery Time of Thyratrons", L. Malter and E. O. Johnson, *RCA Review* (June) 1950

"Studies of Thyratron Behavior, Part II — A Study of the Effect of Grid Potential Variations During the Afterglow Period Upon the Recovery Time of a Thyratron", E. O. Johnson and L. Malter, *RCA Review* (June) 1950

"A Study of Cochannel and Adjacent-Channel Interference of Television Signals", *RCA Review* (June) 1950

"UHF Television Field Test", R. F. Guy, *Electronics* (April) .. 1950

"Ultra-High-Frequency Antenna and System for Television Transmission", O. O. Fiet, *RCA Review* (June) 1950

"The Vidicon — Photoconductive Camera Tube", P. K. Weimer, S. V. Forgue and R. R. Goodrich, *Electronics* (May) 1950

"Wide Range 600-7000 MC Local Oscillator", Peter Janis, *Tele-Tech* (April) 1950

Note—Omissions or errors in these listings will be corrected in the yearly index.

GORDON L. FREDENDALL received the Ph.D. degree from the University of Wisconsin. From 1931 to 1936 he taught electrical engineering and mathematics, and engaged in research work in mercury-arc phenomena at the University of Wisconsin. Since 1936 he has been with Radio Corporation of America, working on television research. He is at present located in Princeton, N. J., at RCA Laboratories Division. Dr. Fredendall is a Senior Member of the Institute of Radio Engineers.

E. DUDLEY GOODALE received the B.S. degree in Electrical Engineering from Union College in 1928 and the B.S. and M.S. degrees in Electrical Engineering from the Massachusetts Institute of Technology in 1930 and 1931. From 1932 to 1937 he was engaged in vacuum tube engineering work with the RCA Manufacturing Company at Harrison, New Jersey. In 1937 he transferred to the Development Group of the National Broadcasting Company in New York where he has been directly associated with television development activities since that time. Mr. Goodale is a member of Eta Kappa Nu, Sigma Xi, the Institute of Radio Engineers, the Society of Motion Picture and Television Engineers, and is a licensed Professional Engineer in New York State.

ROBERT L. HARVEY received the B.S. degree in Electrical Engineering from the University of Tennessee in 1928. After graduation he became a test engineer, and later a member of the receiver engineering group, of the General Electric Company. In 1930 he joined the RCA Manufacturing Company and engaged in receiver production design, receiver advanced development, and later research on receiver circuits and component parts, which included some early work on powdered iron cores. Since 1942 he has been with the RCA Laboratories Division in Princeton, N. J. Mr. Harvey is a member of Sigma Xi and a senior member of the Institute of Radio Engineers.

J. LEWIS HATHAWAY received the B.S. degree in Electrical Engineering from the University of Colorado in 1929. In the same year, he joined the National Broadcasting Company where, as a member of the Development Group, he has since been engaged in all fields of the company's engineering activities. While on leave of absence from 1941 to 1944, he served as a Special Research Associate at Harvard University performing underwater sound development work. Mr. Hathaway was appointed Assistant Manager of Engineering Development of the National Broadcasting Company in 1948. He is a Senior Member of the Institute of Radio Engineers and a Member of the Radio Pioneers.

IMRE J. HEGYI received the B.S. degree in Chemistry in 1942, from the Johns Hopkins University, and the M.S. degree in Chemistry in 1946 from the Polytechnic Institute of Brooklyn. From 1942-1943 he was associated with the Davison Chemical Co. and from 1943-1947 with Baker and Company. In 1947 he joined the Chemico-Physics section of the RCA Laboratories Division, Princeton, N. J. Mr. Hegyi is a member of Sigma Xi, American Chemical Society, American Crystallographic Association, and Institute of Radio Engineers.

ROBERT B. JANES received the B.S. degree in physics from Kenyon College in 1928. He did graduate work in physics at Harvard and the University of Wisconsin where he received a Ph.D. in 1935. From 1929 to 1931 he served as instructor in physics at Colgate University and from 1931 to 1935 as research assistant at the University of Wisconsin. From 1935 to 1943, Mr. Janes was an engineer at the Harrison, N. J. plant of RCA where he worked on television camera tubes and phototubes. Since 1943 he has been in the Tube Department of RCA at Lancaster, Pennsylvania. He was in charge of the development and design of television camera tubes until 1950, when he was appointed Manager of the Development Group responsible for camera tubes, storage tubes, and phototubes.

HUMBOLDT W. LEVERENZ received the B.A. degree in chemistry from Stanford University in 1930. He studied physics and chemistry as an Exchange Fellow of the Institute of International Education at the University of Munster, Westphalia, Germany from 1930-1931. He was a chemico-physicist in the Research and Engineering Department of RCA Manufacturing Co., Inc. from 1931 to 1938 at Camden, N. J., from 1938 to 1941 at Harrison, N. J., and from 1941 to the present time with RCA Laboratories Division. He studied development, manufacture, and tactical use of radar indicators in England during March to May, 1944 as a special representative of the Office of Scientific Research and Development. Mr. Leverenz is a fellow of the American Physical Society and a member of The American Chemical Society, Sigma Xi, and Phi Lambda Upsilon.

WEN YUAN PAN received the E.E. Degree from Stanford University in 1939, and the Ph.D. Degree in Electrical Engineering in 1940. He served in an advisory capacity to the China Defense and Supplies in 1941 and to the Chinese Delegation to the International Civil Aviation Conference in 1944. He was engaged as a research scientist at the Radio Research Laboratory at Cambridge, Massachusetts, during the war years and was invited to be a member of the Advisory Committee of the United Nations Telecommunications in 1946. Since 1945, he has been with the RCA Victor Division at Camden, New Jersey. Dr. Pan is an honorary member of the Veterans' Wireless Operators Association, a member of Sigma XI and Senior Member of the Institute of Radio Engineers.

RALPH C. KENNEDY received the B.A. degree from San Jose State College in 1943 and the M.A. and E.E. degrees in Electrical Engineering from Stanford University in 1945 and 1946 respectively. After serving as Transmitter Engineer and Chief Engineer at several broadcast stations, he joined the Hewlett-Packard Company as an Engineer in 1943, where he worked on Oscillators and UHF Signal Generators for the Armed Forces. In 1944 he became a Transmitter Engineer at KNBC, the National Broadcasting Company transmitter in San Francisco. In 1946 he was transferred to the Development Group of the National Broadcasting Company in New York as a Development Engineer. Since then he has worked on various problems concerned with Sound Broadcasting and Remote Pickup Broadcasting. For the past two years Mr. Kennedy has been engaged in various phases of television development. He is currently engaged in work toward a Doctor's Degree at Brooklyn Polytechnic Institute. Mr. Kennedy is a Member of the American Mathematical Society.

ALEXANDER A. ROTOW, born in Tomsk, Russia, received the B.S. degree in Electrical Engineering and in Physics from the University of Belgrade in Yugoslavia. After graduation, and until the outbreak of World War II, he was employed by the Ikarus airplane factory in Belgrade as radio engineer and later as manager of the physical laboratories. He took part in World War II first as a reserve lieutenant of the Yugoslav Royal Air Force and later with the United States Army in Italy as a civilian engineer in the Headquarters of the Allied Military Government. In 1948 he came to the United States and since that time has been associated with the Tube Department of the RCA Victor Division at Lancaster, Pa., working on camera tube development. Mr. Rotow is engaged in part-time graduate work at Franklin and Marshall College and is a member of the American Association for the Advancement of Science.

CHARLES L. TOWNSEND was born on July 9, 1909 and, except for one year in Hollywood as a sound engineer, has been associated with radio broadcasting since 1927. Mr. Townsend joined the Engineering Department of the NBC Chicago office in 1931 and was transferred to New York in 1937 for television technical and operational development. With the advent of World War II he was engaged in development work on NBC contracts with NDRC and the United States Navy. These included television reconnaissance projects and participation in the guided missile program. With the conclusion of the war, he returned to television operations as Television Supervisor of the Television Film Studio. In 1948 he returned to Chicago as the Operations Supervisor of the NBC television plant then under construction in that city. Mr. Townsend was appointed by NBC in 1949 to the position of Technical Film Director and returned to New York to assume his new responsibilities.